7-1-2014

Biophysical Interactions in the Straits of Florida: Turbulent Mixing Due to Diel Vertical Migrations of Zooplankton

Cayla Whitney Dean
Nova Southeastern University, cd821@nova.edu

Nova Southeastern University Oceanographic Center

Biophysical Interactions in the Straits of Florida: Turbulent Mixing Due to Diel Vertical Migrations of Zooplankton

By:

Cayla Whitney Dean

Submitted to the Faculty of
Nova Southeastern University Oceanographic Center
in partial fulfillment of the requirements for
the degree of Master of Science with a specialty in:
Marine Biology

Nova Southeastern University
July 2014

Thesis of
Cayla Dean

Submitted in Partial Fulfillment of the Requirements for the Degree of

Masters of Science:

Marine Biology

Nova Southeastern University
Oceanographic Center

July 2014

Approved:

Thesis Committee

Major Professor:_____
Alexander Soloviev, Ph.D.

Committee Member:_____
Tamara Frank, Ph.D.

Committee Member:_____
Amy C. Hirons, Ph.D.

Acknowledgements

I thank my major advisor Dr. Alexander Soloviev for providing me the opportunity to work on this project and seeing potential in me. His support and guidance throughout the project contributed to my growth as a researcher and scientist. He also helped me forge connections with many other scientists that I would not have had the opportunity to meet without his assistance. These connections will provide many opportunities for my future work and education. Dr. Soloviev provided support and advice on all physical aspects of this project and greatly furthered my knowledge of physical oceanography. I am grateful to my committee members, Dr. Tamara Frank and Dr. Amy Hirons. Dr. Frank was invaluable in assisting with many questions regarding the biological phenomenon this project addresses. She was also a great resource in helping to plan my future career and educational steps. Dr. Hirons provided invaluable data from the biological samples and data collected during the first phase of the project.

I acknowledge the support from the project, Calypso LNG LLC for the first four years of data collection, and the Office of Naval Research ONR Award # N00014-10-1-0938 for funding data collection for the final year of data collection. I also acknowledge the University of Miami/Gulf of Mexico Research Initiative, Award S120021:"Consortium for Advanced Research on Transport of Hydrocarbon in the Environment (CARTHE)" for support of data analysis. I thank CARTHE for the opportunity to network with other scientists at the top of their field and to present my work at their semiannual meetings. I also thank the NSUOC student government association for travel support to present my partial thesis work at the Ocean Sciences Meeting of 2014.

Finally, I thank my family and friends for their unconditional support, love and encouragement throughout my education. They have provided me with a drive to pursue my education to the furthest extent and without their support I would not have made it this far.

Abstract

Diel vertical migrations (DVM) comprise the largest animal migration on the planet and are a phenomenon present in all bodies of water on Earth. A strong sound scattering layer undergoing DVM was observed in the Straits of Florida via a bottom-mounted Acoustic Doppler current profiler (ADCP) Workhorse Longranger 75 kHz (Teledyne RD Instruments) located at the 244 m isobath. ADCP average backscatter showed a clear periodicity corresponding with sunrise and sunset times indicating the presence of a nocturnal DVM. Analysis of the ADCP backscatter data indicated zooplankton swimming velocities were faster during sunrise than sunset times. In several cases the zooplankton swimming velocity appeared to be faster at the beginning of the descent, after which the swimming velocity decreased. Analysis of ADCP velocity data indicated a measureable decrease in the northward component of the current velocity field during migrations (sunrise and sunset) compared to three hours prior. This was presumably associated with an increase in drag due to turbulent friction associated with DVM. A non-hydrostatic computational fluid dynamics (CFD) model with injection of Lagrangian particles was utilized to simulate the effects of DVM on the velocity field and turbulence signature of the Florida Current. A domain simulating a section of the Florida Current was created and zooplankton were represented by particle injection with a discrete phase model. The model was run with and without particles, holding all other parameters the same, for comparison. Idealized temperature stratification and velocity profiles were set for both summer and winter conditions to observe seasonal differences. For each case, velocity and turbulence with particles were compared to results without particles to confirm the changes in profiles were due to the zooplankton (Lagrangian particles). In several cases there was an observable change in average x-velocity profiles due to the injection of particles into the domain. In all cases there was an observable increase in subgrid turbulent viscosity in the wake of the injected particles. This effect was much stronger in the winter case, most likely due to stratification of the water column which gave a near critical Richardson number. These results indicated that DVM does in fact have an effect on the velocity profile and turbulence signature in a strong current under certain conditions and that there was a seasonal difference due to stratification profiles.

Keywords: diel vertical migration, zooplankton, computational fluid dynamics, turbulence, velocity.

Table of Contents

List of Figures

List of Tables

1. INTRODUCTION

1.1 Diel Vertical Migrations

Diel vertical migration (DVM) is a migration pattern in which organisms migrate from the depths of the ocean to the surface and back on a daily basis (Iwasa, 1982; Richards et al., 1996). Knowledge of and interest in DVM dates back to at least the late 1800s (Loeb, 1893) but the mechanism triggering this phenomenon is still poorly understood (Cohen and Forward, 2009). DVMs compose the largest animal migrations on Earth and they occur in all of the world's oceans, lakes, and ponds that contain habitats where the risk of predation and resource concentration are significantly higher in the upper layers than in the lower (Andersen et al., 1991). Ianson et al. (2004) proposed from conservative assumptions that 15% of zooplankton biomass migrates. DVM appears to have evolved independently in many diverse groups of organisms, indicating that there is some major selective advantage for this behavior (Enright, 1977). Migration does not occur in lakes which have no difference in food concentration in upper and lower layers (Gliwicz, 1987). In addition, Bollens and Frost (1989) demonstrated that the introduction of predators induced DVM in an environment where migrations did not occur in the absence of predators. Organisms can migrate distances ranging from a couple of centimeters to hundreds of meters (Lampert, 1989). Many of these organisms actively seek out or avoid certain environmental conditions by swimming vertically. Those organisms with swim bladders can maintain a preferred position in the water column by actively maintaining neutral buoyancy (Huebert et al., 2010). Figure 1-1 shows examples of the most common migrators and the extremely high density of organisms that can undergo DVM.

Figure 1-1. Examples of zooplankton that undergo DVM. Top left is an example of a euphausiid (http://www.cmarz.org/). Top middle is an example of a chaetognath (http://taxondiversity.fieldofscience.com/). Top right are fish larvae (http://images.fineartamerica.com/). Bottom left is a copepod (http://taxondiversity.fieldofscience.com/). Bottom right is a school of migrating krill showing the large density of organisms migrating.

1.1.1 DVM Patterns

There are three different patterns of DVM that organisms follow: nocturnal, twilight, and reverse. Nocturnal DVM, or 'Type I' migration, is the most common pattern (Hutchinson, 1967). It is represented by a single ascent at sunset and descent at sunrise. Reverse DVM or 'Type II' migration is the opposite of nocturnal. The organisms descend at sunset and ascend at sunrise. This pattern has not been recorded in the open ocean; however, it has been found in lakes and coastal marine environments (Enright, 1977; Brodeur, 1994, Cohen and Forward, 2009) where demersal predators are present. The third type of DVM, Twilight DVM, consists of two separate ascents. The organism begins its ascent at sunset, reaches surface waters and then passively sinks through the night, termed midnight sinking or nocturnal sinking, and ascends once again just before sunrise. After sunrise, the organisms sink to a maximum depth for the day (Iwasa, 1982; Haney, 1988; Lampert, 1989; Cohen and Forward, 2002; Huebert et al., 2011). These

patterns are shown in Figure 1-2. These are not the only DVM patterns observed; a continuum exists between the extremes (Haney, 1988). Organisms can exhibit more than one of these general patterns during their life cycle. There are many factors that contribute to the pattern of migration an organism undergoes. Some factors include light cues, tidal cycle, stage of growth, presence/absence of food, season, age, sex, and depth of thermocline, pyconocline or chlorophyll maximum (Haney, 1988; Lampert 1989; Brodeur, 1994; Gray, 1998; Huebert et al., 2010; Irisson, 2010). Gray (1998) found that a stratified water column was not necessary for DVM to occur, but may change the pattern. Patterns of change in DVM can vary among species, larval stage, fat content (Rudjakov, 1970), sex, location or season (Enright, 1977; Andersen et al., 1991; Richards et al., 1996; Gray, 1998; Klevjer and Kaartvedt, 2011). Huebert et al. (2011) indicated that changes in migration patterns occurred with ontogenic stage; smaller zooplankton are typically found in shallower water during the day and move deeper with increasing size. This is most likely due to organisms being larger and denser at later life history stages and, therefore, more visible to predators than smaller stages (DeRobertis, 2002).

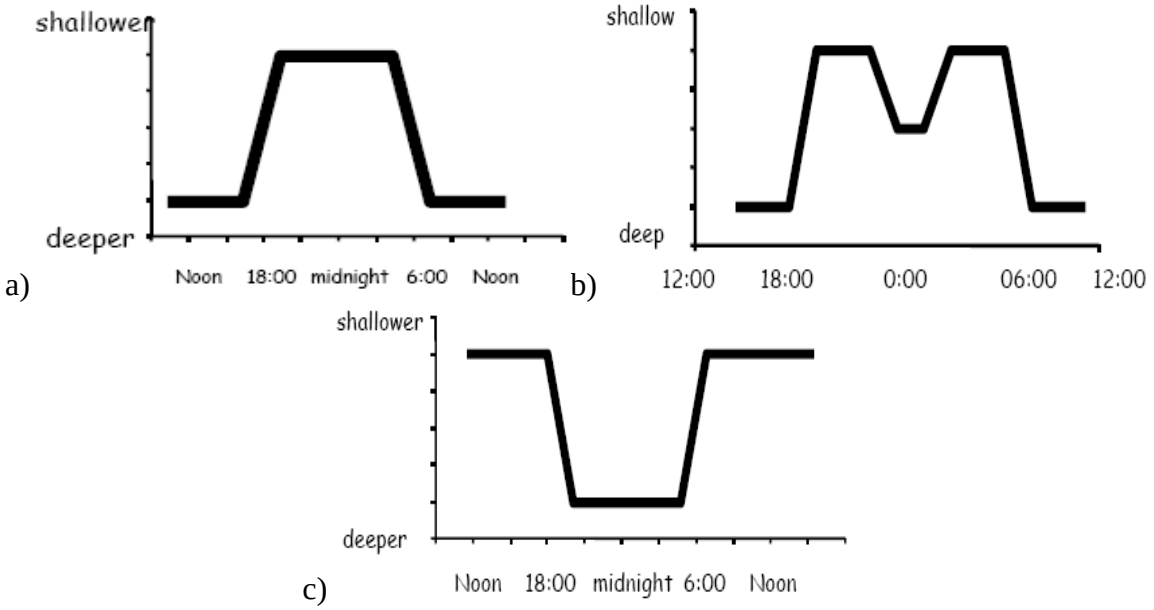

Figure 1-2. DVM patterns a) Nocturnal DVM b) Twilight DVM c) Reverse DVM (courtesy of Dr. Tamara Frank)

1.1.2 Cues

Light is the main physical cue or control mechanism that triggers DVM. This is termed the primary proximate or casual cause because it is the only parameter that changes on a daily basis and provides primary stimulus to trigger timing of migrations (Andersen et al., 1991; Richards et al., 1996). It initiates synchronization of upward motion and the rate of ascent (Haney, 1988). Light can be viewed as an endogenous cue by entraining circadian rhythm orzoo as an exogenous/external cue (Forward, 1988).

While the initiation and synchronization of DVM are triggered by light, it appears that the level of locomotion can be modified by temperature, food, and pressure (Rudjakov, 1970). At dusk a spectral change in the light field occurs, and light shifts toward shorter wavelengths. This shift is observable from approximately 10 to 150 m depth. Below 150 m the shift can no longer be observed, indicating some other cue must be used by species at these depths (Frank and Widder, 1996).

There are three hypotheses that discuss what aspects of the change in light field triggers nocturnal/twilight DVM. These are the absolute intensity-threshold hypothesis, rate of change hypothesis and preferendum hypothesis.

The absolute intensity-threshold hypothesis states that ascent at sunset is initiated once the light intensity decreases below a threshold level and descent at sunrise is initiated as the light intensity increases above threshold intensity (Cohen and Forward, 2009). Studies indicate that it is highly unlikely this is the sole cue used by most species. It is likely that animals are responding to absolute change in intensity along with another cue (Swift and Forward, 1988; Haney et al., 1990).

The preferendum or isolume hypothesis states that zooplankton have a preferred or optimal light intensity (isolume) or range of light intensities, within which they prefer to remain (De Robertis, 2003). Zooplankton will swim or passively sink to move into and remain in their preferred isolume. Several studies indicate that some species appear to be following an isolume such as some invertebrates, while others, such as fish, do not (Frank and Widder, 1997).

The rate of change hypothesis states that the cue for triggering vertical migrations is the rate and direction of change in light from ambient level, not absolute light, which can vary over the course of a day (Cohen and Forward, 2009). According to this hypothesis, light can act as orienting, controlling, and initiating cues (Bainbridge, 1961; Forward, 1985). There is evidence from the field that zooplankton move faster with a faster rate of change of light (Richards et al., 1996). It is likely that some species are cued by changes in absolute light intensity, some are cued by the rate of change intensity, and others are following an isolume. It is also probable that most species use a combination of these cues (Richards et al., 1996; Frank and Widder, 1997; Cohen and Forward, 2009). There are some species that may not be cued by light at all, but are simply following the movements of their prey.

1.1.3 Predator Avoidance

Why do organisms migrate? There have been many hypotheses proposed regarding the ultimate cause of why organisms undergo DVM. The most widely accepted hypothesis is the predator avoidance hypothesis. This hypothesis states that adoption of migratory or non-migratory behaviors is based on the relative abundance of visual

orienting predators, food, and level of satiation (Gliwicz, 1987; Lampert, 1989; De Robertis et al., 2003). The concentration of food at depth is not enough to meet energy requirements of many organisms; therefore, migration to the near surface waters is necessary to meet these demands (Stitch and Lampert, 1981). Predators are more likely to see their prey during the day, leading to the occupation of darker deeper water during the day, and ascent to the surface waters during the evening (Enright, 1977). Assuming predation is based on visual cues, a size bias in the timing of ascent and descent should be present. Smaller animals ascend earlier and descend later than larger organisms because they are less visible to predators (Yamamura, 1998; De Robertis and Jaffe 2000; De Robertis, 2002). This size bias was observed in Oceanographyer Canyon by Frank and Widder (2002) and Saanich Inlet, British Colombia, Canada by Kunze et al. (2006). DVM is a defense behavior and is likely to cause reductions in growth and fecundity. Therefore, food must be in ample supply in the surface waters together with a large number of visual predators to make migration energetically beneficial (Lampert, 1989; Loose and Dawidowicz, 1994).

The abundance of predators and predation rates can change dramatically over seasonal time scales, altering DVM rates and patterns (Iwasa, 1982; Loose and Dawidowicz, 1994). The amplitude of DVM is proportional to the water clarity and the presence or absence of moonlight. Results from Cohen and Forward (2005) suggested that copepod species ascend earlier in the evening when predator abundance is low and later in the evening when high predator abundance is present. The longest migrations will always occur during periods with a new moon at night and cloudless days. These conditions will provide the greatest change in light between day and night. These conditions allow organisms to come closer to the surface at night because they are unlikely to be seen, but they need to go deeper during the day to avoid visually orienting predators (Gliwicz, 1986).

There is quite a bit of support for the predator avoidance hypothesis. It has been shown in the field and laboratory that vertical migrations can be induced in previously non-migrating species by the introduction of predators (Haney, 1988; Bollens and Frost, 1989). Gliwicz (1986) observed that migrations did not occur in lakes where planktivorous fish predators were not present, short range DVM occurred in lakes that had been stocked with fish for decades and long range DVM occurred in lakes that had been stocked for centuries.

1.1.4 Measurements

The deep scattering layer was first discovered in 1942 off the coast of San Diego, California when Sound Navigation and Ranging (SONAR) was first used. An apparent upward migration of the “bottom” was observed in the evening and a downward migration in the morning (Dickson, 1972). It was soon discovered that this phenomenon

had a biological cause, zooplankton undergoing DVM, and was present throughout the world's oceans. The discovery of the deep scattering layer via SONAR provided a new method of studying these migrations. The basic concept behind SONAR is that when a ping is emitted from the instrument, the sound strikes an underwater object that reflects sound and a portion of the sound wave is reflected back to the instrument. For the purposes of biological studies, sound waves do not reflect off of soft fish bodies, but can reflect off of the swim bladders in fish or oil droplets in crustaceans. Echo strength is dependent on size and density contrast of the pinged object. Problems with utilizing this method to study DVM include the inability to detect small zooplankton and fish without swim bladders, or identify taxa present.

Most studies conducted on DVM were accomplished using net sampling methods. These types of studies usually collected samples around the clock, avoiding times directly around sunset and sunrise, when migrations would be occurring. Differences in biomass collected during day samples vs. night samples indicate whether vertical migrations are occurring. Net studies have an advantage over acoustic studies in that they are able to identify species present in migrations. This helps to determine types, size, and swimming speeds (from laboratory experiments) of organisms and how they will interact with the physical characteristics of the water column, such as velocity fluctuations and turbulence signature (Videler et al., 2002; Yen et al., 2003). However, nets can also miss very small organisms depending on the mesh size and larger organisms may be able to swim away avoiding being caught in the net (Ianson, 2004).

Acoustic studies are able to determine exact timing, distance and speed of migrations of a mass of organisms in a large volume of water. The first acoustic Doppler current profiler (ADCP) was developed in 1981 by request of scientists of the Coastal Ocean Dynamics Experiment (Williams, 2010). They desired an autonomous, self-powered, internally recording current profiler. ADCPs measure flow velocity by recording the Doppler shift of transmitted acoustic pulses that return to the sensor after encountering particles, or clusters of scattering particles, in the water column. The Doppler Effect is the change in the observed pitch resulting from relative motion between the observer and the sound wave. The Doppler Shift is the difference between the frequency of received and transmitted sounds proportional to change in speed. Typically, scattering particles move at the same rate as the fluid, unless they are swimming organisms. This property allows the use of an ADCP to detect vertical swimming movements and estimate velocities, especially in times of ascent at sunset and descent at sunrise (Smyth et al., 2006). Increased echo frequency indicates the object is moving towards the instrument. It uses three or four transducers orthogonal to each other and at some horizontal angle. With this, the instrument can determine speed and direction of the flow (Gordon, 1996). The greatest advantage to this instrument is the ability to obtain measurements throughout the water column from a single device. The device sends a series of acoustic

pulses or pings into the water column. As sound moves through the water column, the ADCP measures the reflected sound or backscatter and can potentially provide information on the number of scatterers, but requires a special calibration (Gordon, 1996).

One limitation to ADCP measurements is the lack of resolution to identify and follow individual animals (De Robertis, 2003; Ianson, 2004). ADCPs can only detect scatterers larger than a certain size, based on the frequency of the instrument. Therefore not all migrators can be observed with acoustic measurements. In addition, an ADCP cannot tell the difference between fish, squid or crustaceans that contain swim bladders or oil droplets of equivalent sizes. Observations can also be contaminated by large bubbles or features such as thermoclines. The echo from a "hard" surface is much stronger than the weak echoes from scatterers in the water. Therefore, measurements near the seafloor or surface are not accurate and are usually rejected (Gordon, 1996).

1.1.5 Models

Numerical models are another method of studying DVM and the effect of zooplankton, usually simulated with particles, on mixing and turbulence in a fluid flow. Using a modeling approach, effects from DVM can be simulated in many different conditions and types of fluid flow. It is possible to explore variables of the particles placed in the model, such as organism size, number of migrators present, and swimming speed. Models are a great way to get an approximation of unknown factors in a system. While models can be a great tool for simulating an effect of DVM, it is necessary to validate the model with real world data. The results of the model can then be compared to acoustic and/or net data collected from the field.

No one method is able to fully analyze the effect of DVM in the physical environment. Therefore, several different methods should be utilized simultaneously to get a better understanding. The optimal combination of data would be acoustic measurements, net samples, turbulence profiling with a specialized instrument, laboratory experiments and computation fluid dynamics modeling.

1.2 Biomixing

Oceanography has long been focused on identifying processes that account for the external work required to sustain oceanic circulation. Some of these processes include surface heating and cooling, winds, tidal mixing, and internal waves. From these processes, it has been estimated that 2 to 3 terawatts (TW) of power is required to sustain circulation (Wunsch and Ferrari, 2004; St. Laurent and Simmons, 2006). If only waves and tides are considered, there is an apparent deficit of approximately 1 TW in the energy budget (Munk and Wunsch, 1998; Wunsch, 2000). Dewar et al. (2006) proposed that wind and tide may not contribute as much energy as previously thought. A significant

portion of tidal energy may be dissipated against topographic features or boundaries. Wind energy enters at the surface of the ocean and may dissipate as it propagates to the depth of the ocean. The oceanic biosphere captures approximately 63 TW of solar energy, and while only a small percentage makes it into mechanical energy of swimming this appears to fill the gaps in the energy budget (Dewar et al., 2006; Visser, 2007).

The potential input of energy by marine organisms to the ocean mixing energy budget, known as the concept of biomixing, was first proposed in 1966 by Walter Munk. The concept of biogenic ocean mixing needs a detailed understanding of many processes, including organism behavior and characteristics, mechanisms of mixing stratified fluids by swimming animals and how physical processes affect these factors (Katija, 2012). Biomixing implies that biology has a strong impact on oceanic mixing. On a global scale this would mean that swimming organisms bring cold water from the deep ocean, thereby contributing to global ocean circulation (Dewar et al., 2006). It is possible that DVM could help regulate gas exchange between the ocean and atmosphere, thereby playing a role in the carbon cycle and climate (Kunze et al., 2006). On a local scale this could explain higher levels of surface production that cannot be accounted for by physical mixing mechanisms (Jenkins and Doney, 2003). This could be due to schools of organisms migrating through the thermocline and causing nutrient rich water to mix upward increasing the possibility of phytoplankton growth (Huntley and Zhou, 2004; Visser, 2007).

Swimming-induced turbulence is caused by velocity fluctuations from motion at relatively small scales. Swimming organisms dissipate considerable amounts of mechanical energy. Laboratory studies confirmed that schools of swimming animals create measurable increases in fluid disturbances (Catton et al., 2011) caused by velocity fluctuations from animal motion at small length scales (Huntley and Zhou, 2004). Evaluations based on energetics of swimming organisms indicated that organisms ranging from large zooplankton (0.5 cm) to cetaceans (10 m) can generate turbulent dissipation rates, ε, on the order of 10^{-5} W kg^{-1} in schools and swarms (Huntley and Zhou, 2004; Dewar et al. 2006). This is comparable to dissipation rates associated with major storms and may potentially provide a source of fine-scale turbulent mixing (MacKenzie and Leggettt, 1993). These values are three to four orders of magnitude larger than average dissipation rate in a stratified ocean.

Observations obtained by Kunze et al. (2006) indicated an instantaneous increase in dissipation rates by four to five orders of magnitude in the wake of a migrating school of krill (Fig. 1-3). While this DVM was short in duration, it led to an increase in daily-averaged turbulent eddy diffusivities by two to three orders of magnitude. Subsequent studies showed shear fluctuations at length scales up to one meter larger than the individual organism (Kunze et al., 2007). This indicated that the krill in the study acted as a unit rather than individuals when swimming upward (Kunze et al., 2006). In

aggregations of zooplankton, turbulence will not have time to decay before being encountered by another organism causing an increase of turbulence length and temporal scales (Gregg and Horne, 2009). The net dissipation rate due to a school of swimming organisms depends on the power expended per individual and the number of individuals per unit volume (Dewar et al., 2006). For a school of krill with body length of approximately 1.5 cm, swim speeds of 5 to 10 cm s^{-1}, and density of individuals of about 5000 organisms m^{-3}, the dissipation rate is approximately equal to 10^{-5} to 10^{-4} W kg^{-1} (Huntley and Zhou, 2004) which is consistent with the observations from Kunze et al. (2006). This behavior has also been shown using modeling techniques. Dabiri (2010) used a simple rigid body model and observed overturning length scales larger than the individual animals during a vertical motion of the entire aggregation.

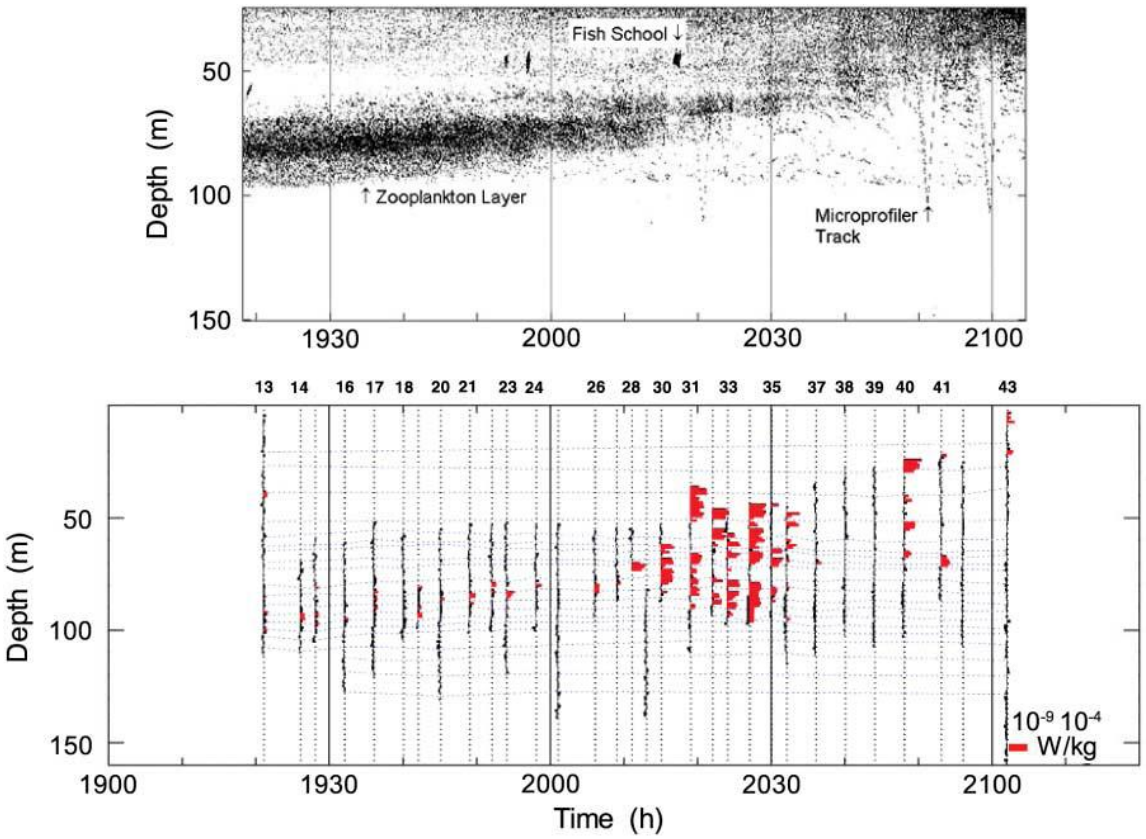

Figure 1-3. Acoustic backscatter data from a 200-kHz echosounder reveals vertical migration of the backscatter layer. The lowering and raising of the vertical microstructure profiler is also evident for some profiles (Kunze et al., 2006).

2 OBJECTIVES

2.1 Significance

DVM occurs in all types of bodies of water on the Earth's surface. This study focused on the migrations occurring in the Florida Current throughout the Straits of Florida. These DVMs are of particular interest because they occur in a very strong western boundary current in a confined area between the southern end of Florida and the Bahamas. This restricted space creates a very fast flow with unusual properties. Due to these properties, many larvae and zooplankton flow through this passage allowing for dispersal throughout the western Atlantic Ocean. The velocity and strength of the Florida Current varies greatly with depth, which influences the flow pattern of any zooplankton entrained in the current (Huebert et al., 2011).

The Florida Current has historically been attractive to study because of its geographically constrained location and proximity to shore. Pillsbury (1891) performed the first study to quantitatively measure the strength and direction of transport in the Florida Current by measuring average surface velocities at six anchor stations between Fowey Rocks and Gun Cay. In the late 1960s, Schmitz and Richardson (1968) made measurements of the Florida Current using new current meters and dropsondes, instruments which provide vertical averages of horizontal current velocity, to take absolute current measurements and determine the structure of the current. At the same time these new instruments became available, computing power began expanding rapidly and numerical models became more sophisticated (Leaman et al., 1987).

Due to the constrained area of Florida Current flow, it has a very high transport rate. The Florida Current has been estimated to have a mean transport rate of 30×10^6 m^3 s^{-1}, or 20 Sv, with a maximum flow in summer and minimum in winter (Anderson et al., 1985; Leaman et al., 1987). Due to the strong topographic changes and wind effects, the Florida Current experiences many different types of motions, including coastal countercurrent, undercurrent, meanders, and eddies, over different spatial and temporal scales. Temporal scales can range from a few days to seasonal and, interannual time frames (Schott et al., 1988; Lee and Williams, 1999). Niiler (1968) and Soloviev et al. (2003) reported current oscillations with approximately 10 hour periods. There have also been reports of strong undercurrents below the Florida Current (Düing and Johnson, 1971; Leaman et al., 1987; Soloviev et al., in review). This type of motion makes this part of the Subtropical Atlantic Gyre difficult to fully understand.

Knowledge gained from this study could have many significant impacts on the scientific community. Results will add to our knowledge of the flow of the Florida Current. We have a comprehensive understanding of the basic physical properties of the Florida Current, but biophysical properties are poorly understood in most systems. This study seeks to add to the knowledge base of biological influence on the physical environment through turbulent mixing. These results will also add to the ever expanding knowledge base of DVM and how migrations affect the physical environment. Much research has been conducted on each aspect of this study, but limited work has been

completed on the interaction of the biological migration and the physical properties of a current.

The effect of turbulence caused by DVMs in the Florida Current, could impact mixing throughout the water column. DVM could be important for mixing nutrients, organic matter, and gases through the thermocline (Andersen et al., 1991; Kunze, 2009; McManus, 2012). This is specifically important when looking at the possibility of future oil spills. A drilling project located in the loop current is being initiated off the northern coast of Cuba (Gibson, 2014). If a spill or a leak occurs in this area, the flow would take oil directly into the Florida Current and in the path of migrating zooplankton. These organisms would migrate through the oil slick and disperse it through the water column as they migrate, causing emulsification. This oil, now dispersed throughout the water column, will stick to the organisms and could potentially kill zooplankton, including fish and crustacean larvae. Therefore, the ability to produce accurate models of the effects of migrating zooplankton on biomixing is critical to making management decisions regarding allowable locations of drilling projects (if domestic) and producing an effectual plan of action should an oil spill occur.

2.2 Hypotheses

ADCP data was utilized to test whether zooplankton DVM had a statistically significant effect on physical oceanographic conditions of the water column. The effect observed from field data was reproduced using computation fluid dynamics software. ADCP and modeling data were compared to determine if zooplankton DVM in the Straits of Florida cause a statistically significant change in the northward current velocity component and/or the turbulence signature, enhancing mixing of the Florida Current. Data from each season was analyzed separately to test if there were seasonal differences in DVM strength. ADCP data was used to calculate average zooplankton vertical swim velocities during migration. This information was used to determine if there was a difference in swim speed in sunrise vs. sunset.

3 METHODS

3.1 Study Site

The Florida Current is a subsidiary feature of the Subtropical Atlantic Gyre and has similar physical properties as the rest of the western boundary current system, which is comprised of the Loop Current in the Gulf of Mexico, the Florida Current in the Straits of Florida and the Gulf Stream in the North Atlantic Ocean. The Florida Current has a strong influence on the circulation on the continental shelf off southeastern Florida (USCG, 2008; Soloviev et al., in review). It begins as the Yucatan Current, which flows as the Loop Current through the Gulf of Mexico and through the Straits of Florida as the Florida Current. This portion flows through the narrow passage between the southern end

of Florida and northern Cuba, and then turns toward the north, flowing between Florida and the western Bahamas. As the current continues northward, it becomes the Gulf Stream near the Georgia/South Carolina border as it approaches the Mid Atlantic Bight (Fig. 3-1) (Lee and Williams, 1999; Huebert et al., 2011).

a) 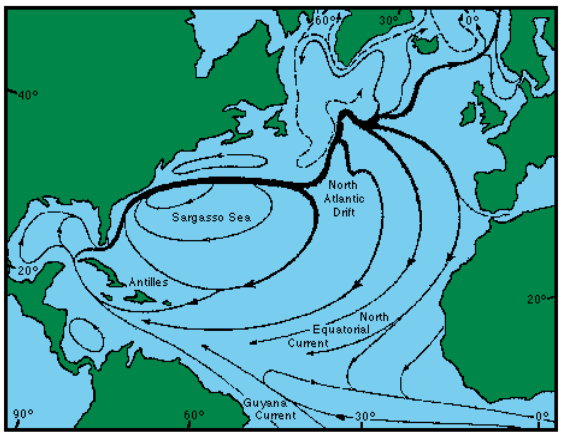

b) 

Figure 3-1. Maps of the flow of the Gulf of Mexico. a) An overview of the entire North Atlantic Gyre http://solarsytem101.blogspot.com/2011_02_01_archive.html. b) A closer look at the Straits of Florida (our study area) http://www.spacedaily.com/images-lg/topographical-map-straits-of-florida-current-lg.jpg

3.2 Data Collection

The majority of data for this study were collected during previous Nova Southeastern University Oceanographic Center (NSUOC) projects. Physical data were collected using a bottom mounted Teledyne RD Instruments ADCP (Workhorse Longranger 75 kHz) equipped with four transducers with a 20 degree inclination from vertical (Fig. 3-2) (USCG, 2008). For the first four years of data collection, the ADCP was located off the coast of Pompano Beach, FL (26.1911°N, 79.9739°W) at a 240 m isobath. Measurements were taken once every hour from January 23, 2007 at 15:00 GMT through October 19, 2010 at 14:17 GMT. This data set was used to address seasonal variability. The ADCP was then relocated to the Florida Straits off Dania Beach at a 244 m depth isobath (26.0315ºN, 79.9937°W) and measurements were taken every 5 minutes from December, 16 2010 at 11:00 GMT until October 11, 2011 at 14:30 GMT. The battery of the instrument was changed twice at this location resulting in three data sets which were approximately one season each. These groups are termed winter (December 16, 2010 at 11:00 through February 8, 2011 at 7:20), spring (February 9, 2011 at 11:00 through April, 26 2011 at 14:30), and summer (April 27, 2011 at 13:00 through October 11, 2011 at 17:50). An ADCP located at the 11m isobath (26.0731°N, 80.1014°W) was used for tidal, wave and coastal information. Locations of data collection are shown in Figure 3-3.

a) 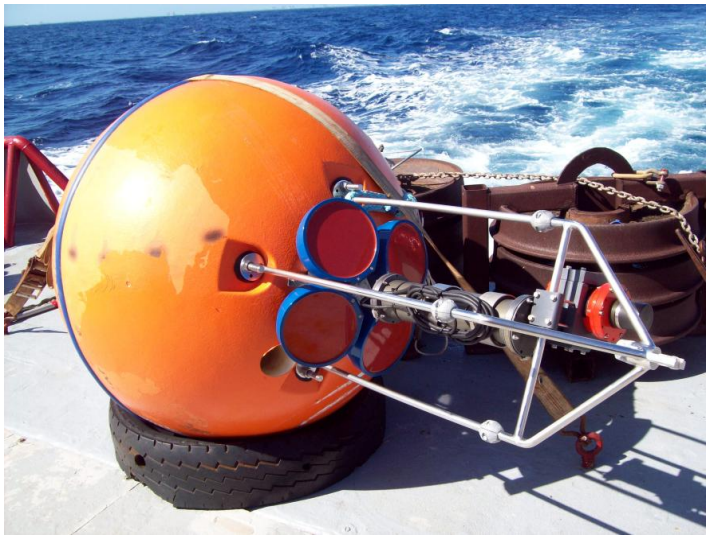  b)

Figure 3-2. Instrumentation: a.) The mooring that the instrument was deployed on; b) Teledyne RD Instruments ADCP (Workhorse Longranger 75 kHz) equipped with four transducers with a 20 degree inclination from vertical

a) 

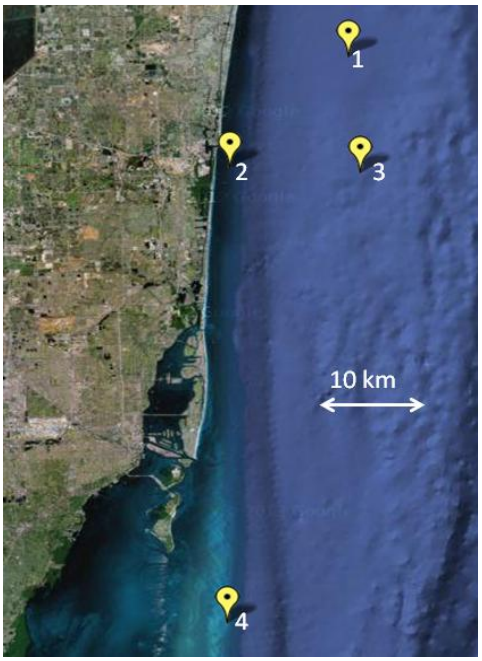

b)

Figure 3-3. Map of the sites where instruments were located. a) Large scale area where the study was conducted. b) Magnified white box from a). 1. ADCP mooring at 240 m isobath (Pompano). 2. ADCP mooring on 11 m isobath, shallow water measurements. 3. ADCP mooring at 244 m isobath (Dania Beach). 4. NDBC wind speed data Fowey Rocks.

Zooplankton and ichthyoplankton samples were collected via bongo and Tucker trawl nets to identify species present at deep water sites within and nearshore of the Florida Current. These samples were used to calculate zooplankton community

compositions and densities. Daytime and nighttime samples were collected at five stations from nine to twenty-four km offshore at shallow (25 m) and deep (200 m) depths. Two bongo nets were used at both depths and all five sites. One net was 202 µm mesh and the other net was 335 µm mesh. Both nets had flow meters attached in order to calculate the volume of seawater passing through for each tow, allowing for zooplankton density calculations. A Tucker mid-water trawl net with 760 µm mesh and attached flow meters collected zooplankton samples from the 0-25 m, 25-200 m and 200-0 m. Zooplankton samples from the bongo and Tucker nets were preserved in 5% seawater buffered formalin solution and then transferred to 70% ethanol solution for storage. For this project, data from the Tucker and bongo nets at sample Site 3 (the same location as the ADCP) provided taxa composition, the size range of the organisms, typical swimming velocities, and typical zooplankton density/biomass in day versus night samples (USCG, 2008). These data were needed to correctly set aspects of the computation fluid dynamics model.

Additional physical data was compiled through a variety of sources to assist in the analysis of the ADCP data. Sunrise and sunset times were collected from http://aa.usno.navy.mil/cgi-bin/aa_rstablew.pl. Full and new moon times were obtained from http://eclipse.gsfc.nasa.gov/phase/phases2001.html. Wind speed and direction were obtained from the National Oceanic and Atmospheric Administration's National Data Buoy Center (NOAA NDBC) at the Fowey Rocks station (Fig. 3-3), which recorded a measurement every five minutes. Tidal information was determined from the pressure sensor on the ADCP mooring.

3.3 Data Analysis

ADCP data were accessed using WinADCP software and exported in .mat format to be analyzed using Matlab software. Matlab was used to reproduce the contour plots of backscatter from the ADCP with additional information overlaid including sunrise, sunset, full, and new moon times. Zooplankton swim speeds were approximated by calculating the rate of change in the average backscatter at sunrise and sunset. The length of time of migration was determined on the x-axis (seconds) and the distance migrated was determined from the y-axis (meters). This information was used to calculate the rate of change of backscatter during migration. The zooplankton vertical swim velocity was estimated by dividing the difference in distance by difference in time giving a velocity. This calculation was performed for individual days and averaged over each season for the Dania Beach data set. Averages over each season were obtained by averaging the backscatter signal from each seasonal data set for 60 before and after sunset/sunrise. The rate of change in backscatter signal was then calculated from this average backscatter contour. Matlab was also used to analyze the northward current velocity component of the Florida Current at sunrise/sunset compared with data from three hours prior to determine if there was any change in velocity due to DVM. The sunrise and sunset

averages were calculated for 60 minutes before and after sunrise or sunset. Only cases when the Florida Current was present, northward velocity greater than 0.75 m s^{-1}, were considered. A 95% confidence interval was calculated for the average northward velocity profiles.

3.4 Computational Fluid Dynamics Model

ANSYS Fluent, commercial computational fluid dynamics (CFD) modeling software, was utilized to simulate the same biological/physical phenomena in an idealized situation. This was simulated using a 50 by 50 by 250 m domain with a one meter resolution mesh representing a section of the Florida Current (Fig. 3-4). For each model case a two hour spin up was run initially to allow the model to solve the flow equations. From this spin up, two separate cases were run, one with particles and one without particles for comparison. All models were run with a five second time step for 1440 steps (2 hours) with maximum 20 iterations per step. For every model run, gravity and energy equations were turned on. Even with increased computational power it was prohibitive to fully solve the three-dimensional Navier-Stokes equations in a turbulent flow. Therefore, some simplifying assumptions were made. Turbulence was modeled using Large Eddy Simulation/Wall Adapting Local Eddy Viscosity Model (LES WALE) which filtered the time-dependent Navier-Stokes equations (Eqn. 1 through 4).

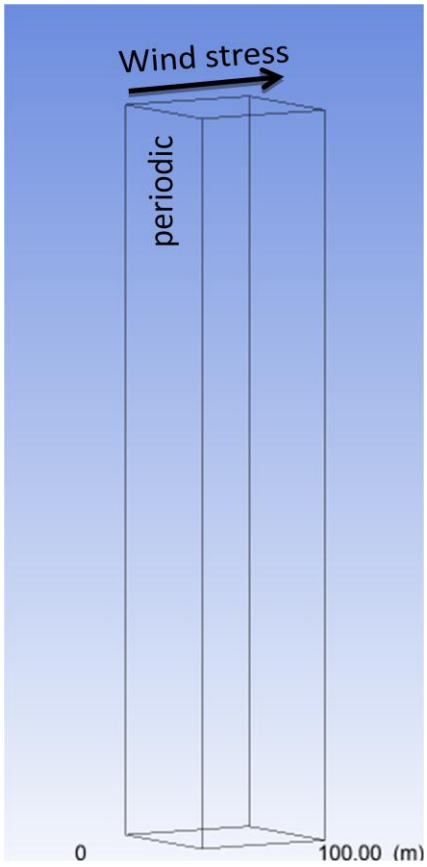

Figure 3-4. Domain used for ANSYS Fluent CFD model

$$\frac{\partial \rho}{\partial t} + \frac{\partial}{\partial x_i}(\rho \bar{u}_i) = 0 \quad (1)$$

$$\frac{\partial}{\partial t}(\rho \bar{u}_i) + \frac{\partial}{\partial x_j}\left(\rho \bar{u}_i \bar{u}_j\right) = \frac{\partial}{\partial x_j}\left(\sigma_{ij}\right) - \frac{\partial \bar{\rho}}{\partial x_i} - \frac{\partial \tau_{ij}}{\partial x_j} \quad (2)$$

where σ_{ij} is the stress tensor due to molecular viscosity defined by

$$\sigma_{ij} = \left[\mu\left(\frac{\partial \bar{u}_i}{\partial x_j} + \frac{\partial \bar{u}_j}{\partial x_i}\right)\right] - \frac{2}{3}\mu \frac{\partial u_i}{\partial x_i}\delta_{ij} \quad (3)$$

and τ_{ij} is the subgrid-scale stress defined by

$$\tau_{ij} = \rho\overline{u_i u_j} - \rho \bar{u}_i \bar{u}_j \quad (4)$$

In the WALE model the eddy viscosity was modeled by:

$$\mu_t = \rho L_s^2 \frac{\left(S_{ij}^d S_{ij}^d\right)^{3/2}}{\left(\bar{S}_{ij}\bar{S}_{ij}\right)^{5/2} + \left(S_{ij}^d S_{ij}^d\right)^{5/4}} \quad (5)$$

where L_s and S_{ij}^din the WALE model are defined, respectively as

$$L_s = \min\left(xd, C_w V^{1/3}\right) \quad (6)$$

$$S_{ij}^d = \frac{1}{2}\left(\bar{g}_{ij}^2 + \bar{g}_{ji}^2\right) - \frac{1}{3}\zeta_{ij}\bar{g}_{kk}^2, \bar{g}_{ij} = \frac{\delta \bar{u}_i}{\delta x_j} \quad (7)$$

In Fluent the default value of the WALE constant C_w is 0.325 (Fluent Theory Guide).

It was very important to set accurate initial boundary conditions to allow the model to solve the flow equations and, therefore, converge faster. Periodic boundary conditions were imposed to allow infinite fetch and to allow the particles to stay in the domain indefinitely. At the top boundary of the water column, specified shear was set at 0.048 Pa to simulate a 5 m s^{-1} northerly wind and at -0.048 Pa to simulate a 5 m s^{-1} southerly wind. Heat flux was also set at the top boundary to simulate a more realistic environment. For summer conditions, the heat flux was set at 100 W m^{-2} during the day (immediately before sunset) and -20 W m^{-2} during night (immediately after sunset). For winter, the heat flux was set at 20 W m^{-2} before sunset and -100 W m^{-2} after sunset. Similar surface heat fluxes were set at sunrise. The bottom boundary was set to no slip condition, indicating that the fluid sticks to the wall. The side walls of the domain were set with 0 Pa specified shear.

Not all options could be preset within the current ANSYS Fluent platform. To counter this, a user defined function was written using C++ language to define initial temperature and velocity profiles to simulate stratification of the Florida Current. Stratification profiles were significantly different in summer and winter conditions and the effect of Richardson number (Ri) determined from these profiles was of critical

importance. When Ri values approach 0.25, the critical value, the flow can become more unstable and, therefore, more turbulent. Below this critical value, smaller disturbances to the flow will create larger increases in turbulence.

Average profiles of the initial temperature and velocity are shown in Figure 3-5. In this study actual stratification information was not collected, so idealized profiles were used. The mixed layer was set to extend deeper in the water column during winter than in summer. The thermocline began at 75 m depth and a shallow layer at the top of the thermocline, from 75 to 85 m, occurred where the stratification was very strong, giving a Richardson number (Ri) less than critical value. In summer conditions, the mixed layer was set much shallower, beginning at 40 m depth, and the thermocline was a much thicker layer. This stratification profile gave a much higher Ri not approaching critical values. For both summer and winter conditions, the thermocline extended to 150 m depth. The Ri gives an indication of whether a flow will be stable or subject to overturning. In the winter thermocline, the Ri was less than 0.25 which was below the critical value indicating the flow was not stable and likely to overturn at least on local scales based on current shear. In summer, the Ri was greater than 0.25 and did not approach critical values, indicating a stable flow.

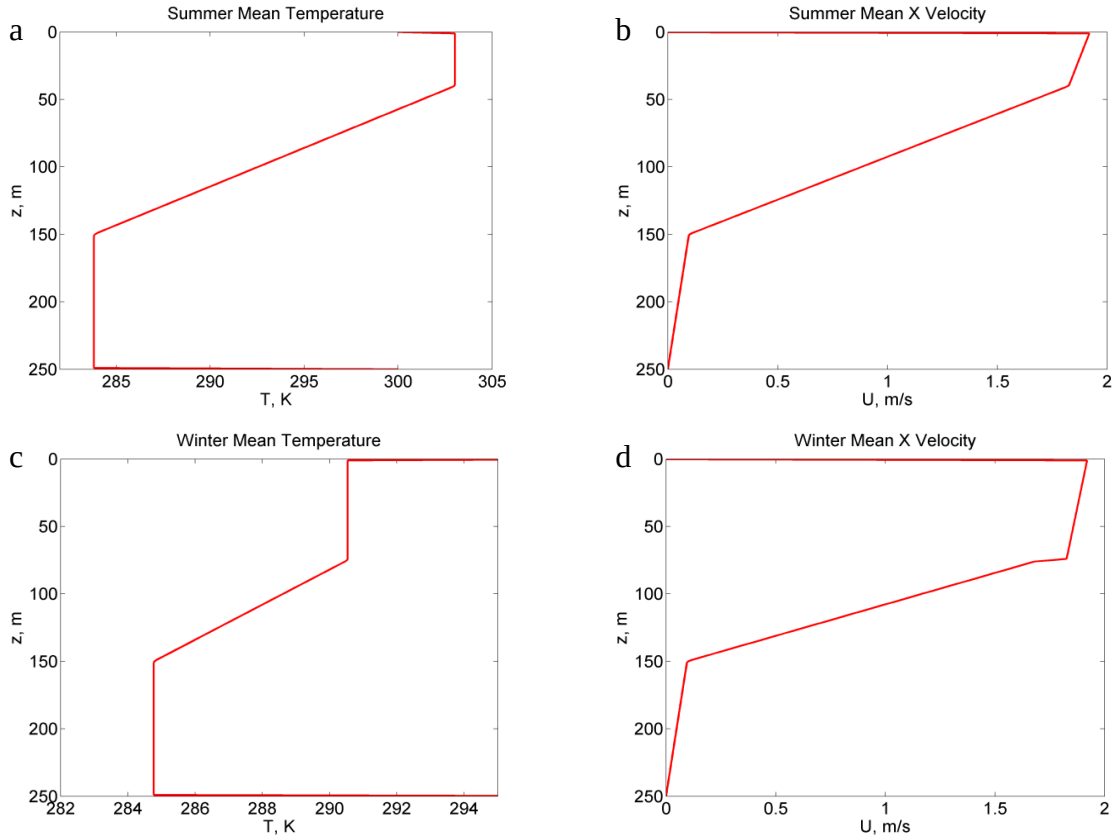

Figure 3-5. Initial stratification conditions for temperature and velocity in summer and winter cases. a) Temperature profile (K) for summer b) X velocity (m s^{-1}) for summer c) Temperature profile for winter (K) d) X velocity profile for winter (m s^{-1})

The model used a pressure-based solver with the SIMPLE scheme for pressure-velocity coupling. For spatial discretization, Standard Scheme was used for pressure, Least Squares Based was used for gradient, Bounded Central Difference was used for momentum, and Second Order Upwind was used for energy. The time-stepping scheme was set to Second Order Implicit. The liquid material within the domain was set to water and a Bousinessq approximation was used to allow faster convergence of the model. This approximation treats density as a constant value in all solved equations except the buoyancy term in the momentum equation.

$$(\rho - \rho_0)g \approx -\rho_0\beta(T - T_0)g \tag{8}$$

where ρ_0 is the constant density of the the flow, T_0 is the operating temperature and β is the thermal expansion coefficient. Density of water was set to 998.2 kg m^{-3}. The operating density was set to 0 to account for hydrostatic pressure and operating temperature was set to 288.15 K which was within the range of temperatures defined to simulate the Florida Current.

To model zooplankton, particles were injected into the domain in ANSYS Fluent using a discrete phase model (DPM). DPM allows simulation of a discrete second phase in a Lagrangian frame of reference. The fluid, or first phase, was treated as a continuum by solving the Navier-Stokes equations. The dispersed, or second, phase consisted of spherical particles dispersed in the continuous phase and was solved by tracking a large number of particles. Fluent computes particle trajectories individually at specific intervals during the calculation. Unsteady tracking of particles was enabled so Fluent advances each particle a specified number of particle time steps before the flow solution is updated. The particles and the flow develop together in time. A coupled DPM was selected making the effects of the particles influence the flow solution and interact with the continuous phase. Number of continuous phase iterations per DPM iteration was set to two. This controlled the frequency that the particles were tracked and the solution updated. The option to update DPM sources with each flow iteration was selected so the particle source term was recalculated every iteration.

In the coupled DPM model, the mass flow rate of a particle injection is required, which determines the number of particles injected per unit of time. To aid in the determination of the mass flow rate of particles injected in the CFD model, zooplankton biomass (mL m^{-3}) and concentrations (# m^{-3}) from several previous studies were referenced and converted to a mass flow rate (kg s^{-1}), utilizing several simplifying assumptions. For studies that indicated number of organisms per cubic meter, the organisms were assumed to be spherical particles with 0.01 m diameter. For all studies, zooplankton were assumed to have the same density as water (1000 kg m^{-3}). This was calculated for only the top 100 m of the domain as this is the area that DVM was observed from the acoustic data in this study.

Calculation of mass flow rate was possible due to the zooplankton samples collected. This study determined zooplankton biomass by the method of displacement of volume (Beer, 1976). At the location of the ADCP, biomass values ranged from 0.001 to 1.13 mL m^{-3}. The maximum value was used for this calculation since zooplankton studies typically are underestimates. The mass flow rate was determined by multiplying the biomass (1.5 mL m^{-3}) for this study site (Criales et al., 2004) by the volume of the domain to obtain mL of organism per cubic meter. Milliliters were converted to cubic meters and then multiplied by the density of zooplankton resulting in kilograms of particles (Eqn. 8). Particles were only injected at one time step so the calculated value served as the mass flow rate (kg s^{-1}) for particle injection into the domain.

$$1.13\frac{mL}{m^3} * 250000m^3 * \frac{1cm^3}{1\ mL} * \left(\frac{1\ m}{100\ cm}\right)^3 * 1000\frac{kg}{m^3} = 282.5\ kg \tag{9}$$

One study was performed close to our study area by oceanographers and biologists from Southeast Fisheries Science Center and University of Miami Rosenstiel School of Marine and Atmospheric Sciences (UM RSMAS). This project was known as SEFCAR and utilized a 1 m^2 and a 10 m^2 MOCNESS (Multiple Opening/Closing Net and Environmental Sampling System). They observed biomasses ranging from 0.05 to 1.5 mL m^{-3} (Criales et al., 2004) calculated from displacement volume (Beer, 1976). The same calculation as in equation 8 was made for data from this study (9).

$$1.5\frac{mL}{m^3} * 250000m^3 * \frac{1cm^3}{1\ mL} * \left(\frac{1\ m}{100\ cm}\right)^3 * 1000\frac{kg}{m^3} = 375\ kg \tag{10}$$

In a study performed by Kunze et al. (2006), a very high concentration of euphausiids was observed via acoustic measurements. They observed 10,000 organisms m^{-3}. The number of organisms was multiplied by the volume of the top 100 m of the domain to obtain the total number of organisms present. It was then multiplied by the organisms' density and by the volume of the particle (Eqn. 9). Particles were only injected at one time step, so this value can be taken as the mass flow rate (kg s^{-1}).

$$10000\frac{\#}{m^3} * 250000m^3 * 1000\frac{kg}{m^3} * 5.24 \times 10^{-7}m^3 = 1.31 \times 10^6\ kg \tag{11}$$

These calculations provided a range of possible mass flow rates to use for this simulation. DPM with differing mass flow rates were tested to determine what concentration of particles was needed to show an effect on turbulence signature and velocity profiles.

Injection type was set to standard, so a single parcel of particles was injected at each time step. The number of particles in the parcel, NP, was determined by

$$NP = m_s\frac{\Delta t}{m_p} \tag{12}$$

where NP is the number of particles in a parcel, m_s is the mass flow rate of the particle stream, Δt is the time step, and m_p is the particle mass. The spherical drag law was set to

approximate drag of the particles. The drag coefficient, C_D, for spherical particles is defined by

$$C_D = \alpha_1 + \frac{\alpha_2}{Re} + \frac{\alpha_3}{Re^2} \tag{13}$$

where α_1, α_2, and α_3 are constants over several ranges of Re (Morsi and Alexander, 1972).

The physics of the DPM is described by ordinary differential equations while continuous flow is expressed as partial differential equations. This means that the DPM has its own numerical mechanisms and discretization schemes. The trapezoidal scheme was chosen for the high order tracking scheme which uses a semi-implicit trapezoidal integration. The implicit scheme was chosen for the low order tracking scheme which uses Eulerian integration of

$$\frac{d\bar{u}_p}{dt} = F_D\left(\bar{u} - \bar{u}_p\right) + \frac{\bar{g}(\rho_p - \rho)}{\rho_p} + \bar{F} \tag{14}$$

where $\bar{F}$ is an additional acceleration term, $F_D\left(\bar{u} - \bar{u}_p\right)$ is the drag force per unit particle mass and

$$F_D = \frac{18\mu}{\rho_p d_p^2}\frac{C_D Re}{24} \tag{15}$$

where $\bar{u}$ is the fluid phase velocity, $\bar{u}_p$ is the particle velocity, μ is the molecular viscosity of the fluid, ρ is the fluid density, ρ_p is particle density, and $d_p$is the particle diameter. *Re* is the Reynolds number defined as

$$Re = \frac{\rho d_p |\bar{u}_p - \bar{u}|}{\mu} \tag{16}$$

When the particle reaches hydrodynamic equilibrium, the high order scheme is insufficient because the step length is limited. At this point Fluent switches to the stable lower order scheme and gives larger integration steps.

Initial conditions must be set for the DPM calculations to proceed. An injection was created and properties were assigned to it such as starting position, size, mass flow, and time of injection. Particles were set to a uniform in size of 1 cm diameter. Temperature of the particles was set to 290 K which was within the range of temperatures set by the user defined stratification profiles in both summer and winter cases. Particles were injected from a surface within the first time step of the model. Sunrise was simulated by injecting particles at the top boundary of the domain and sunset was simulated by injecting particles at 110 m depth near the bottom of thermocline. The particle type was set to inert so they obeyed the force balance (Eqns. 10 through 12).

When the DPM model was initiated, inert particles were created to inject at the selected surface. Water particles were created and then density was changed to approximate sinking or swimming behavior and renamed as zooplankton. Water density

was selected because zooplankton were assumed to be very similar to water for most properties. For sunrise, the zooplankton particles were set to a density of 1025 kg m^{-3} to sink through the water column. For sunset, they were set to 986 kg m^{-3} to float to the surface. Turbulent dispersion of particles due to turbulence in the fluid phase was predicted using the stochastic tracking model and activating the discrete random walk model, also called the eddy lifetime model. This model includes the effect of instantaneous turbulent velocity fluctuations on the particle trajectories and is written as

$$u = \bar{u} + u' \tag{17}$$

Next, boundary conditions for the DPM were set at each boundary. This determined the fate of the trajectory of the particles. For sunrise cases, the DPM boundary condition at the top and side boundaries were set to reflect particles and the bottom boundary was set to allow the particles to escape. For sunset cases the top boundary was set to allow particles to escape and the bottom and side boundaries were set to reflect particles back into the domain. The inlet was set to a periodic boundary so particles flowed out one side of the model and back into the other side with the fluid flow. The escape boundary condition allowed particles to leave the domain when they hit a wall. The reflect boundary condition caused the particles to bounce off the wall retaining the same momentum as before the collision and remain in the domain.

Analysis of average velocity profiles and turbulence signatures from model results was conducted by exporting data from the model. For each model run, factors were exported over the entire water column in an ASCII format to be processed in Matlab. A Matlab script was developed to observe average profiles of velocity in the x-direction and subgrid turbulent viscosity for particles versus no particles cases. Contour plots for subgrid turbulent viscosity were taken directly from ANSYS Fluent and images of particle locations were processed using CFD-post, an ANSYS post-processing tool.

4 RESULTS

4.1 Observational Data

4.1.1 Backscatter

4.1.1.1 Velocity Contours

A contour plot of the ADCP northward current velocity taken during the Dania Beach data set in spring is shown in Figure 4-1. This image clearly shows the presence of the strong western boundary current, the Florida Current and its meanders offshore. Warm colors near the surface indicate the Florida Current was present directly above the bottom mounted ADCP instrument with a top speed of approximately 2 m s^{-1}. Cooler colors near the surface indicate the Florida Current had meandered offshore. The Florida

Current did not reach the bottom at this location at any time. It ranged from the surface to approximately 140 m deep and weakened with depth. Meandering of the Florida Current has been documented in many studies (Niiler, 1968; Soloviev et al., 2003).

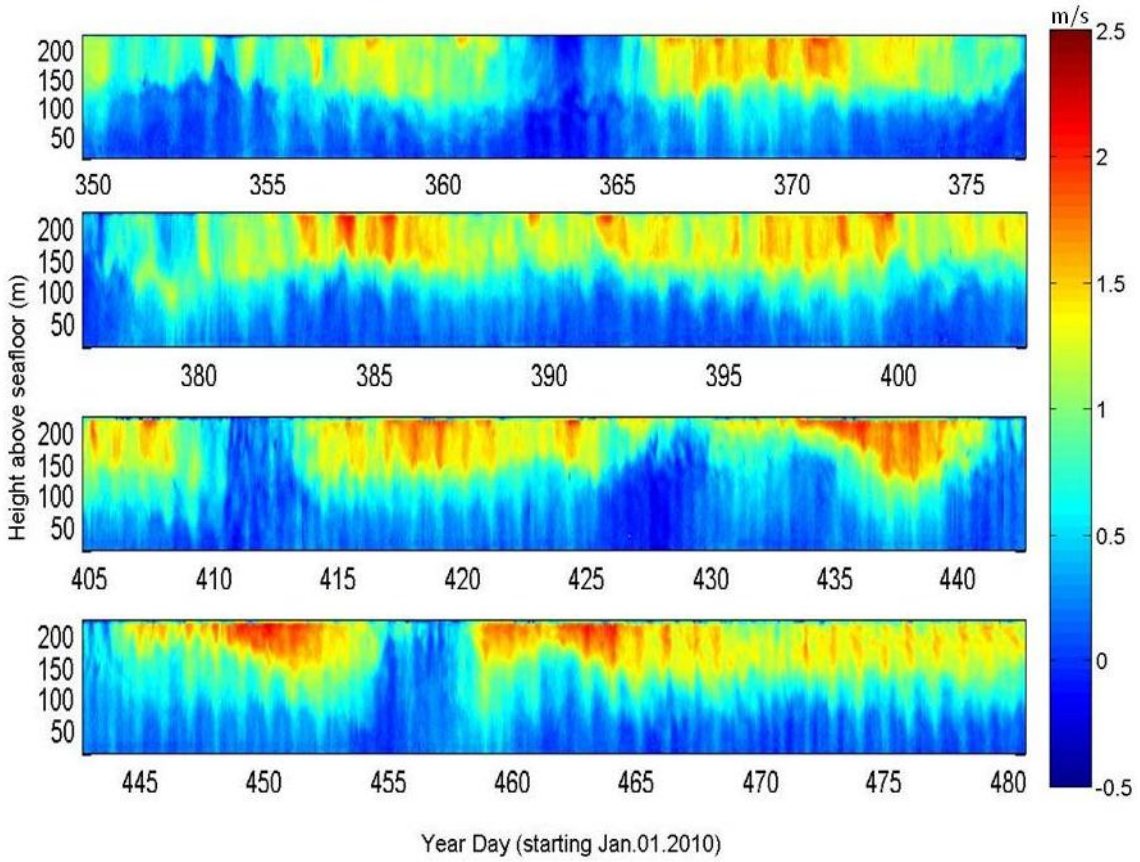

Figure 4-1. Northward current velocity contour plot. Dania Beach spring data set February 9, 2011 to April, 26, 2011

4.1.1.2 Dania Beach

A contour plot of the ADCP backscatter averaged over all four beams is shown in Figures 4-2 through 4-5, separated by season. Part a) of these plots shows the contour plot of backscatter directly as recorded by the instrument. A periodic pattern in the backscatter with higher values in the surface water followed by higher values in mid-depths appeared throughout most of the data set, suggesting the presence of a DVM cycle. To observe if this was DVM, part b) shows the same plot with sunrise indicated by a solid white line, sunset set as a dashed white line, new moon as a solid black line, and full moon as a dashed black line. The sunset and sunrise times clearly coincided with the dramatic changes in backscatter in the surface layers. DVM patterns due to lunar cycle, however, were not analyzed for this thesis.

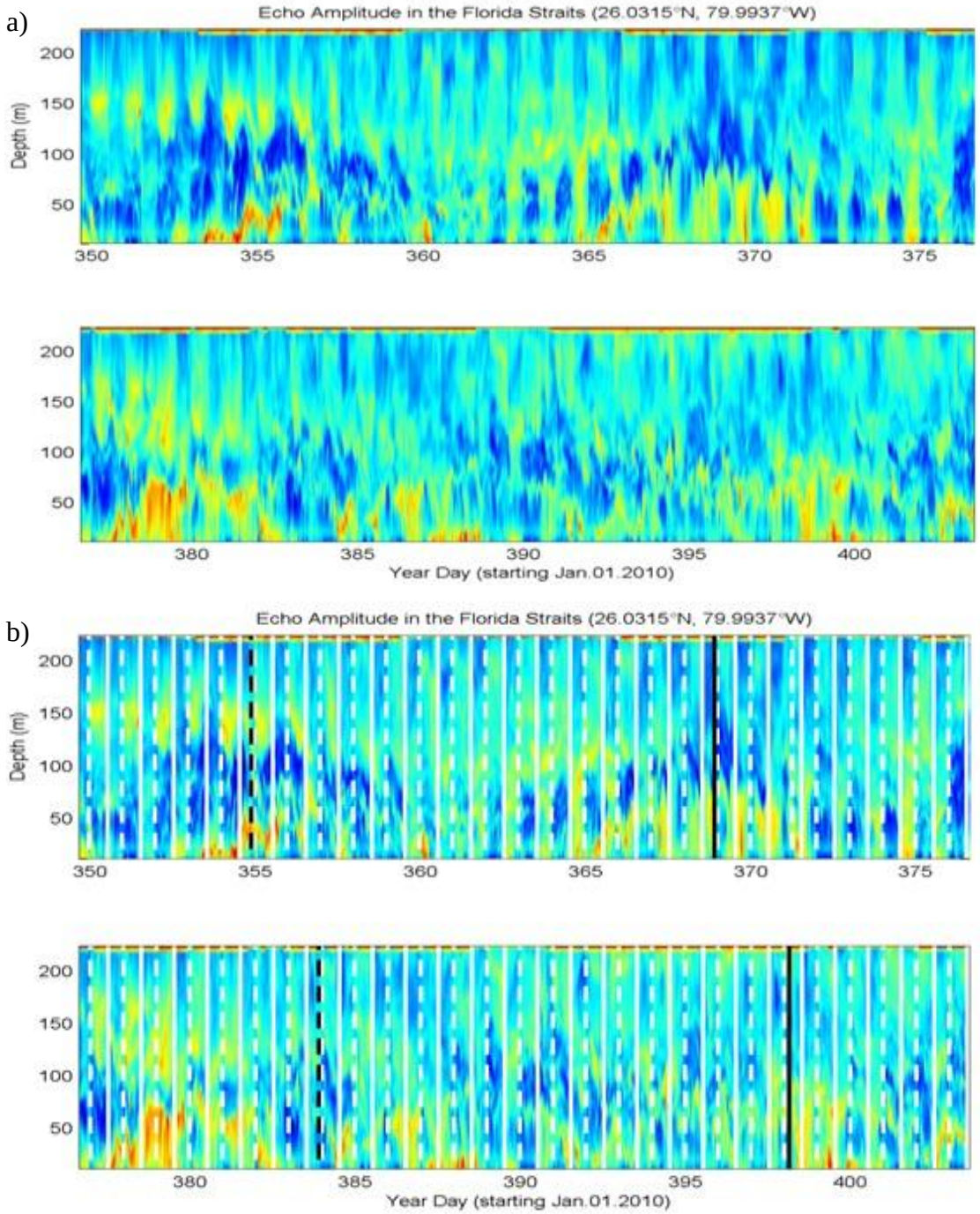

Figure 4-2. a) Beam averaged backscatter from bottom mounted ADCP on Dania Beach (26.0315°N, 79.9937°W) during winter months (December 16, 2010 at 11:00 through February 8, 2011 at 7:20).b) Sunrise indicated by a solid white line, sunset by a dashed white line, new moon by a solid black line and full moon by a dashed black line.

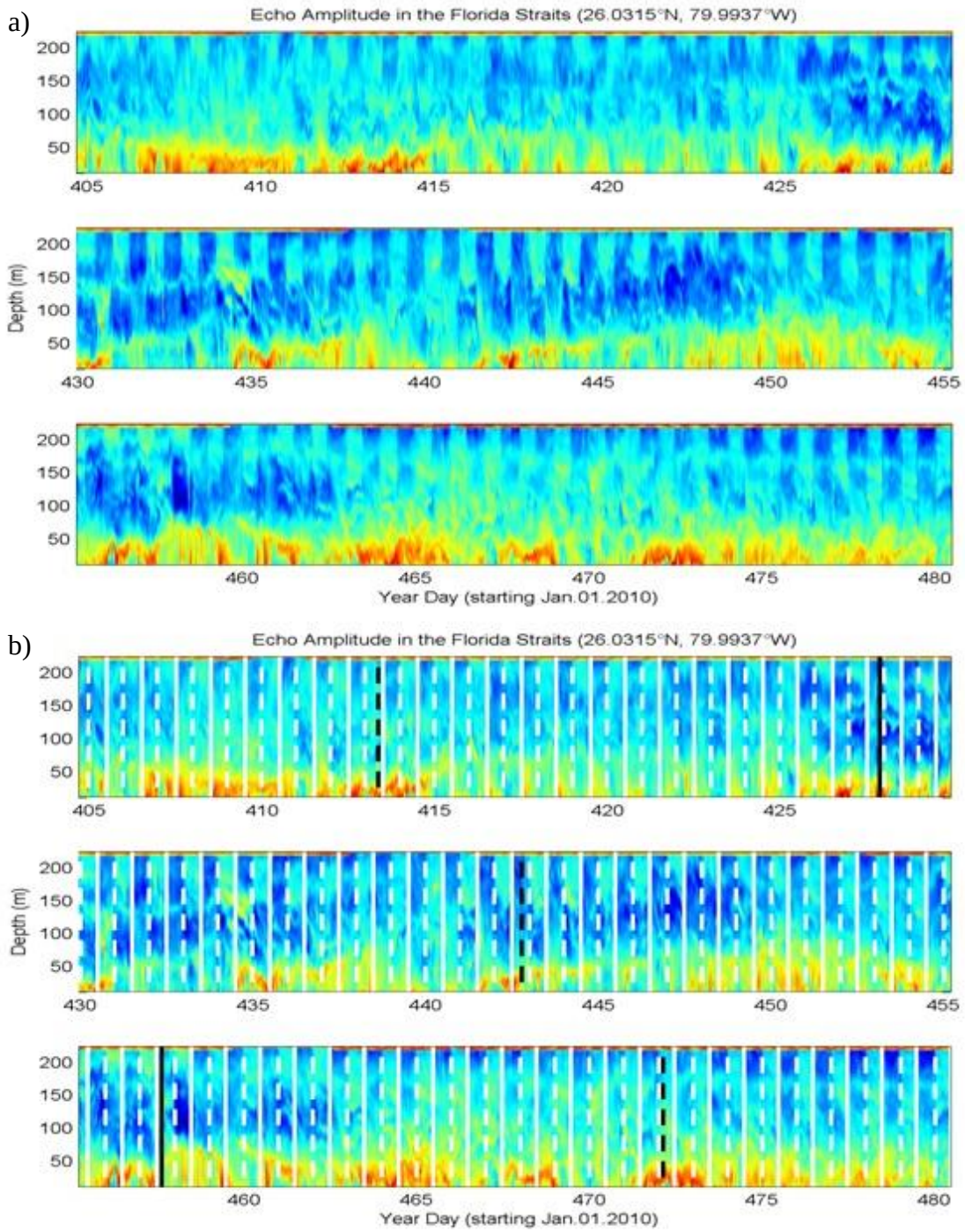

Figure 4-3. a) Beam averaged backscatter from bottom mounted ADCP on Dania Beach (26.0315°N, 79.9937°W) during spring months (February 9, 2011 at 11:00 through April, 26 2011 at 14:30). b) Sunrise times indicated by a solid white line, sunset by a dashed white line, new moon by a solid black line and full moon by a dashed black line.

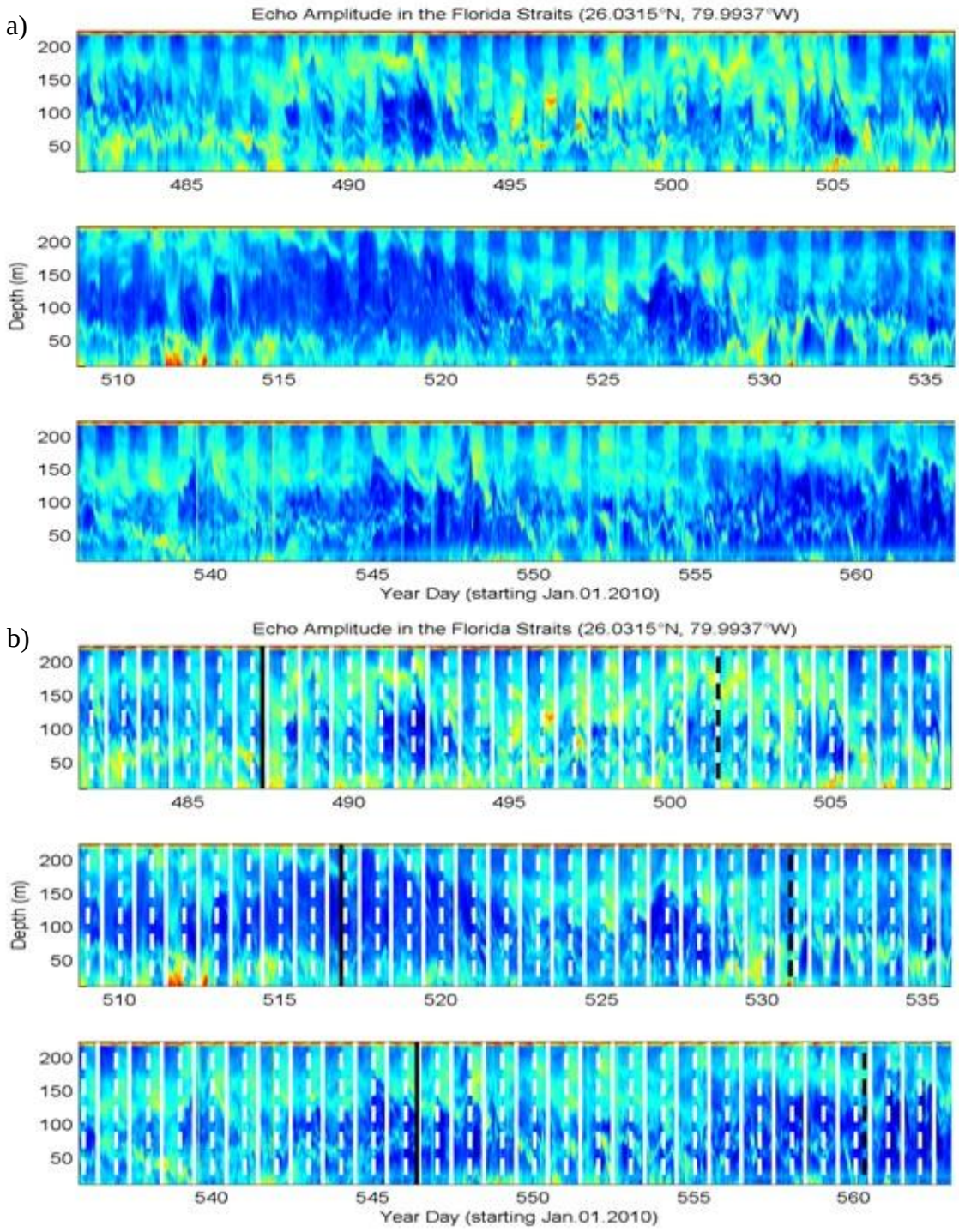

Figure 4-4. A) Beam averaged backscatter from bottom mounted ADCP on Dania Beach (26.0315°N, 79.9937°W) during summer months (April 27, 2011 at 13:00 through July 15, 2011 at 23:45). B) Sunrise times indicated by a solid white line, sunset by a dashed white line, new moon by a solid black line and full moon by a dashed black line.

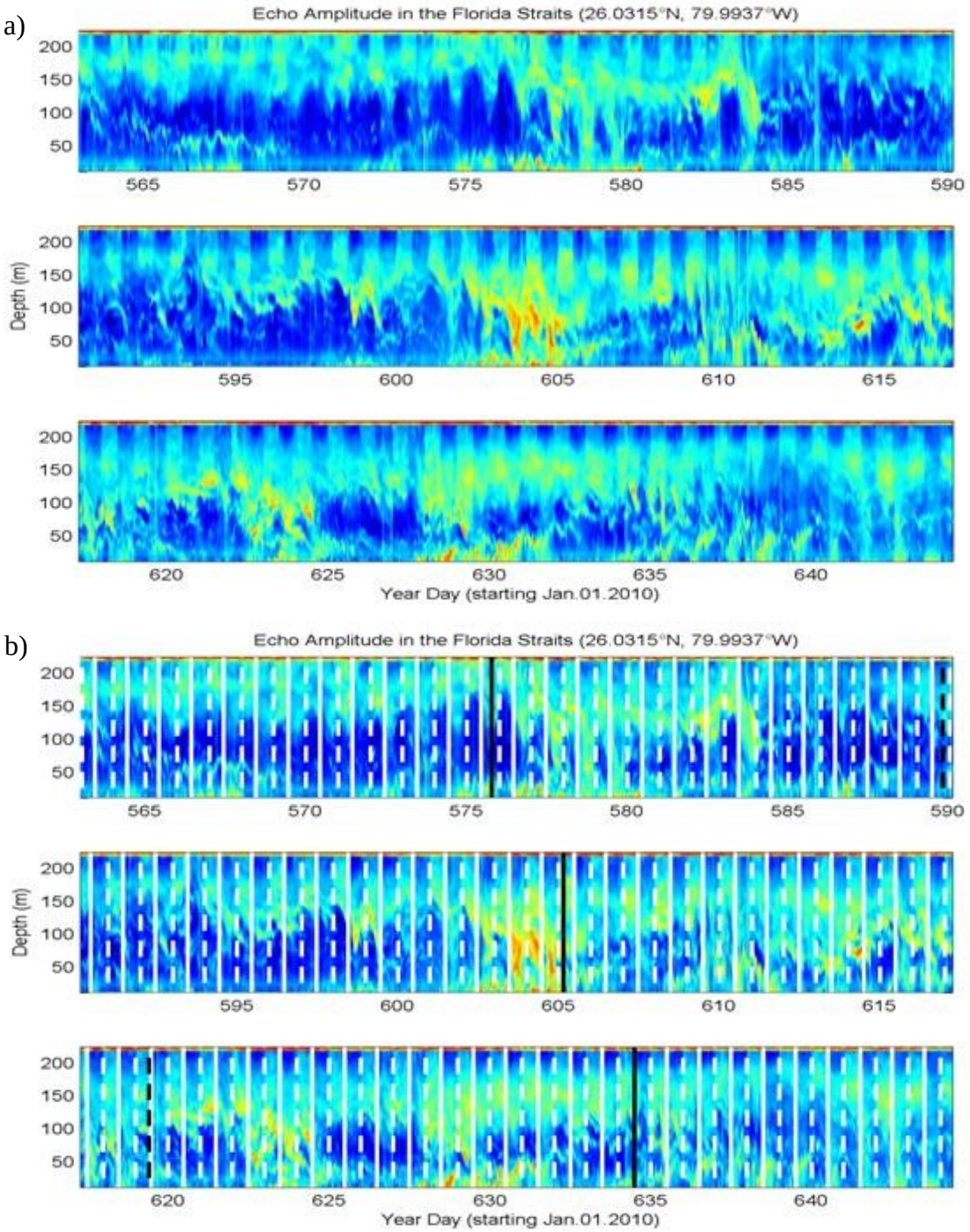

Figure 4-5. a) Beam averaged backscatter from bottom mounted ADCP on Dania Beach (26.0315°N, 79.9937°W) during summer months (July 16, 2011 at 000 through October 11, 2011 at 17:50). b) Sunrise times indicated by a solid white line, sunset by a dashed white line, new moon by a solid black line and full moon by a dashed black line.

4.1.1.3 Pompano

Contour plots of averaged ADCP backscatter from the Pompano four year data sets are shown in Figures 4-6 through 4-17. As with the Dania Beach data set, sunrise times are indicated with a solid white line, sunset times are indicated with a dashed white line, new moon is shown in a solid black line, and full moon is shown with a dashed black line. The same periodicity that was present in the Dania Beach data set appeared to be present the majority of the time in the longer Pompano data set. There was typically a larger concentration of particles, indicated by stronger backscatter, in the surface waters just after sunset which moved back to depth after sunrise. This pattern was expected from DVM. Again, the lunar cycle was not researched further during this study.

4.1.2 Zooplankton Swimming Speeds

Focusing on sunrise and sunset times on the backscatter contour allowed estimation of the rate at which the scatterers moved toward or away from the surface layers. Many cases showed two distinct rates during sunrise but sunset only showed one slope. In the case shown in Figure 4-18, the downward swimming speed at sunrise was initially 4.3 cm s^{-1} and then dropped off to 2.5 cm s^{-1} which was comparable with Kunze et al. (2006) who showed average ascent speeds of 2.5 to 3.5 cm s^{-1} in Saanich Inlet, British Colombia, Canada. At sunset the approximate swim speed was 2.6 cm s^{-1}. Backscatter was averaged at sunrise and sunset times over the course of each season to obtain an average zooplankton swim speed. During the winter season average swimming speed at sunrise was 1.05 cm s^{-1} and at sunset was 0.85 cm s^{-1} (Fig. 4-19). For spring, sunrise had two separate slopes. Initially the decent rate was 2.22 cm s^{-1} for and after approximately 20 minutes, slowed to 0.79 cm s^{-1}. The ascent rate at sunset was 1.28 cm s^{-1} (Fig. 4-20). During summer, the scatterers did not appear to migrate down as far in the water column as during the other seasons. The average sunrise speed was 0.76 cm s^{-1} and sunset was 0.60 cm s^{-1} (Fig. 4-12). Swimming speed was averaged over the full 11 month data set. The average sunrise speed was 1.52 cm s^{-1} and average sunset speed was 0.79 cm s^{-1} (Fig. 4-22). These swim velocities are summarized in Table 4-1.

Table 4-1. Average zooplankton swimming speeds calculated from slope of backscatter

Average Zooplankton Swim Speeds		
	Sunrise	Sunset
Winter	1.05	0.85
Spring	2.22 – 0.79	1.28
Summer	0.76	0.60
All	1.52	0.79

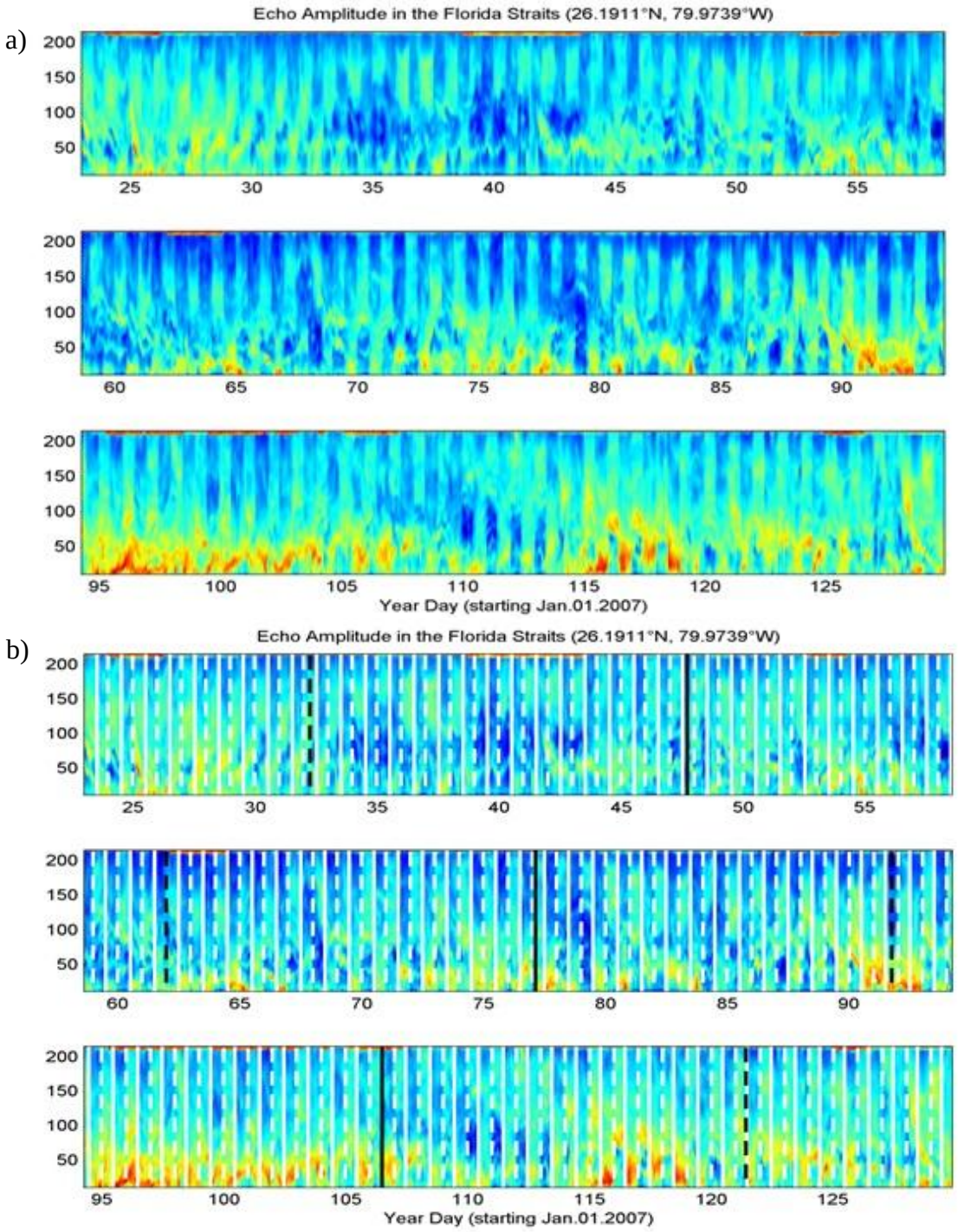

Figure 4-6. a) Beam averaged backscatter from bottom mounted ADCP at Pompano (26.1911°N, 79.9739°W) January 23, 2007 at 23:00 GMT to May 8, 2007 at 21:00 GMT. b) Sunrise times indicated by a solid white line, sunset by a dashed white line, new moon by a solid black line and full moon by a dashed black line.

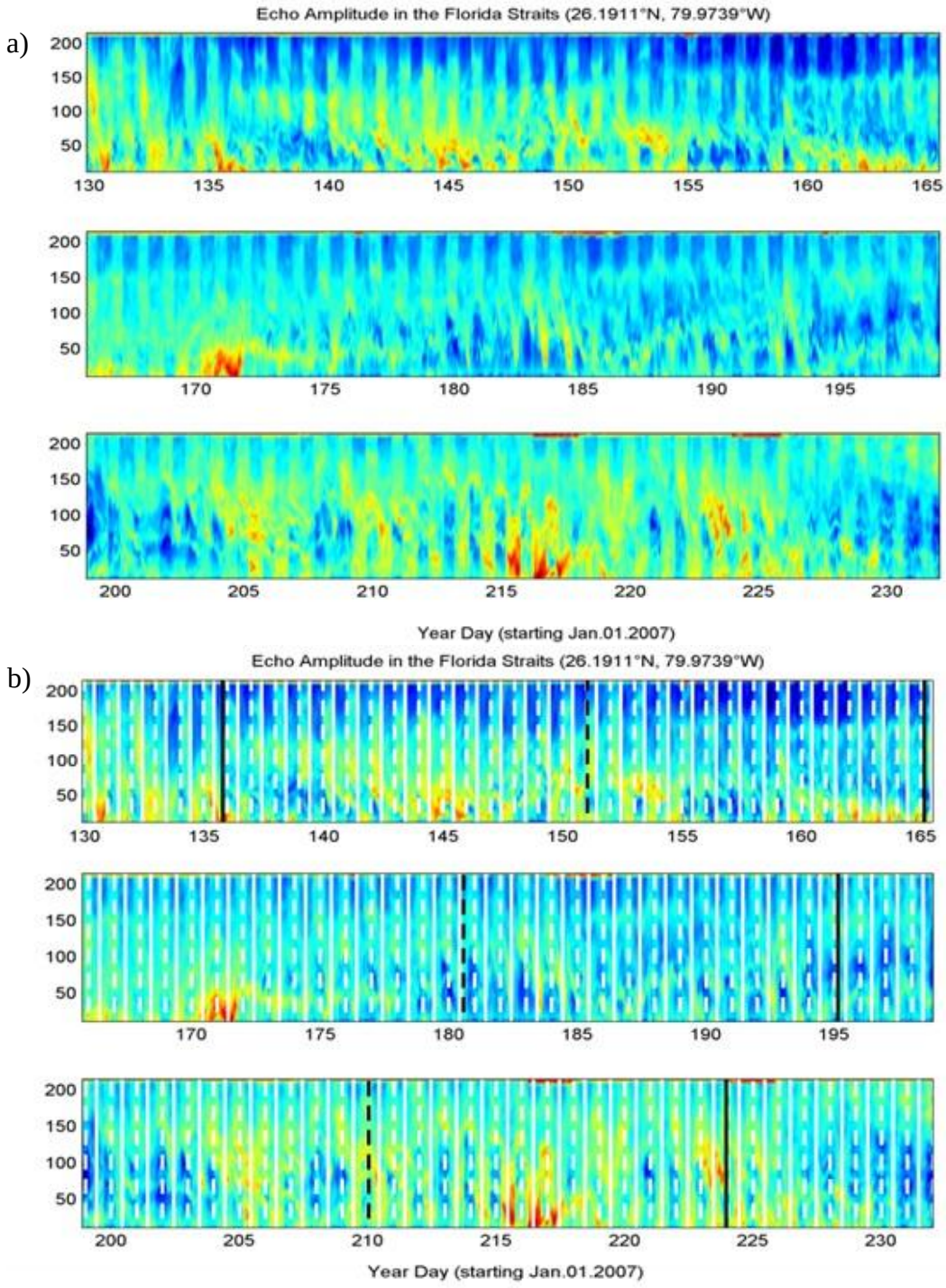

Figure 4-7. a) Beam averaged backscatter from bottom mounted ADCP at Pompano (26.1911°N, 79.9739°W) May 8, 2007 at 22:00 GMT to August 19, 2007 at 0:00 GMT. b) Sunrise times indicated by a solid white line, sunset by a dashed white line, new moon by a solid black line and full moon by a dashed black line.

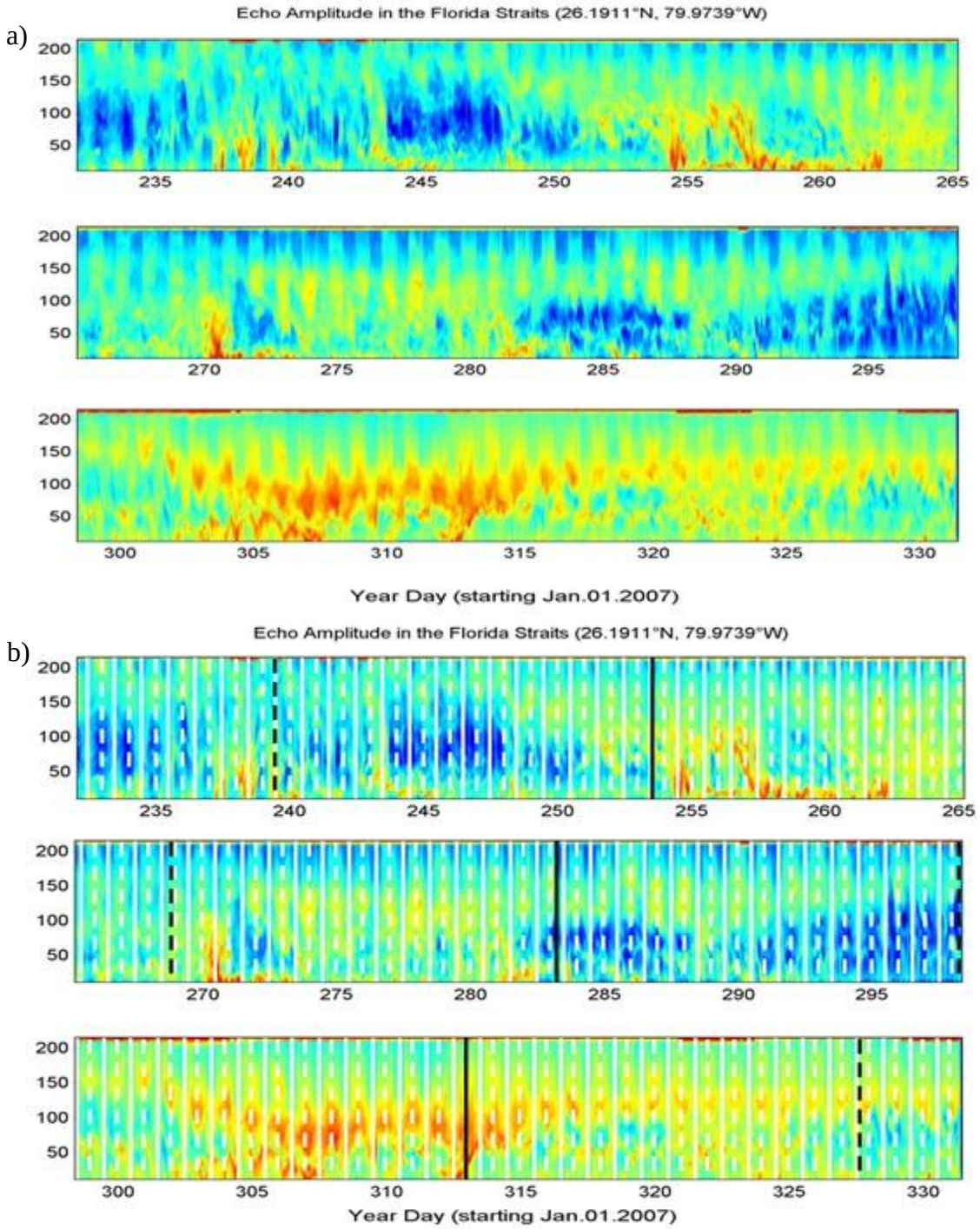

Figure 4-8. a) Beam averaged backscatter from bottom mounted ADCP at Pompano (26.1911°N, 79.9739°W) August 19, 2007 at 1:00 GMT to November 26, 2007 at 10:00 GMT. b) Sunrise times indicated by a solid white line, sunset by a dashed white line, new moon by a solid black line and full moon by a dashed black line.

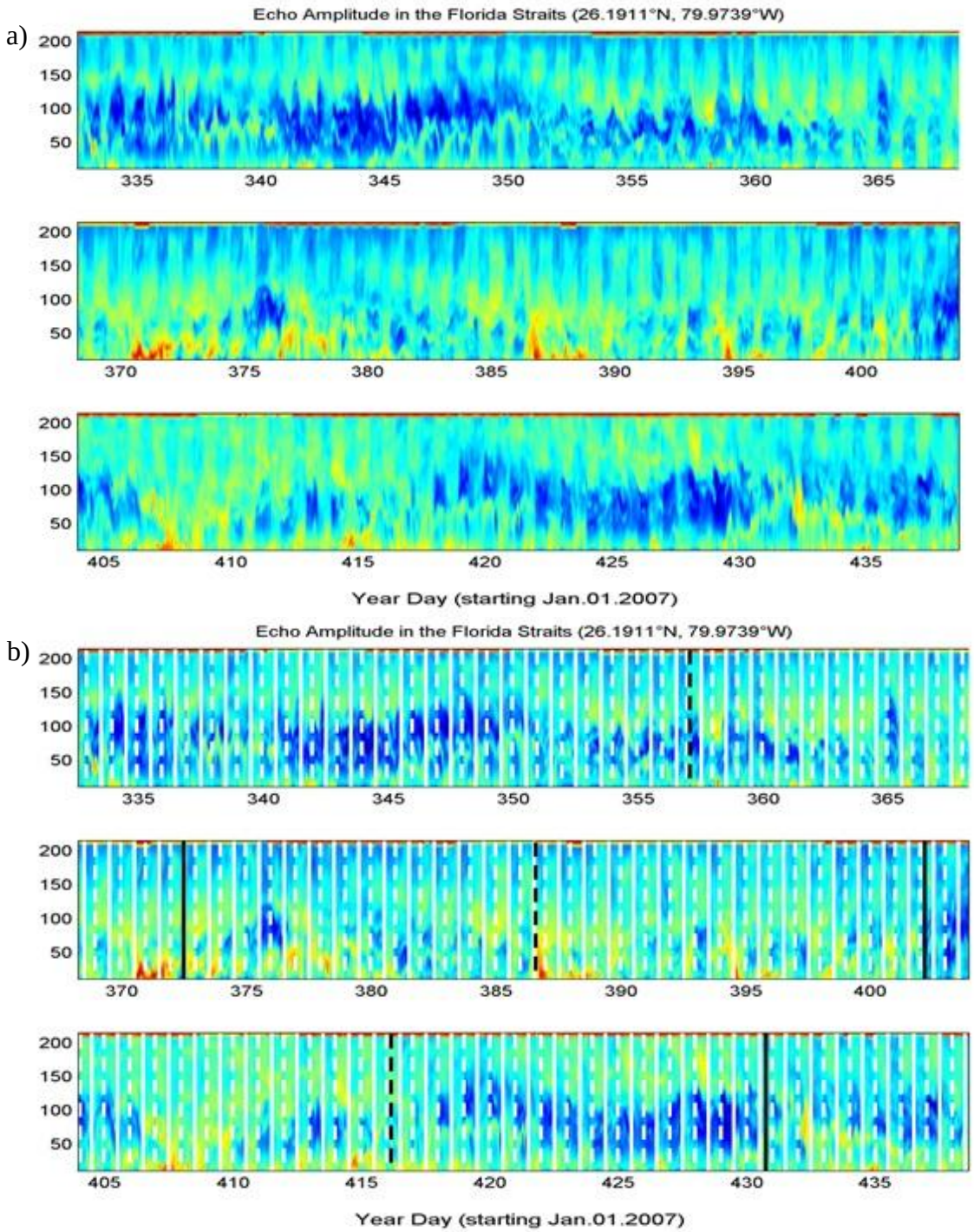

Figure 4-9. a) Beam averaged backscatter from bottom mounted ADCP at Pompano (26.1911°N, 79.9739°W) November 26, 2007 at 11:00 GMT to March 13, 2008 at 15:00 GMT. b) Sunrise times indicated by a solid white line, sunset by a dashed white line, new moon by a solid black line and full moon by a dashed black line.

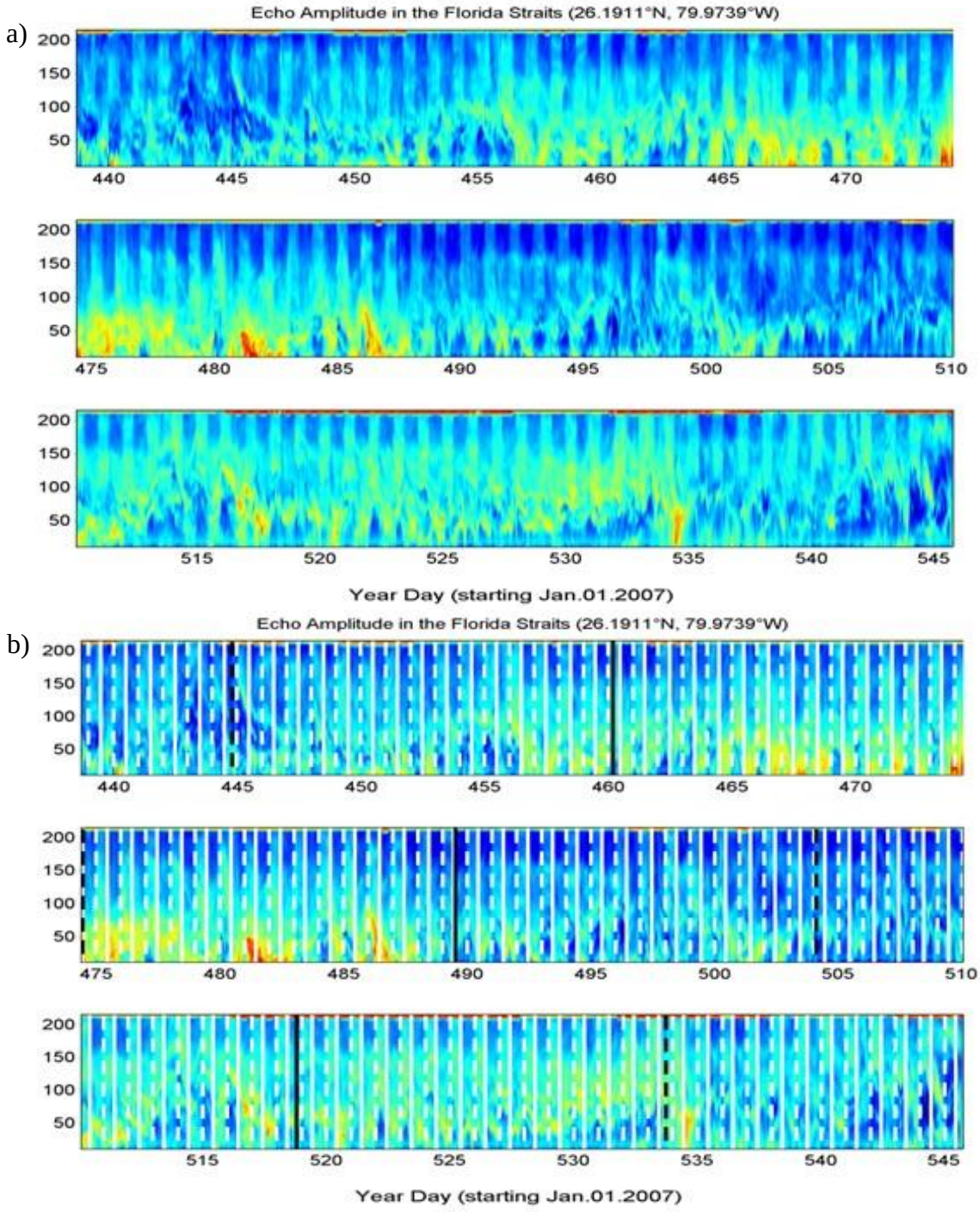

Figure 4-10. a) Beam averaged backscatter from bottom mounted ADCP at Pompano (26.1911°N, 79.9739°W) March 13, 2008 at 16:00GMT to June 28, 2008 at 18:00 GMT. b) Sunrise times indicated by a solid white line, sunset by a dashed white line, new moon by a solid black line and full moon by a dashed black line.

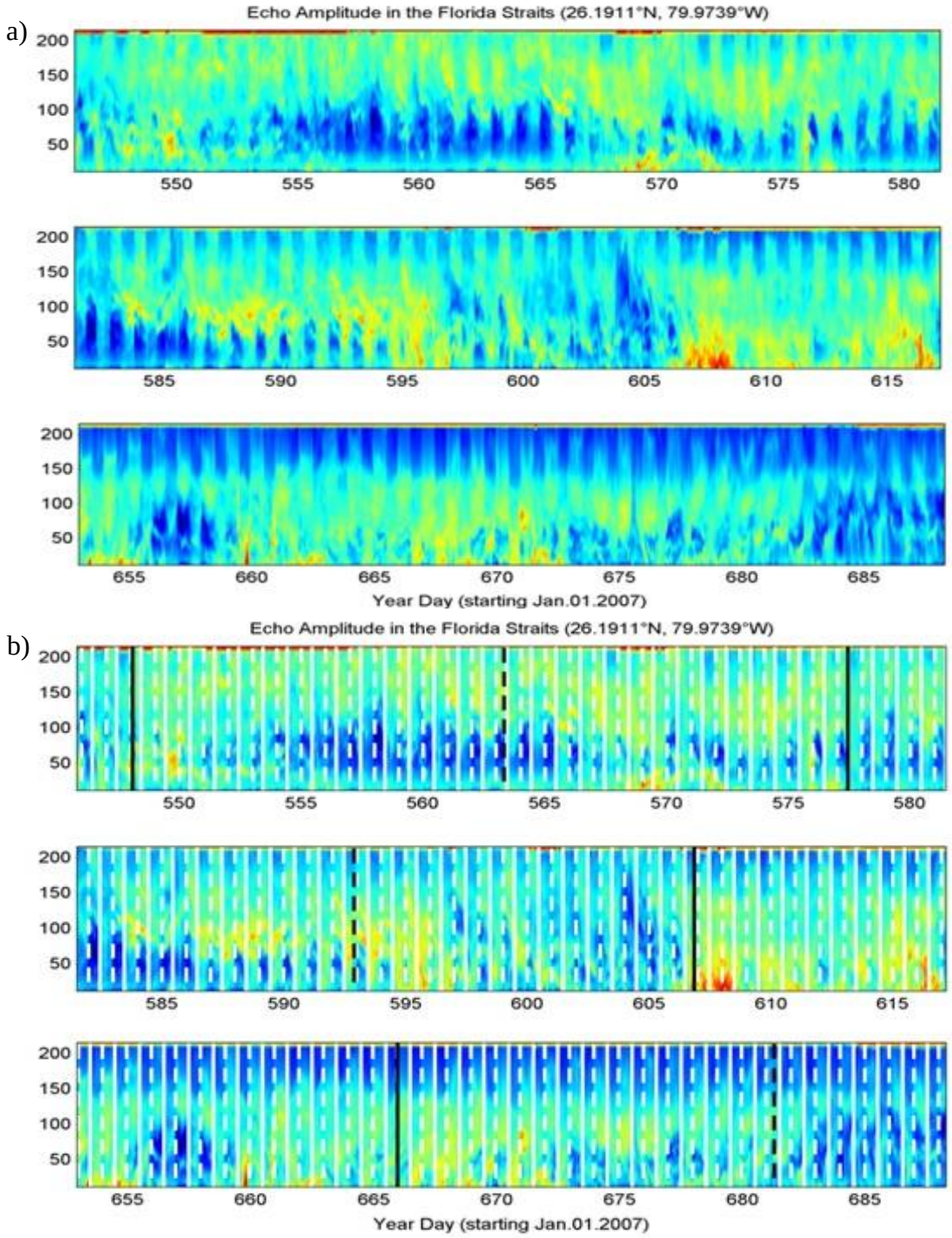

Figure 4-11. a) Beam averaged backscatter from bottom mounted ADCP at Pompano (26.1911°N, 79.9739°W) June 28, 2008 at 19:00 GMT to November 18, 2008 at 6:00 GMT. b) Sunrise times indicated by a solid white line, sunset by a dashed white line, new moon by a solid black line and full moon by a dashed black line.

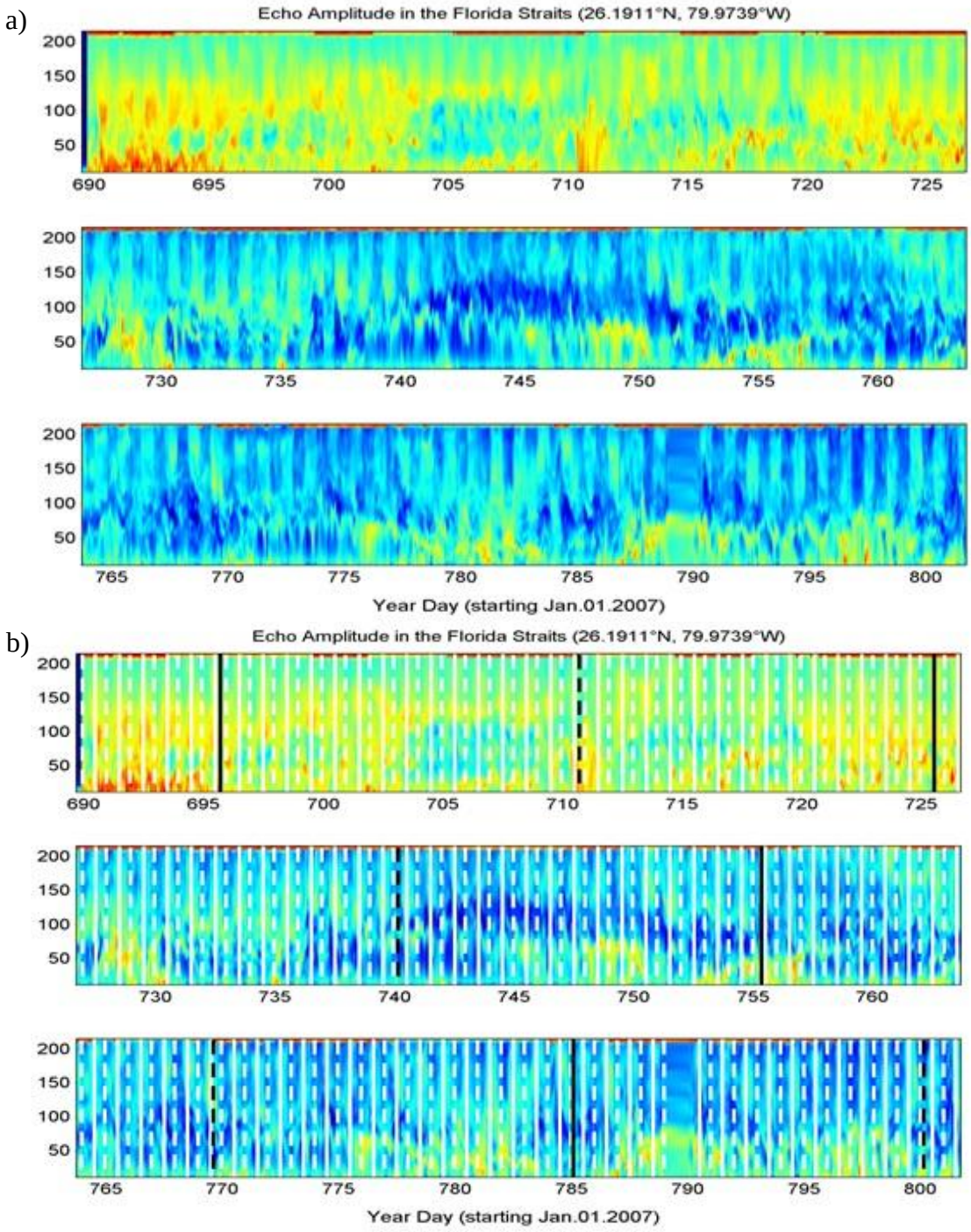

Figure 4-12. a) Beam averaged backscatter from bottom mounted ADCP at Pompano (26.1911°N, 79.9739°W) November 18, 2008 at 7:00 GMT to March 11, 2009 at 17:00 GMT. b) Sunrise times indicated by a solid white line, sunset by a dashed white line, new moon by a solid black line and full moon by a dashed black line.

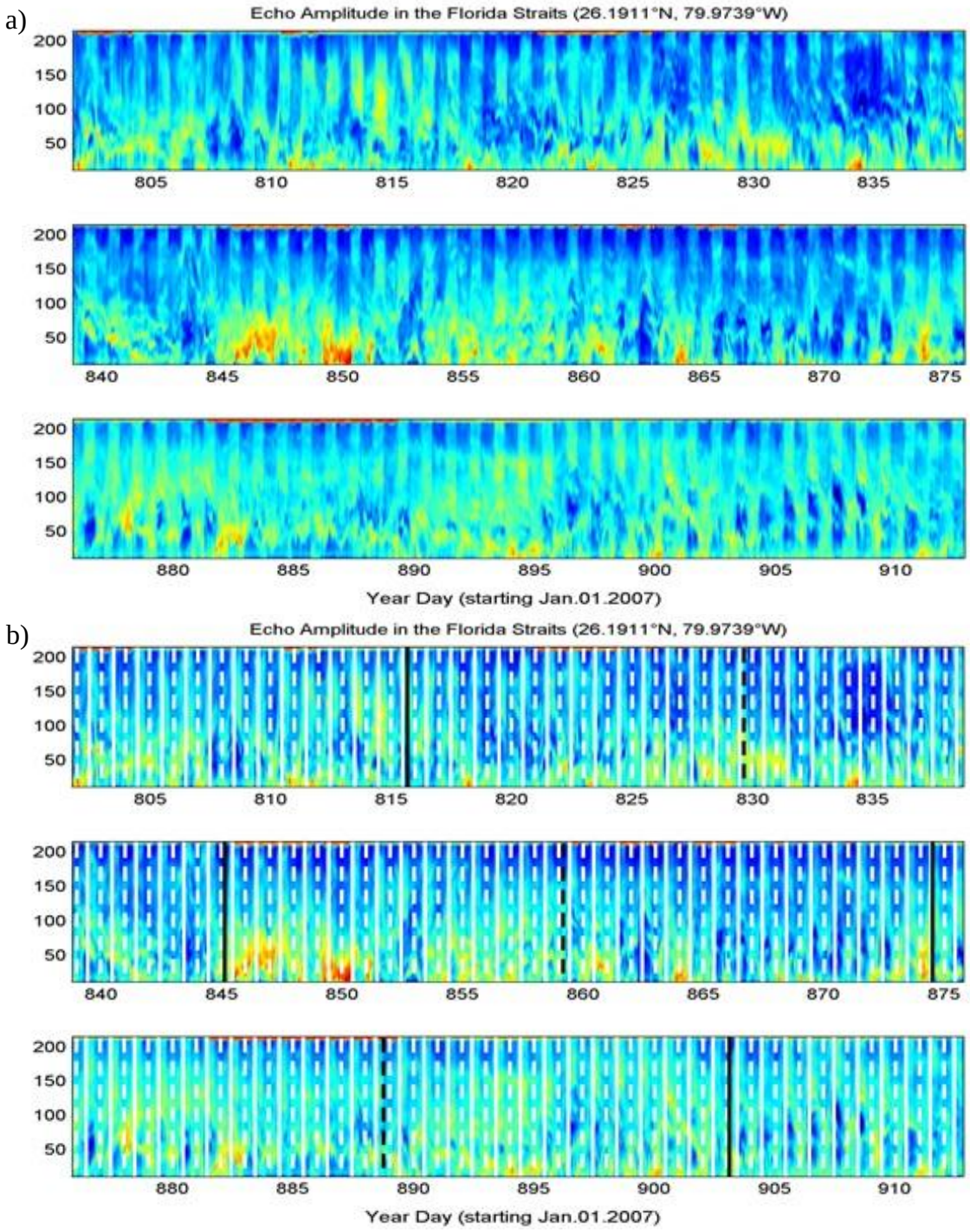

Figure 4-13.a) Beam averaged backscatter from bottom mounted ADCP at Pompano (26.1911°N, 79.9739°W) March 11, 2009 at 18:00 GMT to June 30, 2009 at 20:00 GMT. b) Sunrise times indicated a solid white line, sunset by a dashed white line, new moon by a solid black line and full moon by a dashed black line.

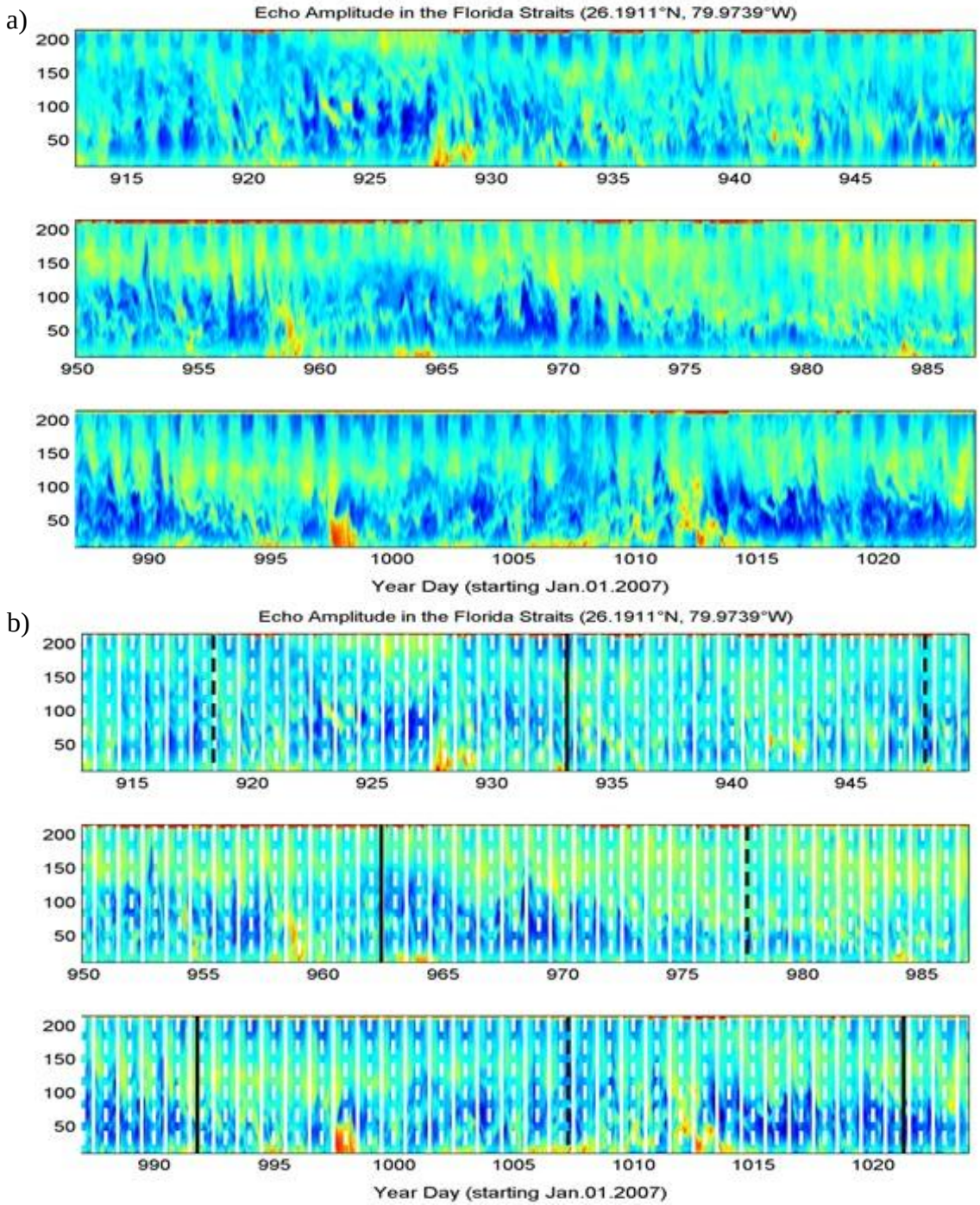

Figure 4-14. a) Beam averaged backscatter from bottom mounted ADCP at Pompano (26.1911°N, 79.9739°W) June 30, 2009 at 21:00 GMT to October 19, 2009 at 23:00 GMT. b) Sunrise times indicated by a solid white line, sunset by a dashed white line, new moon by a solid black line and full moon byn a dashed black line.

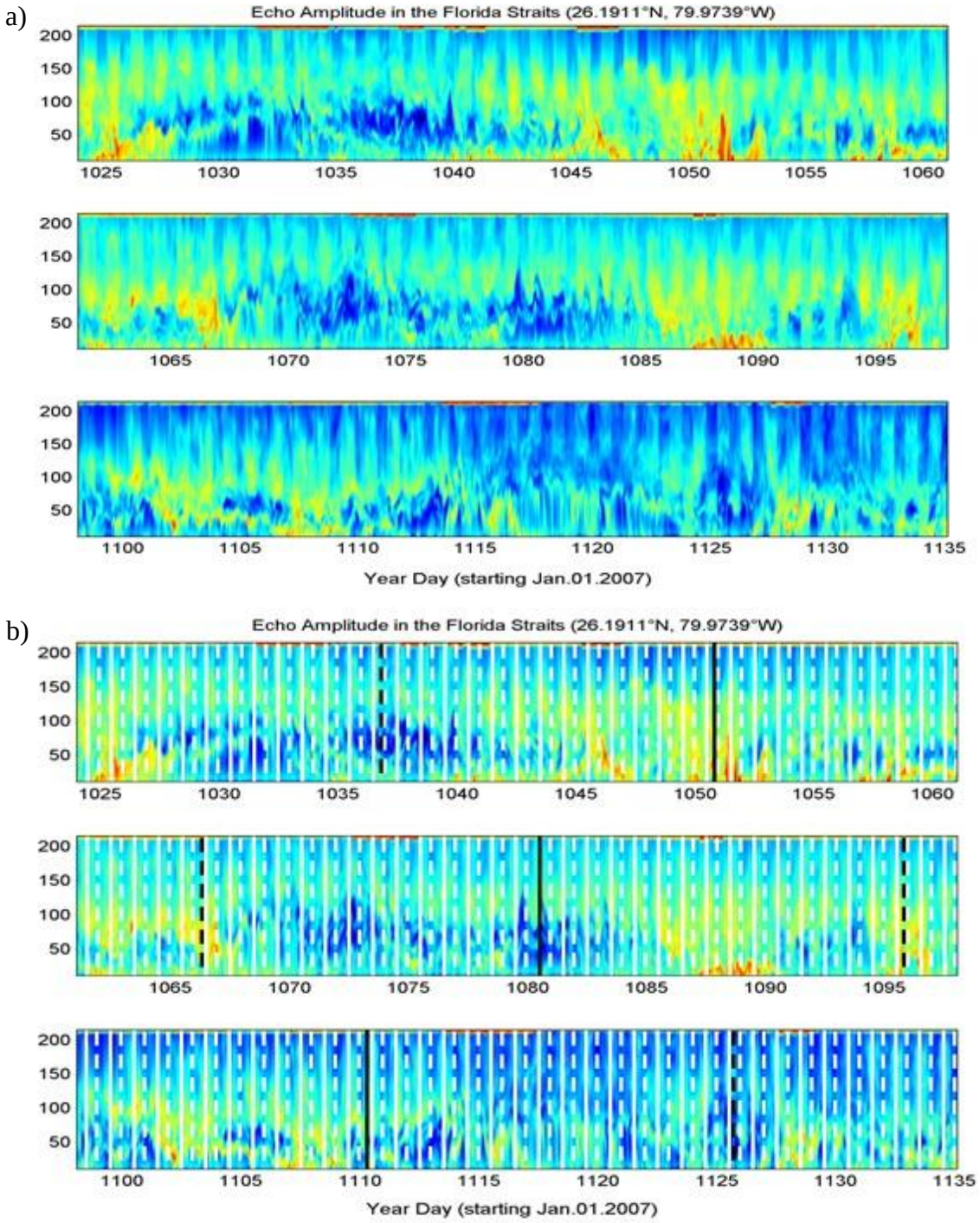

Figure 4-15. a) Beam averaged backscatter from bottom mounted ADCP at Pompano (26.1911°N, 79.9739°W) October 20, 2009 at 0:00 GMT to February 8, 2010 at 2:00 GMT. b) Sunrise times indicated by a solid white line, sunset by a dashed white line, new moon by a solid black line and full moon by a dashed black line.

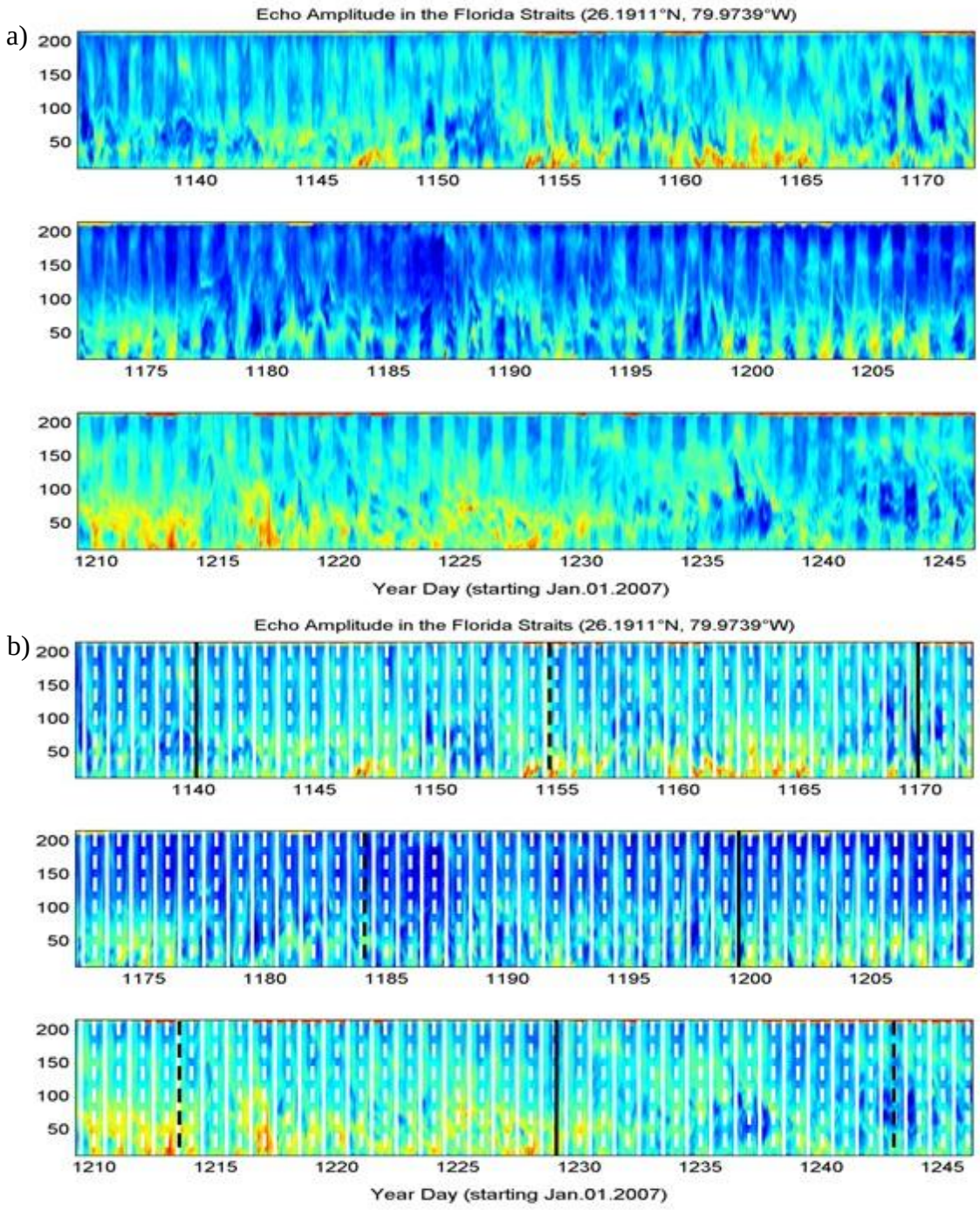

Figure 4-16. a) Beam averaged backscatter from bottom mounted ADCP at Pompano (26.1911°N, 79.9739°W) February 8, 2010 at 3:00 GMT to May 30, 2010 at 5:00 GMT. b) Sunrise times indicated by a solid white line, sunset by a dashed white line, new moon by a solid black line and full moon by a dashed black line.

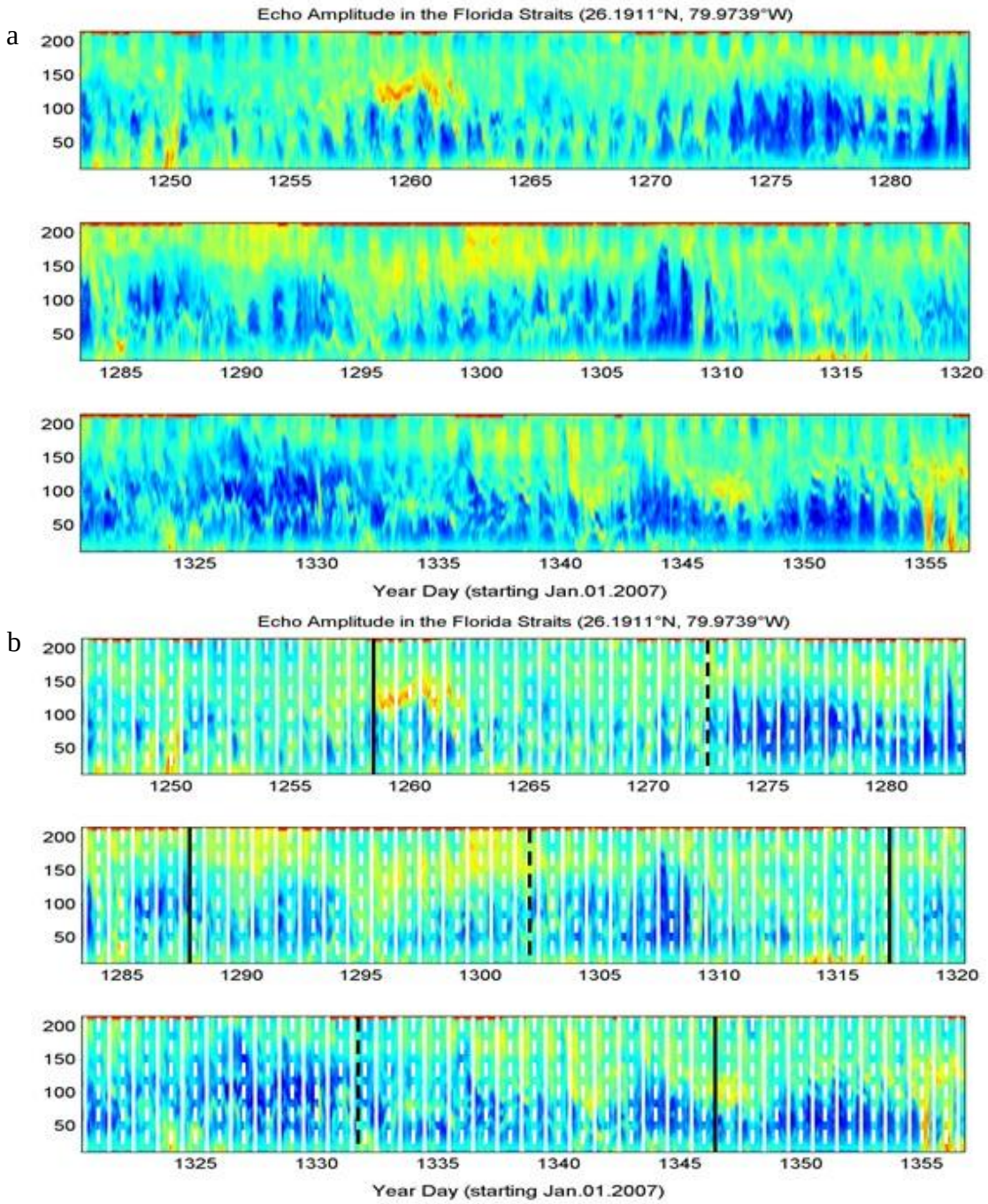

Figure 4-17. a) Beam averaged backscatter from bottom mounted ADCP at Pompano (26.1911°N, 79.9739°W) May 30, 2010 at 6:00 GMT to September 17, 2010 at 18:00 GMT. b) Sunrise times indicated by a solid white line, sunset by a dashed white line, new moon by a solid black line and full moon by a dashed black line.

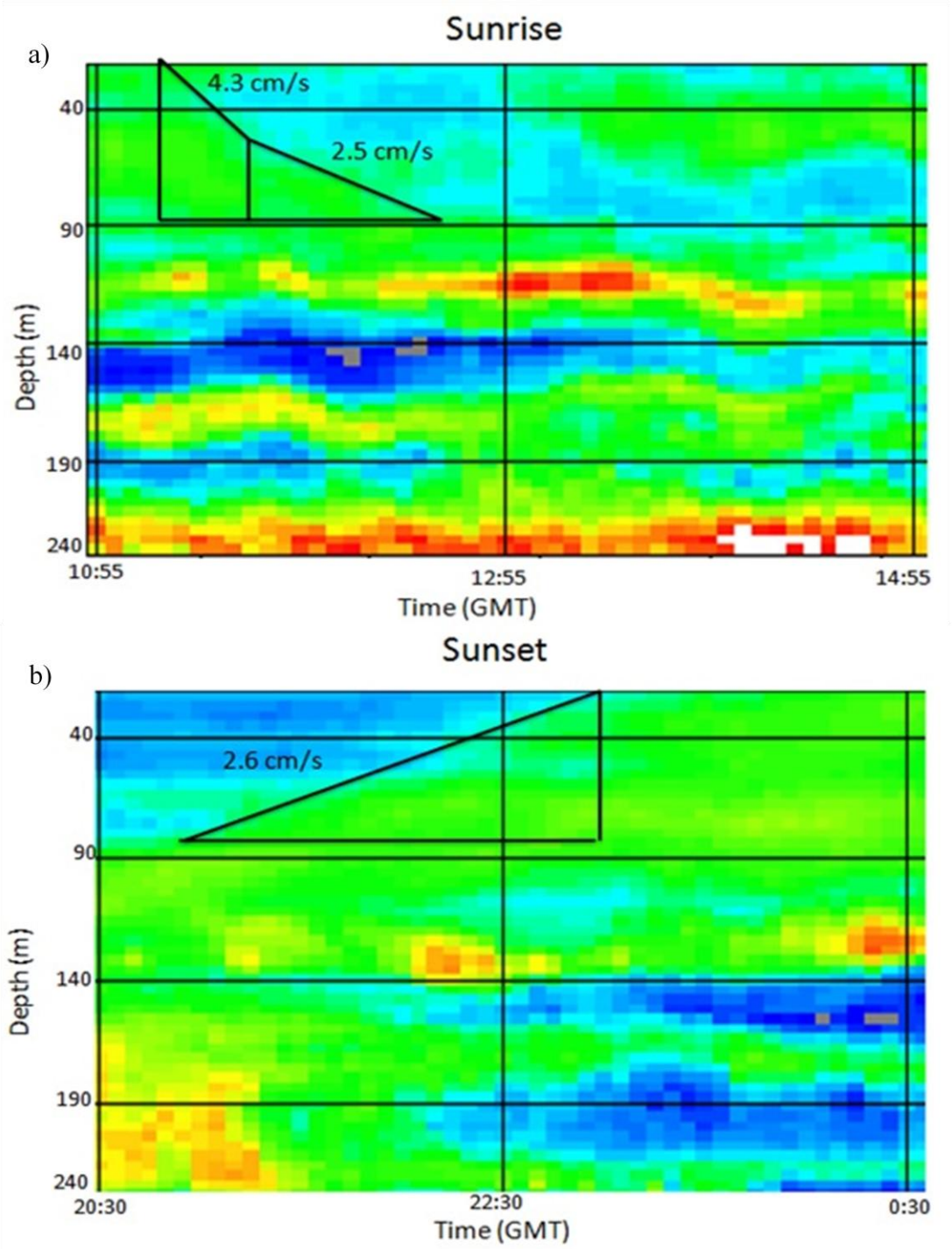

Figure 4-18. Swimming vertical velocity of zooplankton calculated using acoustic (ADCP) backscatter signal in a sunrise and a sunset case. This case showed two different zooplankton velocities (depending on depth) during sunrise while sunset only showed one. Horizontal line of the triangle depicts the length of time that migration occurred, vertical lines indicate depth of migration. Slope formula was used to determine velocity.

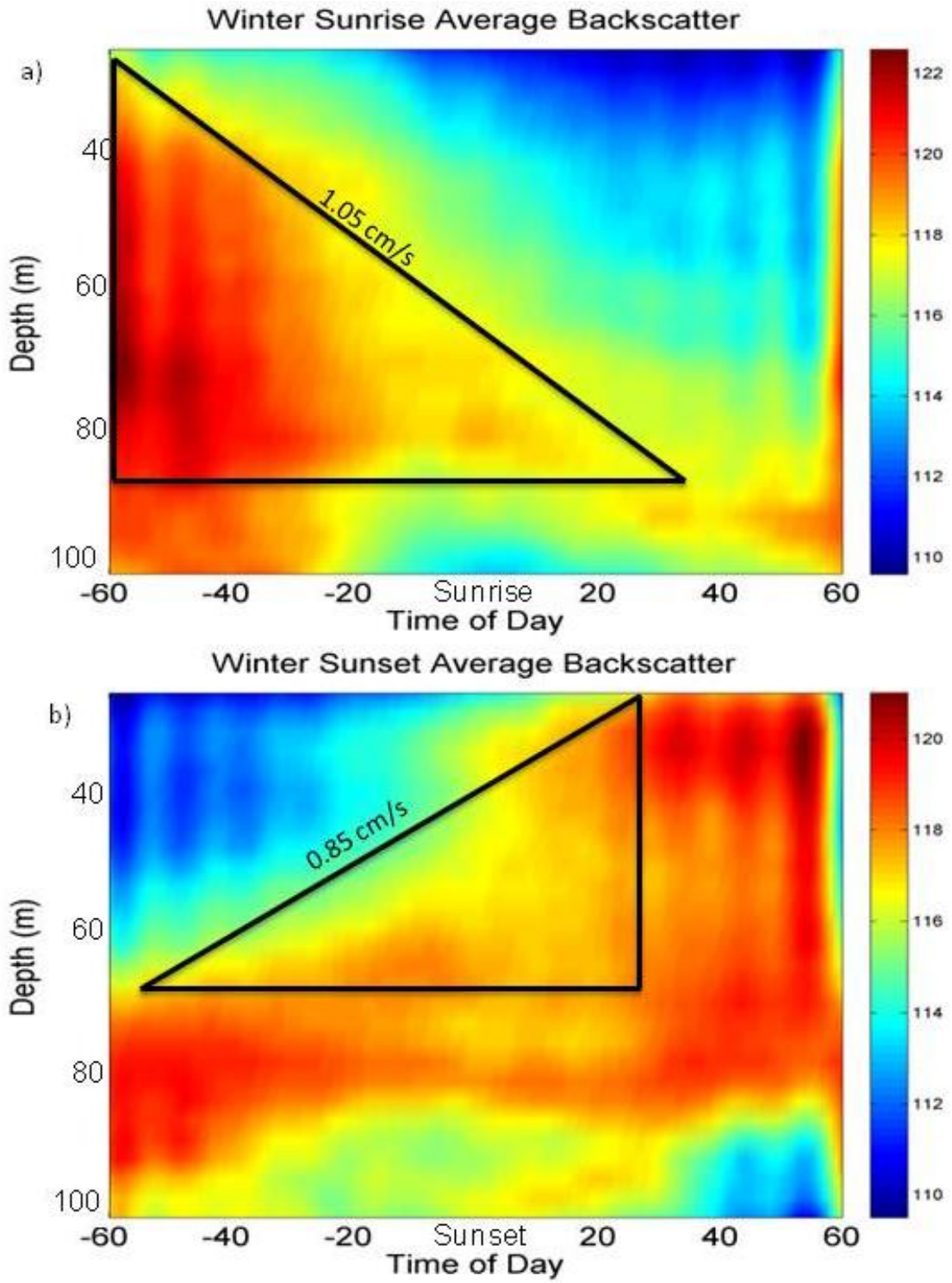

Figure 4-19. Averaged winter zooplankton swim speeds during a) sunrise and b) sunset conditions calculated from ADCP backscatter from winter months (December 16, 2010 to February 8, 2011). Horizontal line of the triangle depicts the length of time that migration occurred, vertical lines indicate depth of migration. Slope formula was used to determine velocity.

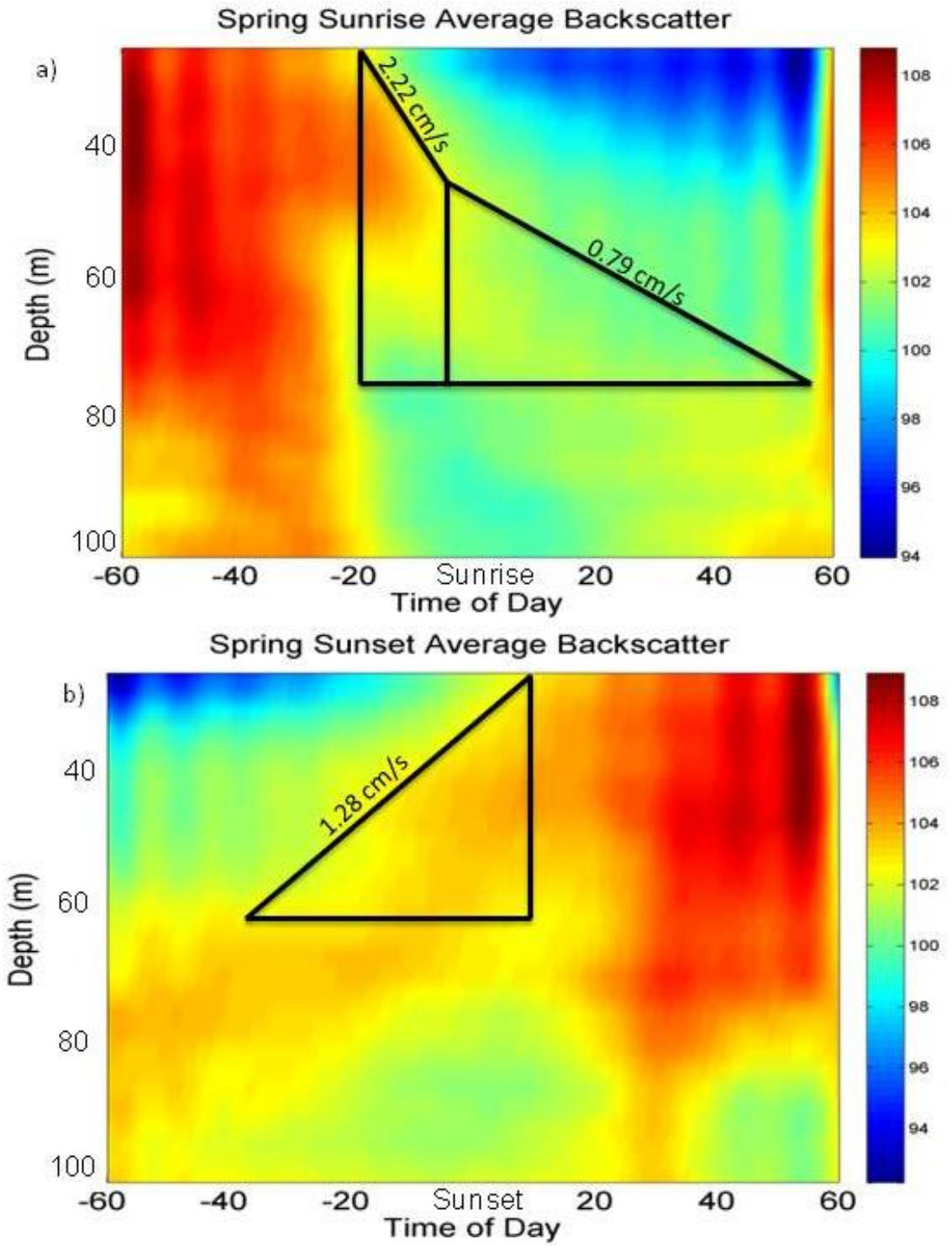

Figure 4-20. Averaged spring zooplankton swim speeds during a) sunrise and b) sunset conditions calculated from ADCP backscatter from spring months (February 9, 2011 to April, 26, 2011). Horizontal line of the triangle depicts the length of time that migration occurred, vertical lines indicate depth of migration. Slope formula was used to determine velocity.

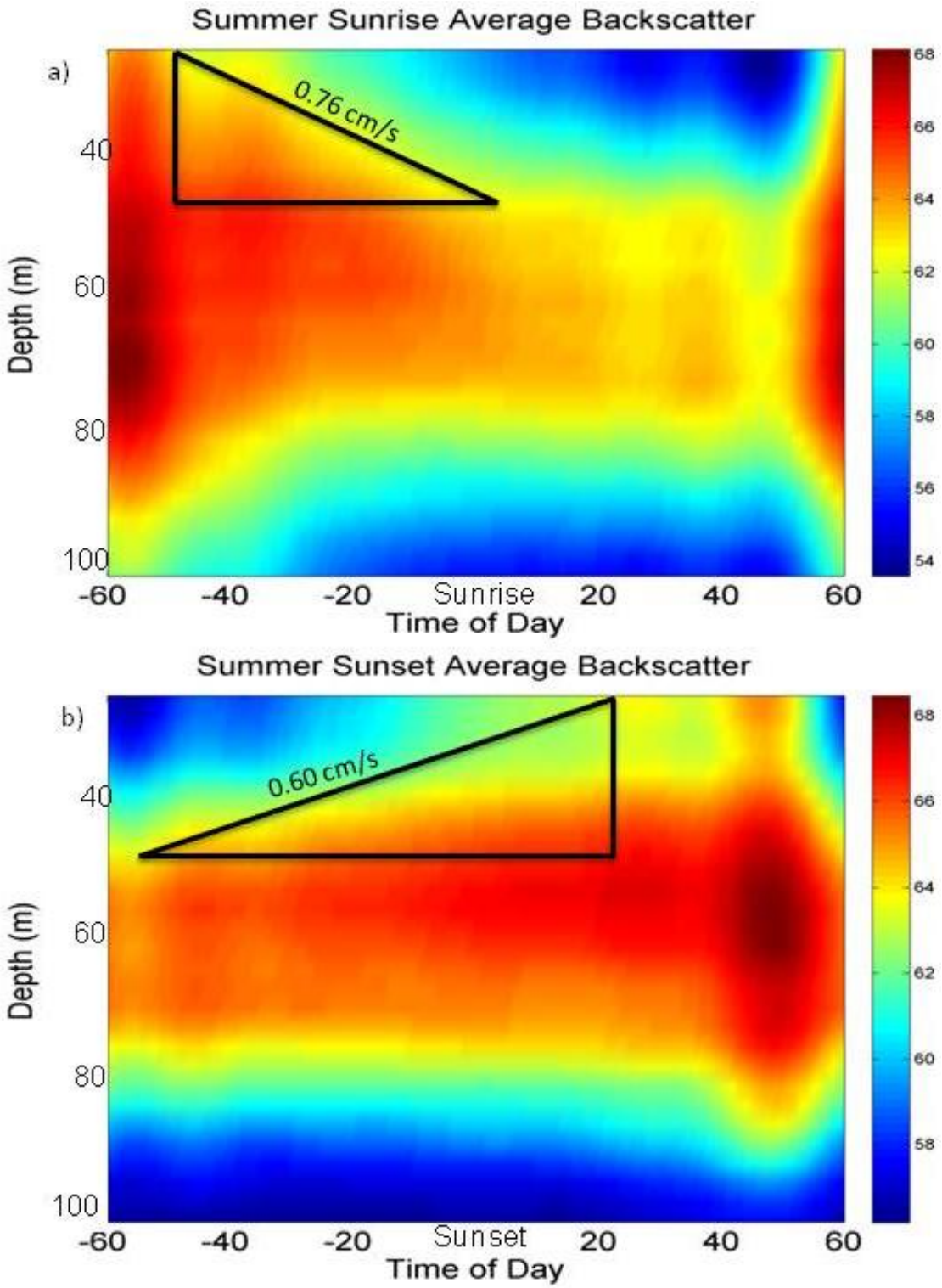

Figure 4-21. Averaged summer zooplankton swim speeds during a) sunrise and b) sunset conditions calculated from ADCP backscatter from summer months (April 27, 2011 to October, 11, 2011). Horizontal line of the triangle depicts the length of time that migration occurred, vertical lines indicate depth of migration. Slope formula was used to determine velocity.

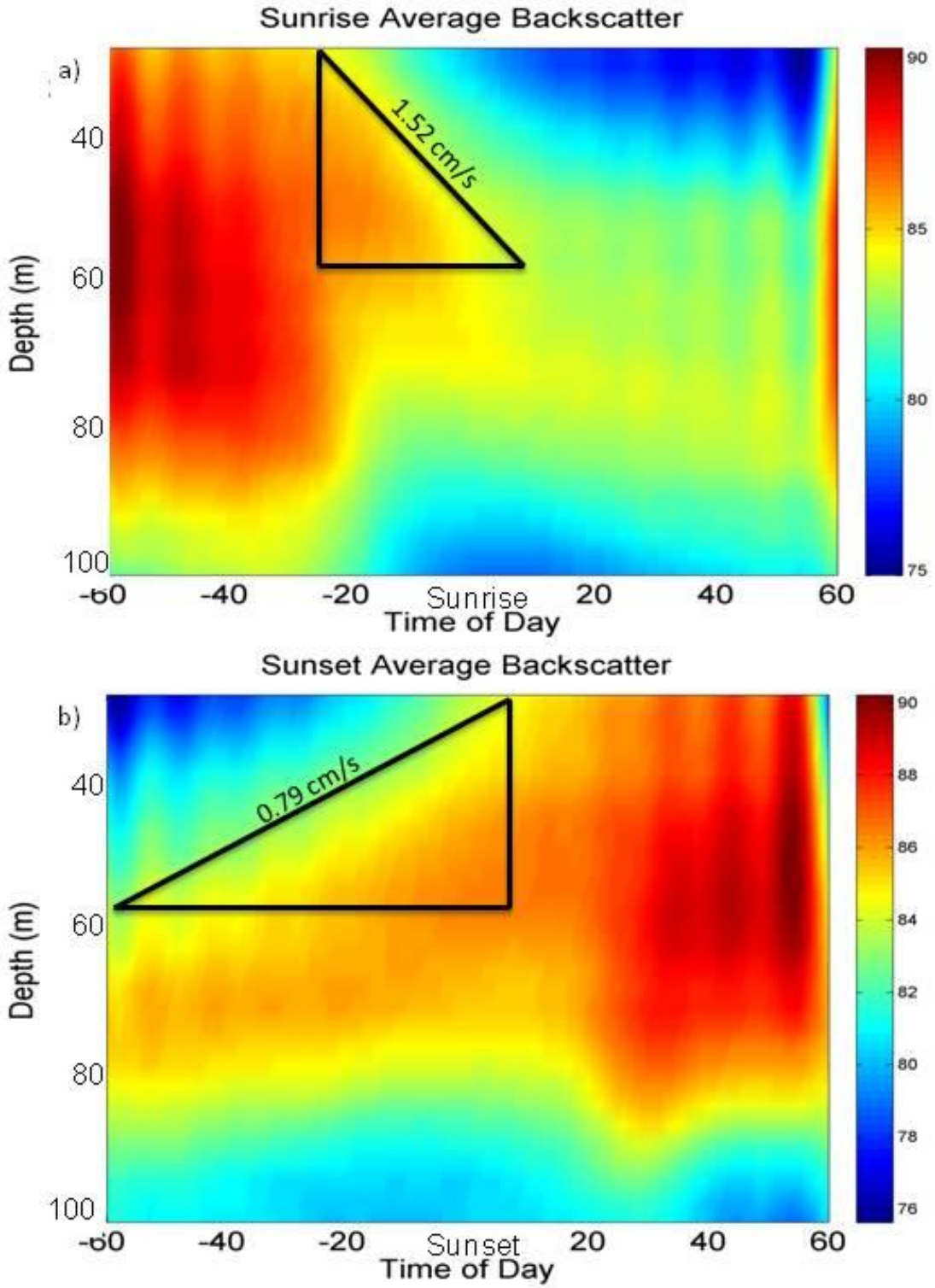

Figure 4-22. Averaged zooplankton swim speeds during a) sunrise and b) sunset conditions calculated from ADCP backscatter from full 11 month data set (December 16, 2010 to October, 11, 2011). Horizontal line of the triangle depicts the length of time that migration occurred, vertical lines indicate depth of migration. Slope formula was used to determine velocity.

4.1.2 Velocity

4.1.2.1 Dania Beach

Northward current velocity profiles were averaged over all sunrise and sunset times for each season and for the complete 11 month data set. These profiles were compared to the averaged profile three hours prior. Only cases within the Florida Current, characterized by a northward current velocity greater than 0.75 m s^{-1}, were considered. A 95% confidence interval was calculated to determine statistical significance. A statistically significant decrease in northward velocity in the top 100 m occurred during time intervals around sunset and sunrise as compared to three hours prior. The decrease in velocity in winter during migration times was not statistically significant with a 95% confidence interval (Fig 4-23). Spring showed no change in average northward velocity profile (Fig 4-24). Summer showed a statistically significant decrease in the northward velocity component during migration as compared to three hours prior (Fig 4.25). The complete 11 month data set showed a statistically significant decrease in the northward component of velocity during migrations as compared to three hours prior (Fig 4-26).

4.1.2.2 Pompano

Northward current velocity profiles were averaged over all sunrise and sunset times for each season and for the complete four year data set. These profiles were compared to the averaged profile three hours prior. Only cases within the Florida Current, characterized by a northward current velocity greater than 0.75 m s^{-1}, were considered. A 95% confidence interval was calculated to determine statistical significance. There were no observable change in velocity in the winter and spring cases (Fig. 4-27 and 4-28). There was an observable decrease in the northerly velocity component in summer and fall cases and when all four years of data were averaged (Fig. 4-29 through 4-31). However, these were not statistically significant at the 95% confidence level.

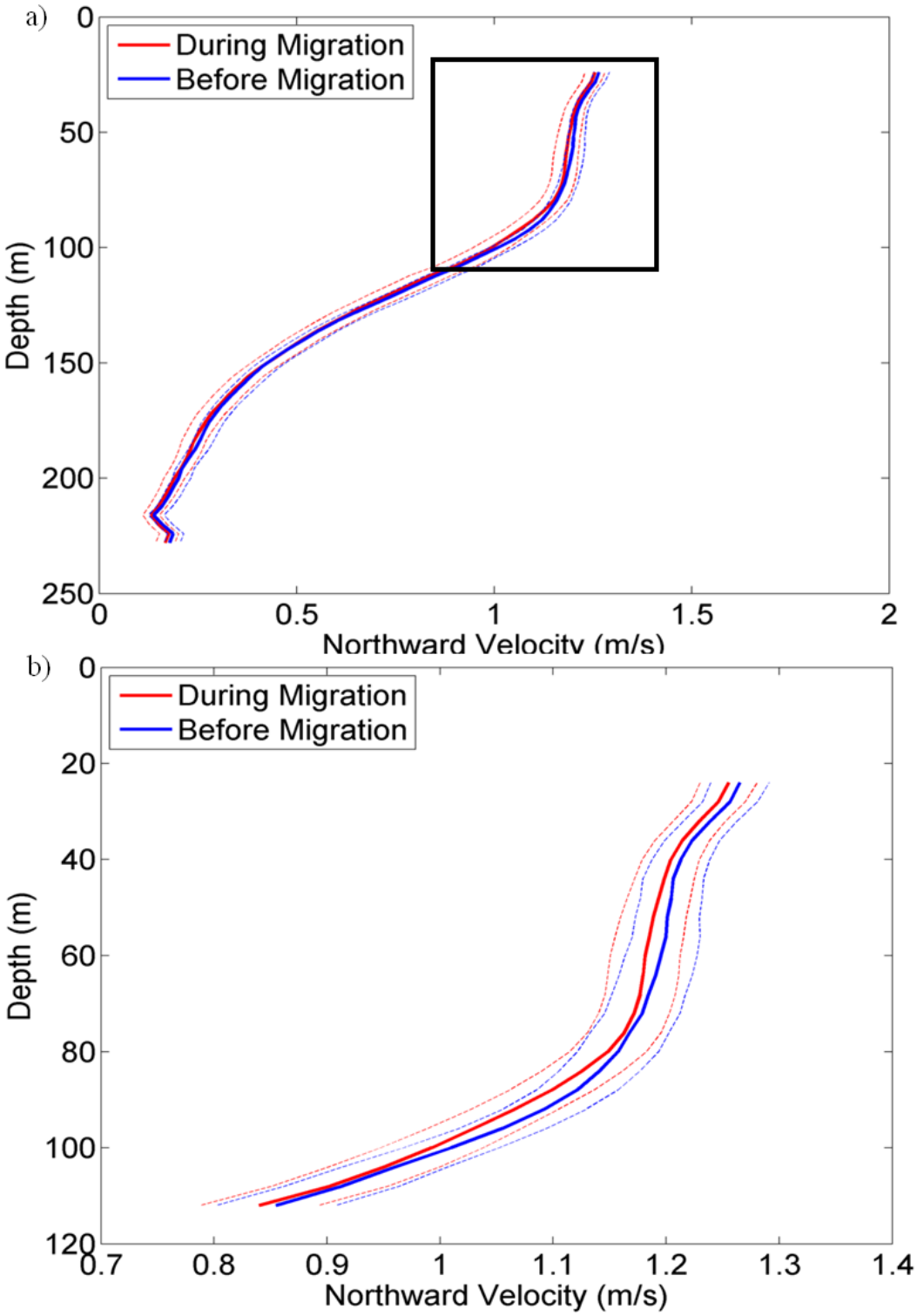

Figure 4-23. Winter northward current velocity profiles of sunrise/sunset compared to three hours prior using a 95% confidence interval (represented with dotted lines) from Dania Beach data set. a) Complete average velocity profile. b) Top 110 m of the profile represented by the black box in part a.

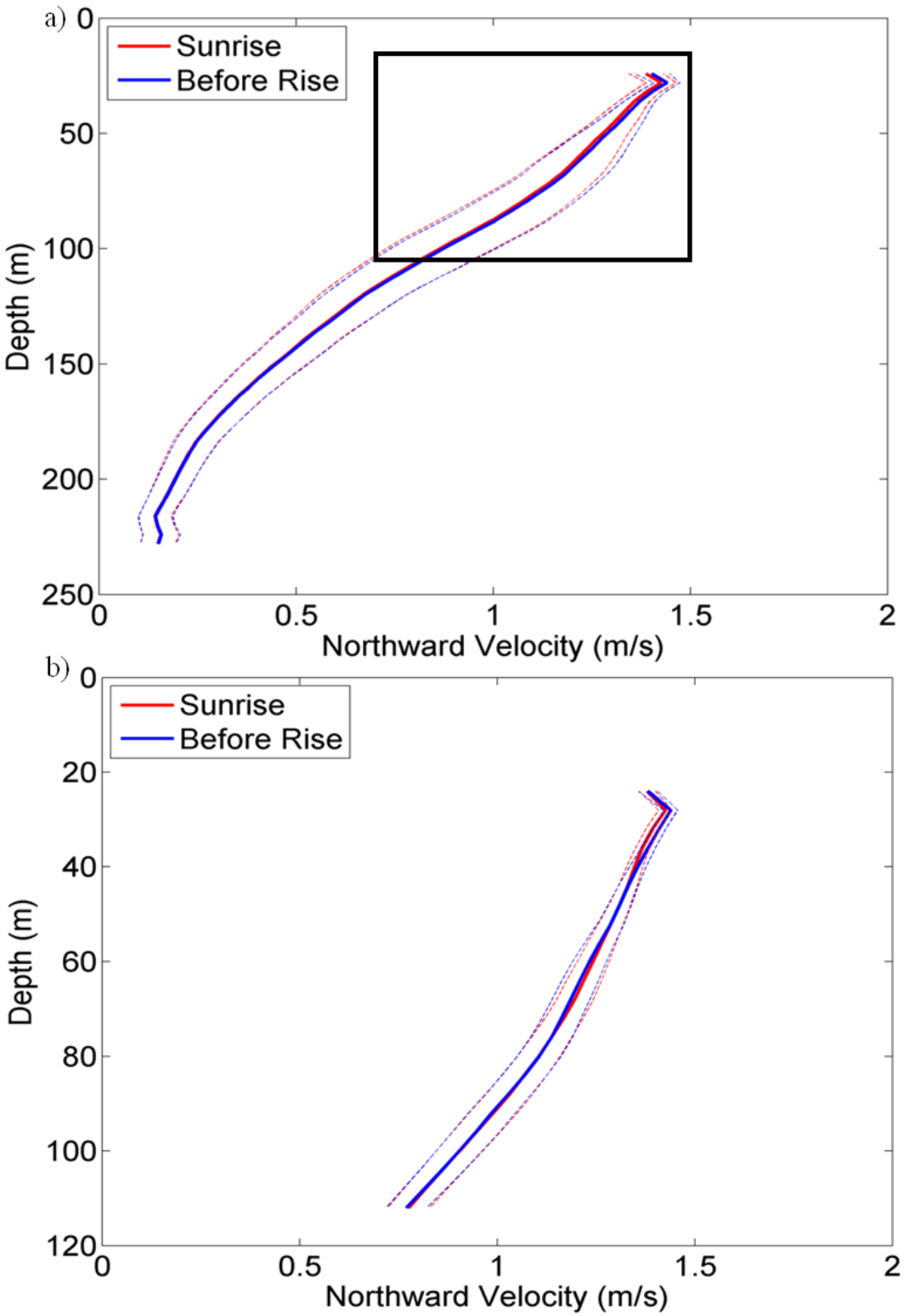

Figure 4-24. Spring northward current velocity profiles of sunrise/sunset compared to three hours prior using a 95% confidence interval (represented by dotted lines) from Dania Beach data set. a) Complete average velocity profile. b) Top 110 m of the profile reprsented by the black box in part a.

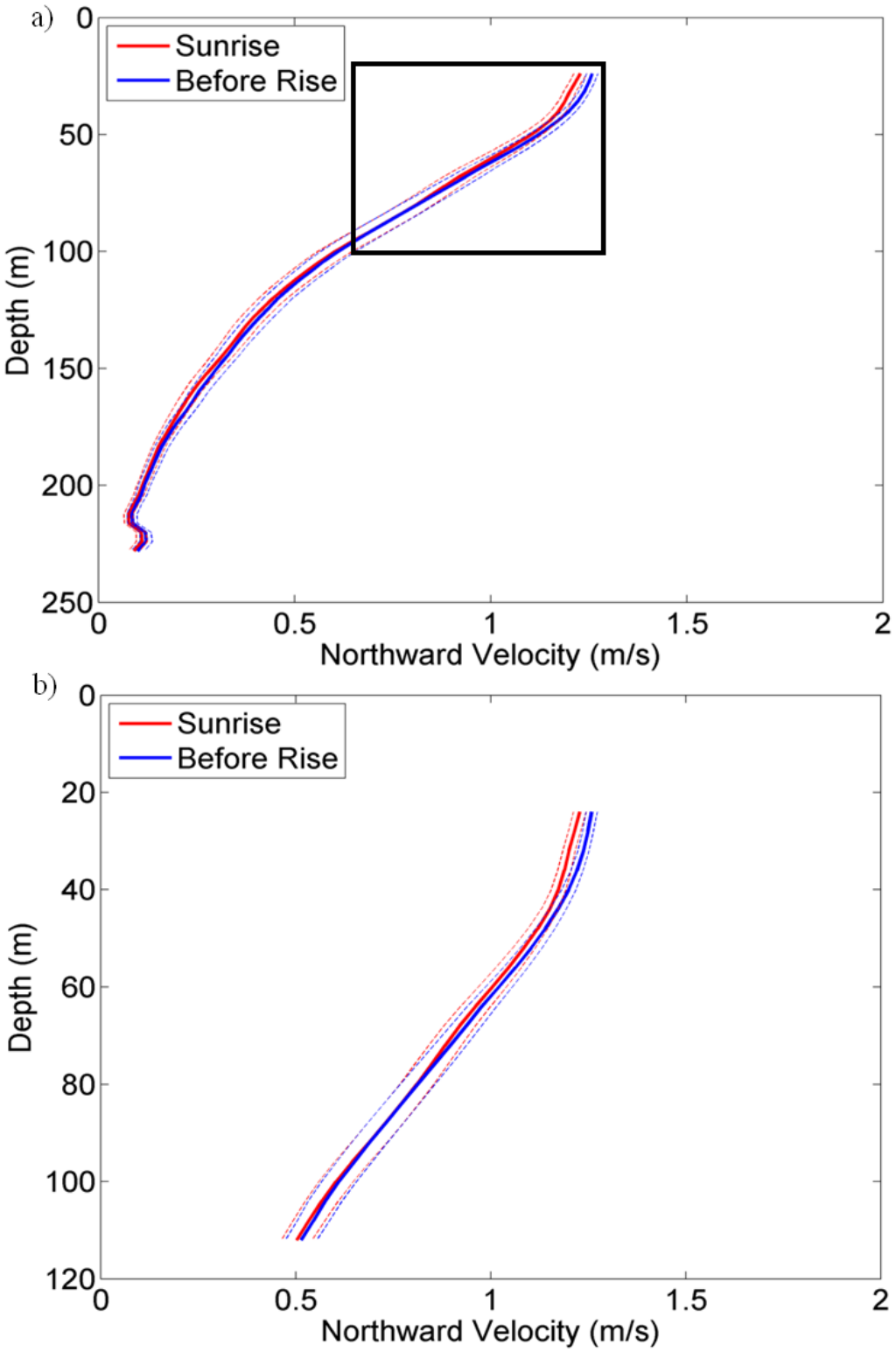

Figure 4-25. Summer northward current velocity profiles of sunrise/sunset compared to three hours prior using a 95% confidence interval (represented by dottend lines) from Dania Beach data set. a) Complete average velocity profile. b) Top 110 m of the profile reprsented by the black box in part a.

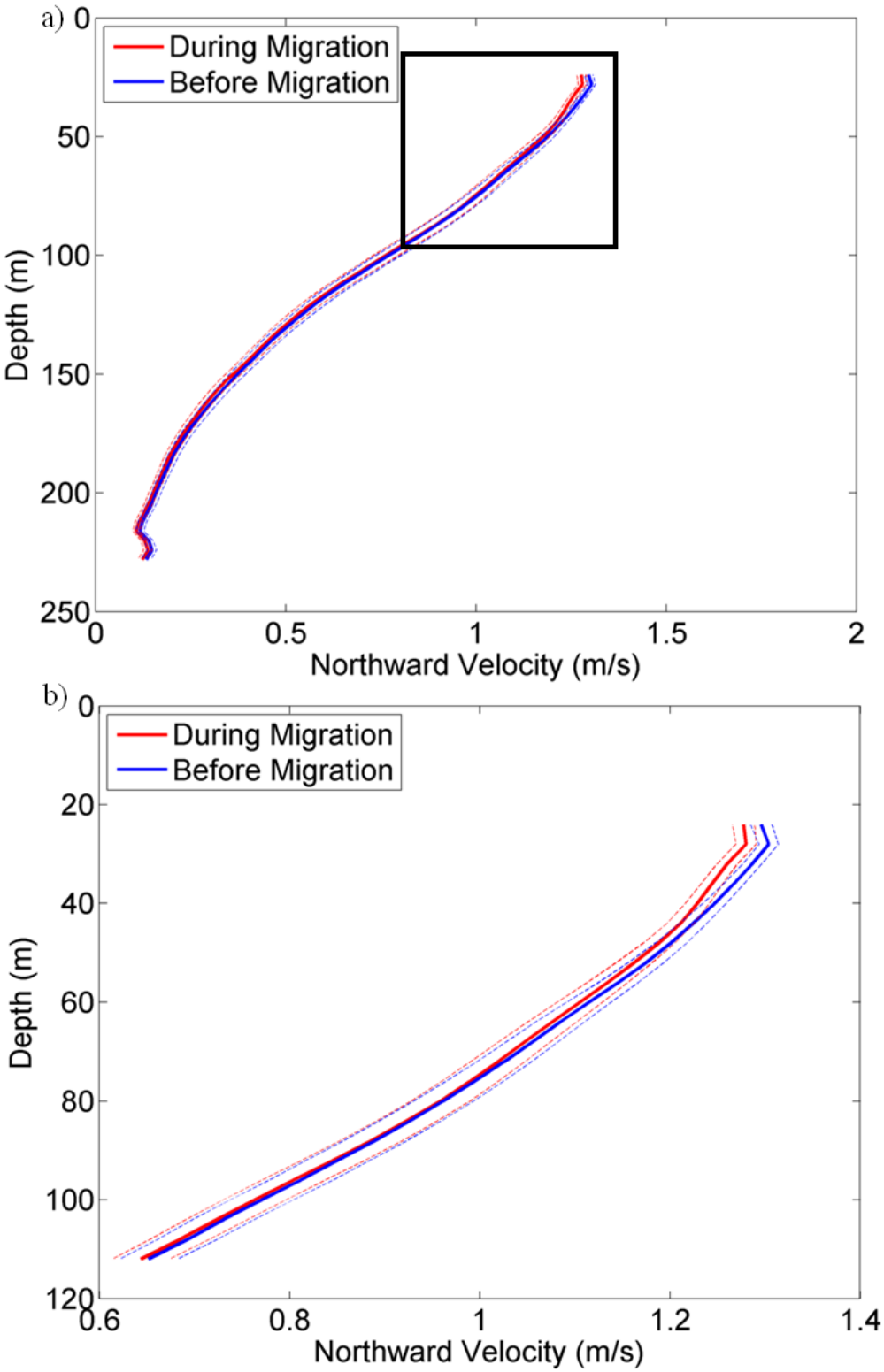

Figure 4-26. Full 11 month data set northward current velocity profiles of sunrise/sunset compared to three hours prior using a 95% confidence interval (reprsented by dotted lines) from Dania Beach data set. a) Complete average velocity profile. b) Top 110 m of the profile represented by the black box in part a.

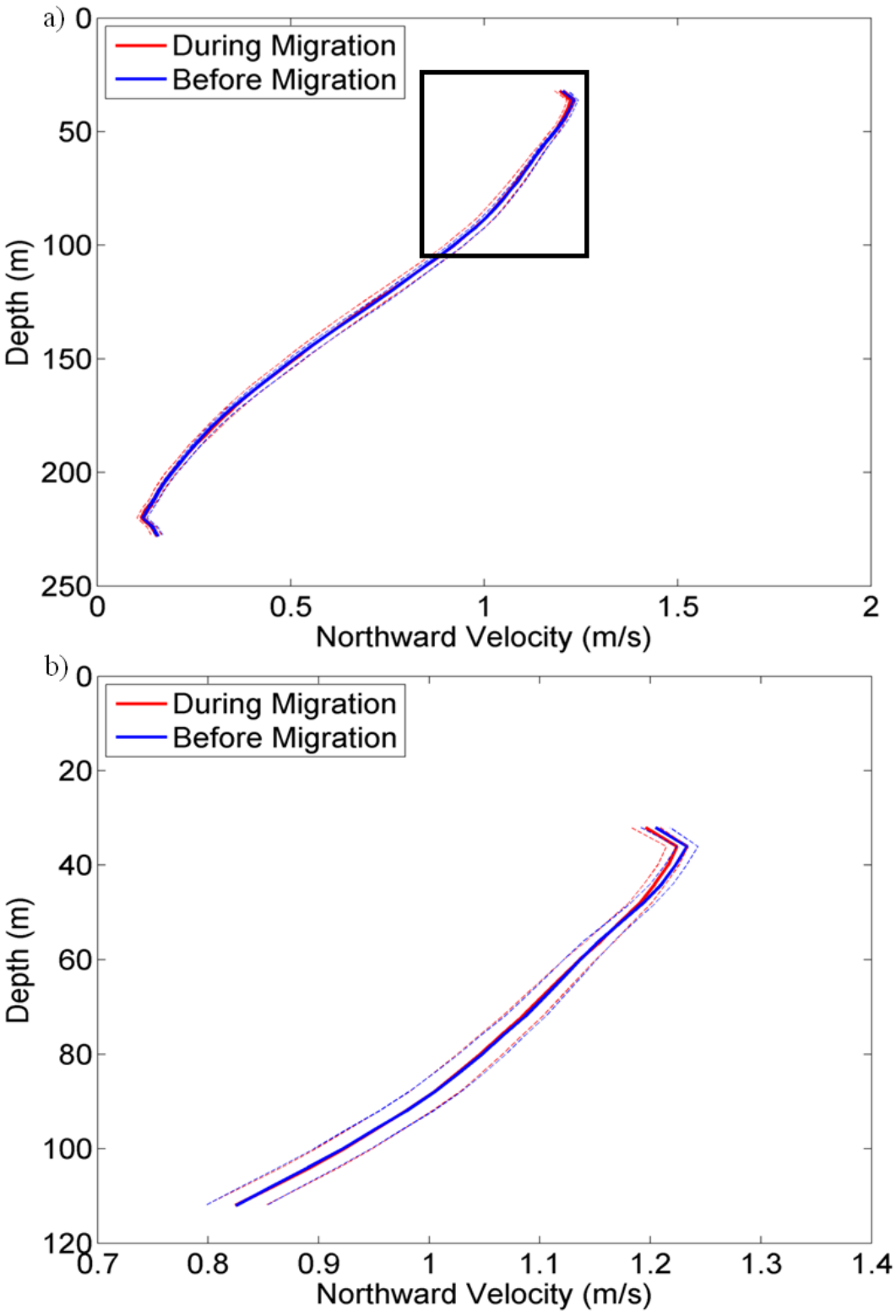

Figure 4-27. Winter northward current velocity profiles of sunrise/sunset compared to three hours prior using a 95% confidence interval (represented by dotted lines) from Pompano 4 year data set. a) Complete average velocity profile. b) Top 110 m of the profile represented by the black box in part a.

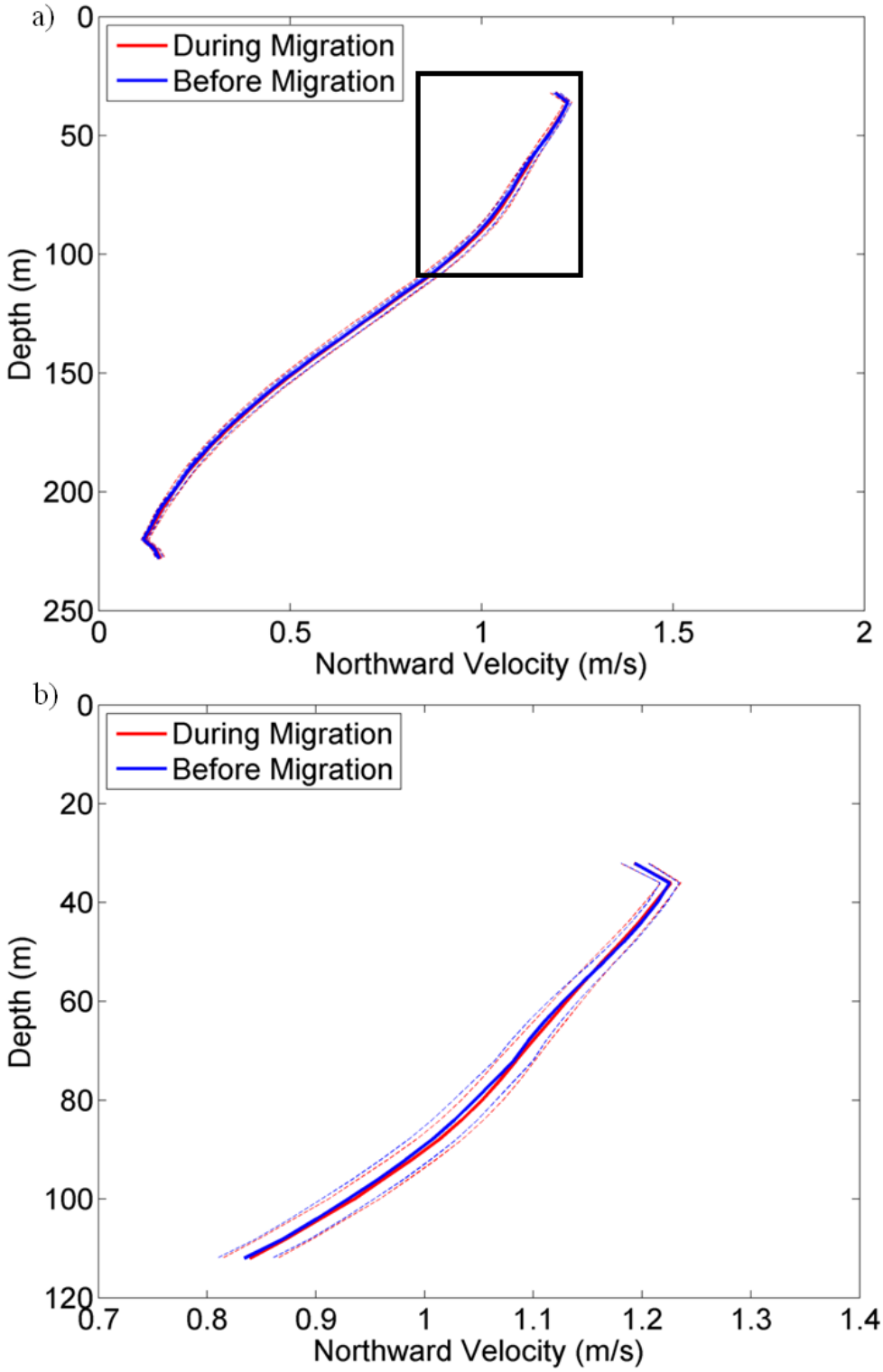

Figure 4-28. Spring northward current velocity profiles of sunrise/sunset compared to three hours prior using a 95% confidence interval (respresented by dotted lines) from Pompano 4 year data set. a) Complete average velocity profile. b) Top 110 m of the profile represented by the black box in part a.

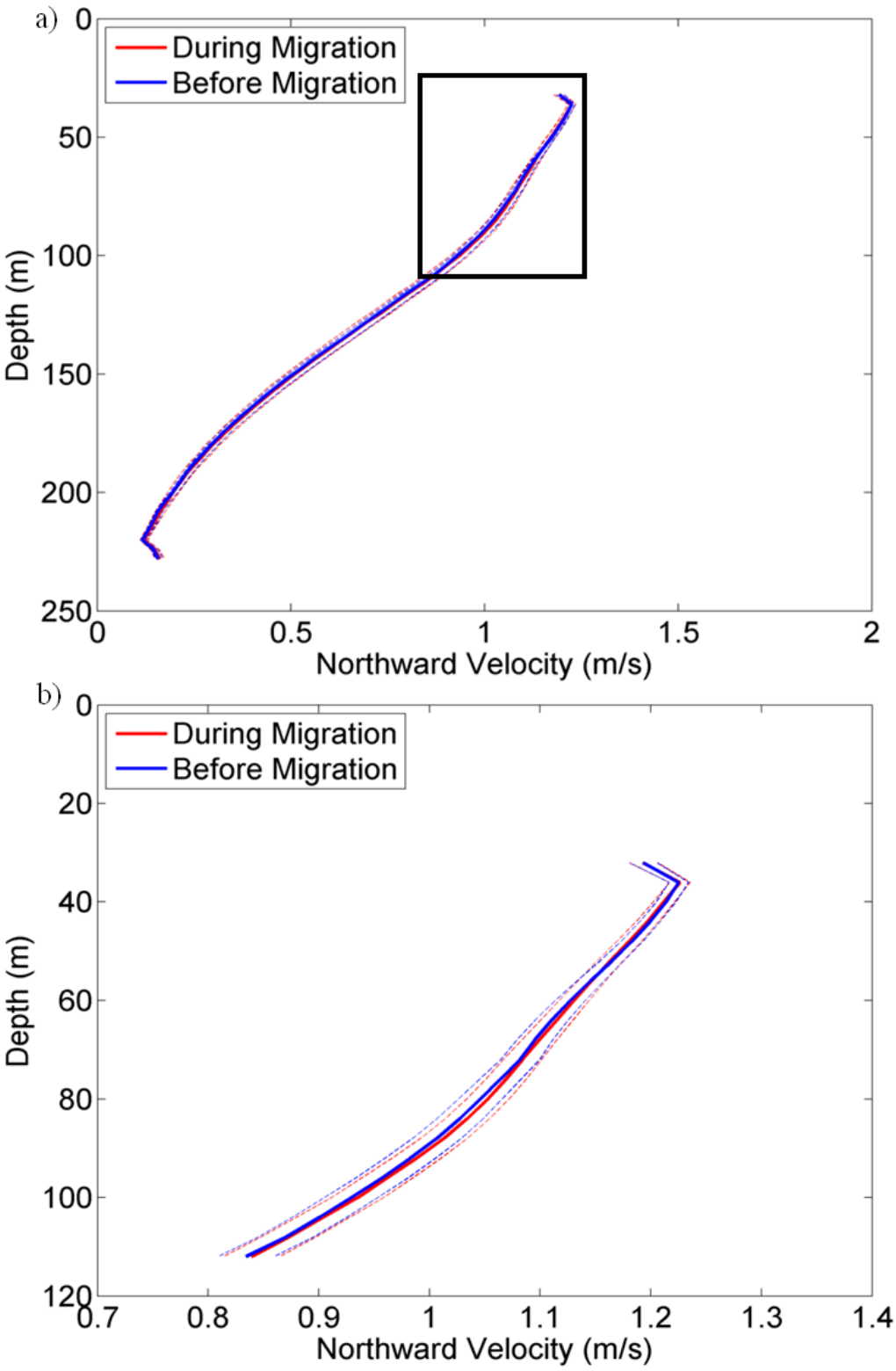

Figure 4-29. Summer northward current velocity profiles of sunrise/sunset compared to three hours prior using a 95% confidence interval (representd by the black box) from Pompano 4 year data set. a) Complete average velocity profile. b) Top 110 m of the profile represented by the black box in part a.

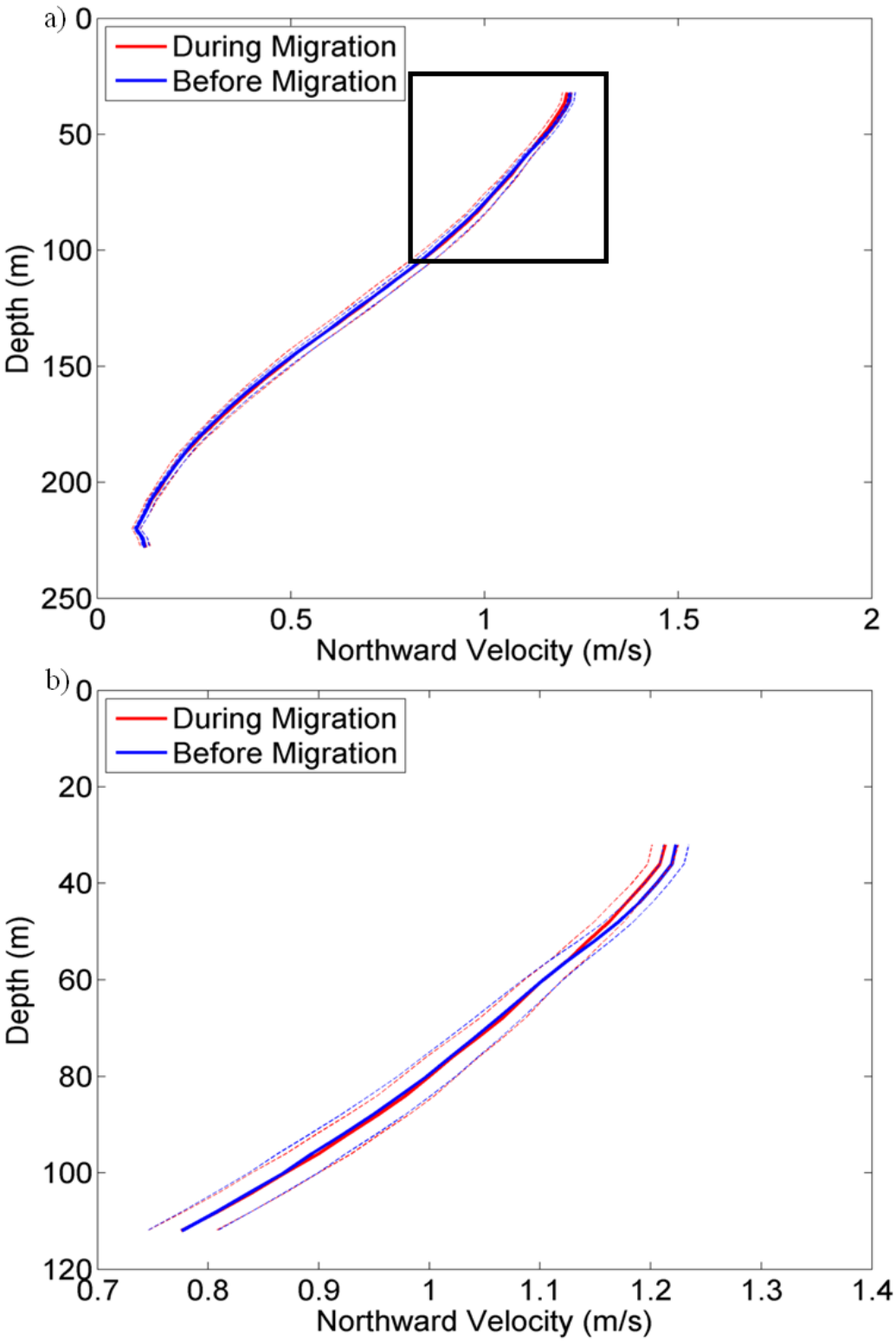

Figure 4-30. Fall northward current velocity profiles of sunrise/sunset compared to three hours prior using a 95% confidence interval (represented by dotted lines) from Pompano 4 year data set. a) Complete average velocity profile. b) Top 110 m of the profile represented by black box in part a.

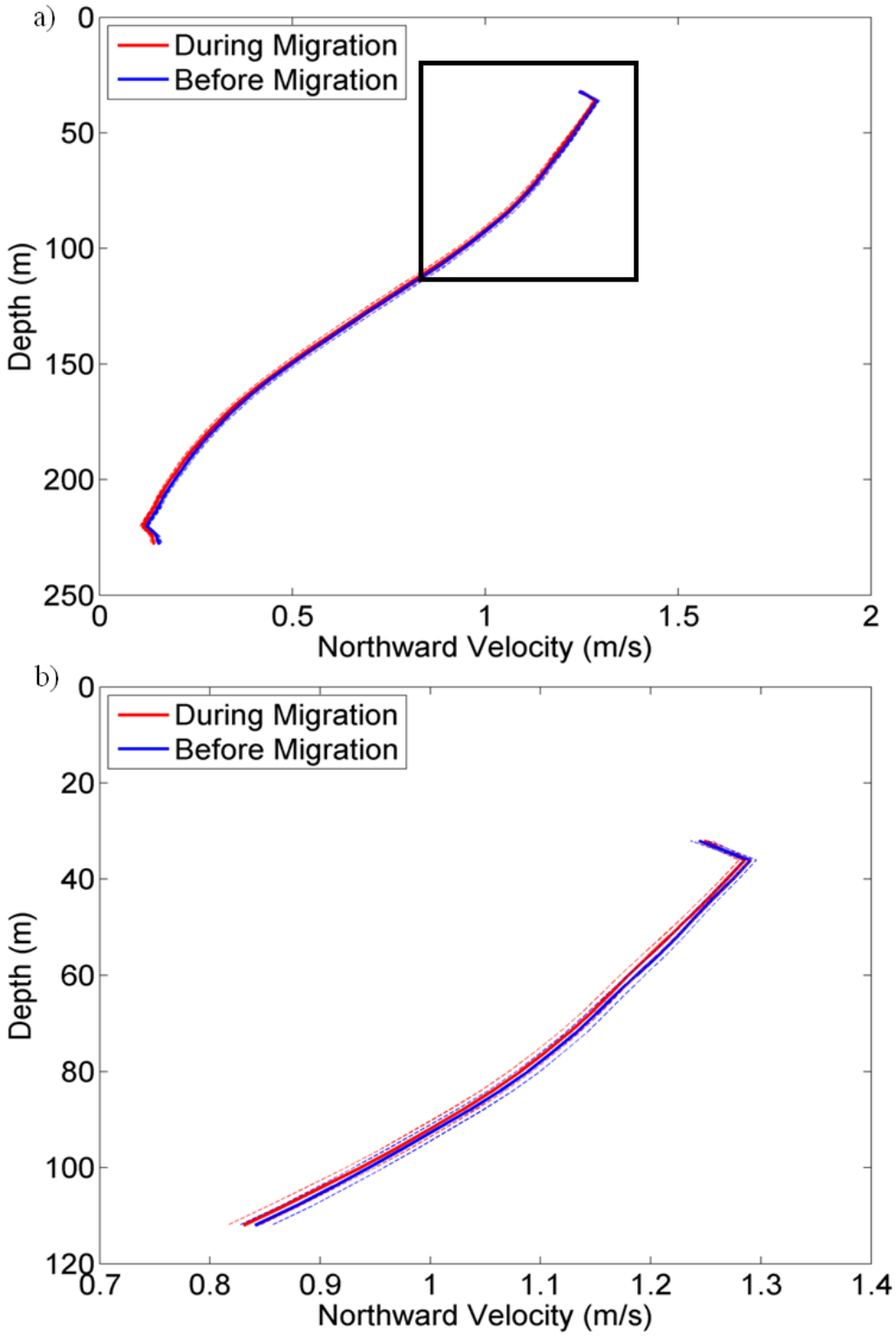

Figure 4-31. Full four year data set northward current velocity profiles of sunrise/sunset compared to three hours prior using a 95% confidence interval (represented by dotted lines) from Pompano 4 year data set. a) Complete average velocity profile. b) Top 110 m of the profile represented by the black box in part a.

4.2 Computational Fluid Dynamics Model

A range of mass flow rates were tested to determine what level of zooplankton density was necessary to create an impact on velocity profiles and turbulence signatures. A mass flow rate of $5x10^4$ kg s^{-1} produced very little effect on turbulence and velocity. A mass flow rate of $2.5x10^5$ kg s^{-1} did produce an impact on turbulence in all cases and velocity in some cases. This mass flow rate is the upper limit for the DPM model because this model cannot handle a volume fraction of particles is larger than 0.1. All results presented below are from this upper limit.

Data from the model runs were analyzed during a time step while the particles were moving through the mixed layer where the stratification was set so the Ri was much lower than the rest of the domain. The same time step was used for the corresponding no particles case. This was at a slightly different time for each model. The particles moved differently in each season due to differences in initial stratification conditions. The Ri was closer to the critical value in winter stratification, make the water column more susceptible to turbulent mixing. This made it slightly more difficult for the particles to penetrate through mixed layer than in summer stratification. The direction of particle movement influenced the time step in which the particles were moving through the mixed layer. In sunrise cases, particles were injected at the top boundary of the domain, therefore, they moved through the mixed layer fairly quickly. In sunset cases, particles were injected near the bottom of the thermocline, so they took longer to rise into the mixed layer. Winter sunrise cases were taken 15 minutes after particles were released from the surface. Winter sunset cases were taken 26 minutes and 40 seconds after particles were released from a 110 m depth, rising toward the surface. Summer sunrise northerly wind case was taken 10 minutes after particles were released from the surface. Summer sunrise southerly wind case was taken 11 minutes and 40 seconds after release from the surface. Sumer sunset cases were taken 30 minutes after the particles were released from a 110 m depth.

4.2.1 Velocity

Average x-velocity profiles were plotted for all model runs. Each case compared a run with particles in the domain to a run with no particles. All other settings for the two runs were exactly the same. In the winter sunrise northerly wind case, there was a slight decrease in velocity in the particles cases compared to no particles in the mixed layer of the water column. The sunrise southerly wind case showed a slight increase in velocity in the mixed layer when particles were present. There were slight distortions in the winter sunset cases (Fig. 4-32). In summer runs, there was a slight distortion of the x-velocity profile in the sunrise northerly wind case and there were no observable effects in any of the other cases (Fig. 4-33). X-velocity profiles were also averaged for each season (Fig.

4-34). There was a slight decrease in average velocity when winter cases were averaged and no difference when summer cases were averaged.

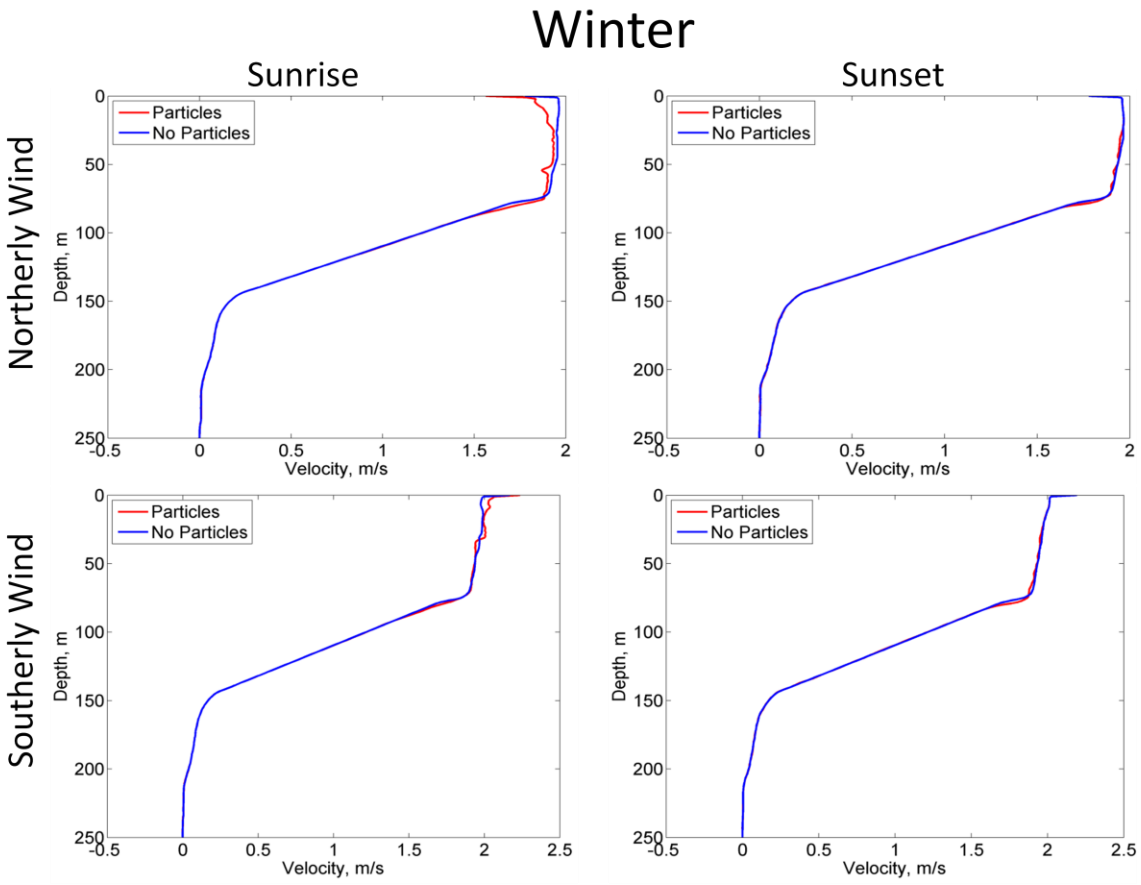

Figure 4-32. Winter average northward velocity profiles from the CFD model.

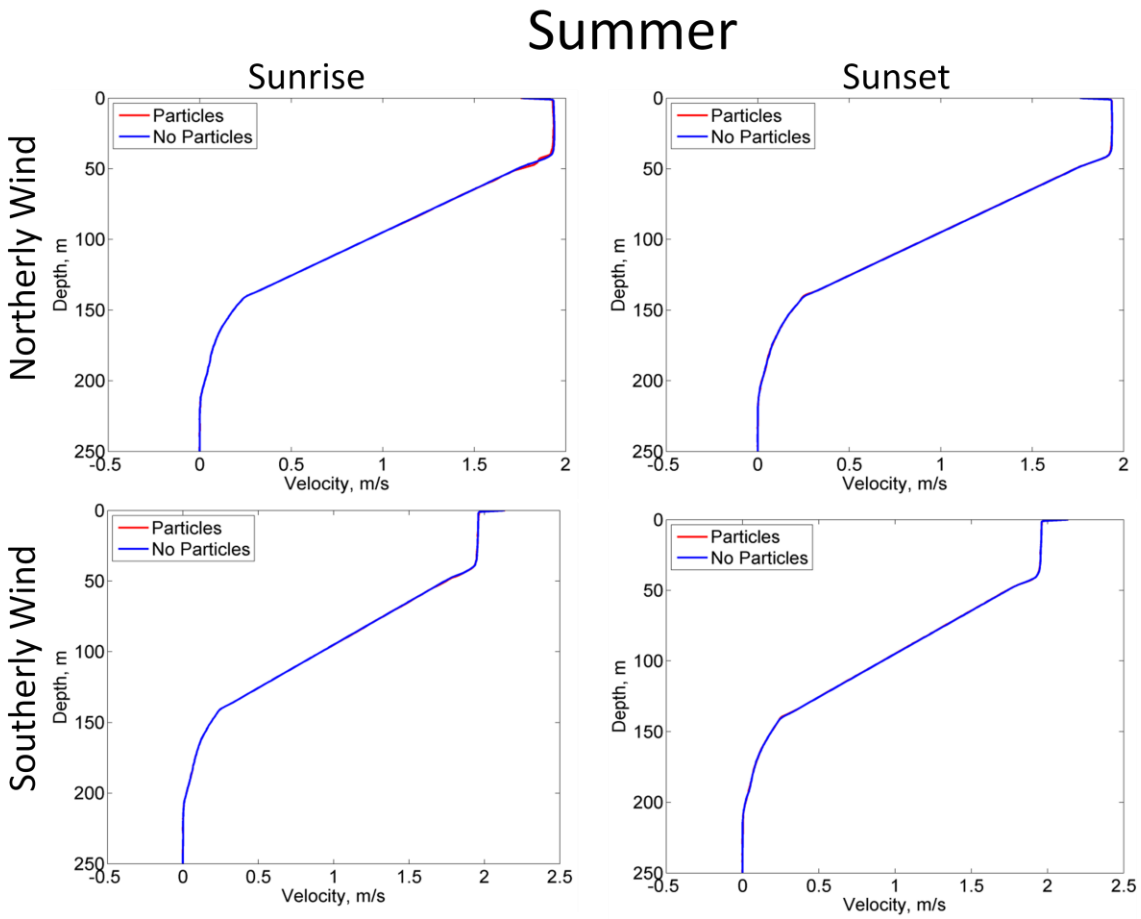

Figure 4-33. Summer average northward velocity profiles from the CFD model.

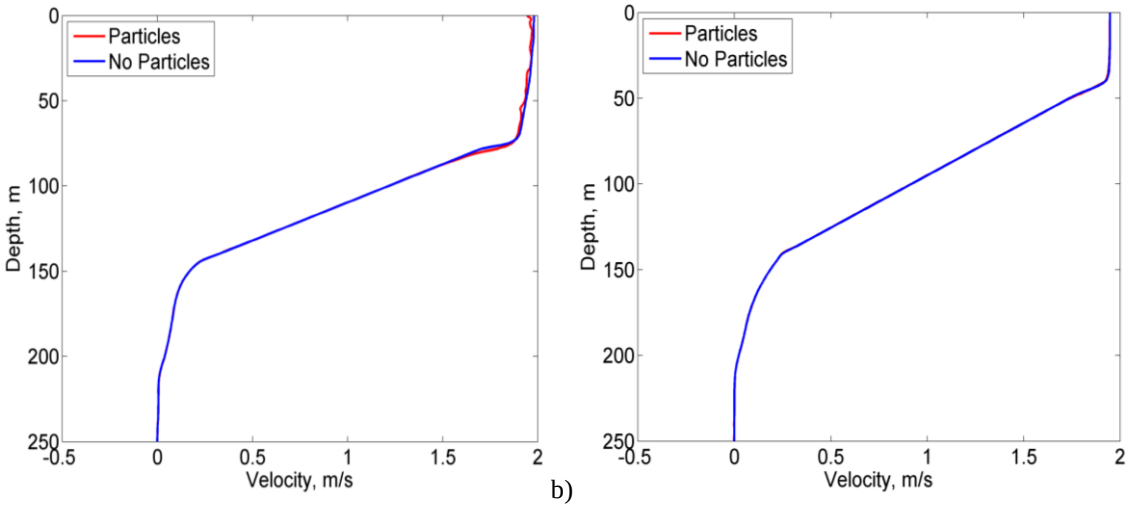

a) b)

Figure 4-34. Season averaged northward velocity profiles from the CFD model. A) Winter cases. B) Summer cases.

4.2.2 Turbulence

Average profiles of subgrid turbulent viscosity were plotted from the model runs. These profiles compared a model run with particles to one with no particles. All other settings in the runs were the same. In the winter cases, there was an obvious increase in turbulence in the mixed layer when particles were present in the average profiles of all cases. This increase was larger in the sunrise cases than the sunset cases (Fig. 4-35). In summer there were observable increases, but smaller than in winter cases, in the subgrid turbulent viscosity average profiles when particles were present in all cases. The effect of particles in sunrise cases was greater than sunset in cases (Fig. 4-36). Average subgrid turbulent viscosity profiles were also averaged for each season (Fig. 4-37). There was an obvious increase in turbulence in both averaged cases. This increase was greater during averaged winter cases. In all cases, turbulence was increased in the bottom boundary layer due to setting a no slip boundary condition at the bottom boundary which causes the fluid to stick to the wall at this boundary.

A contour plot of subgrid turbulent viscosity was exported in particles and no particles cases to compare the level of turbulence in the wake of the particles simulating DVM. Particles tracks were also exported to easily visualize the location of the particles within the domain. All cases showed an increase of subgrid turbulent viscosity in the mixed layer with particles present compared to no particles.

Winter cases had a very high level of turbulence (Figs 4-38 to 4-45). The scales range from $2x10^{-8}$ to 8.7 kg $(m \times s)^{-1}$. The winter cases all showed a substantial increase of turbulence in the mixed layer and all cases showed very low levels of turbulence when no particles were present. All of the cases had some turbulence in the surface layer due to wind stress imposed along the top boundary.

All summer cases showed an increase in subgrid turbulent viscosity in cases with particles compared to those without. The differences were not as strong as in the winter cases. The absolute level of turbulence was lower due to the differences in stratification. The scale ranged from $5x10^{-7}$ to 5.9 kg $(m \times s)^{-1}$ which was much lower than the winter cases. Sunrise cases had an obvious increase of turbulence in the particles case compared to no particles. Sunset cases had a slightly elevated turbulent signature when particles were present, but it was not as obvious.

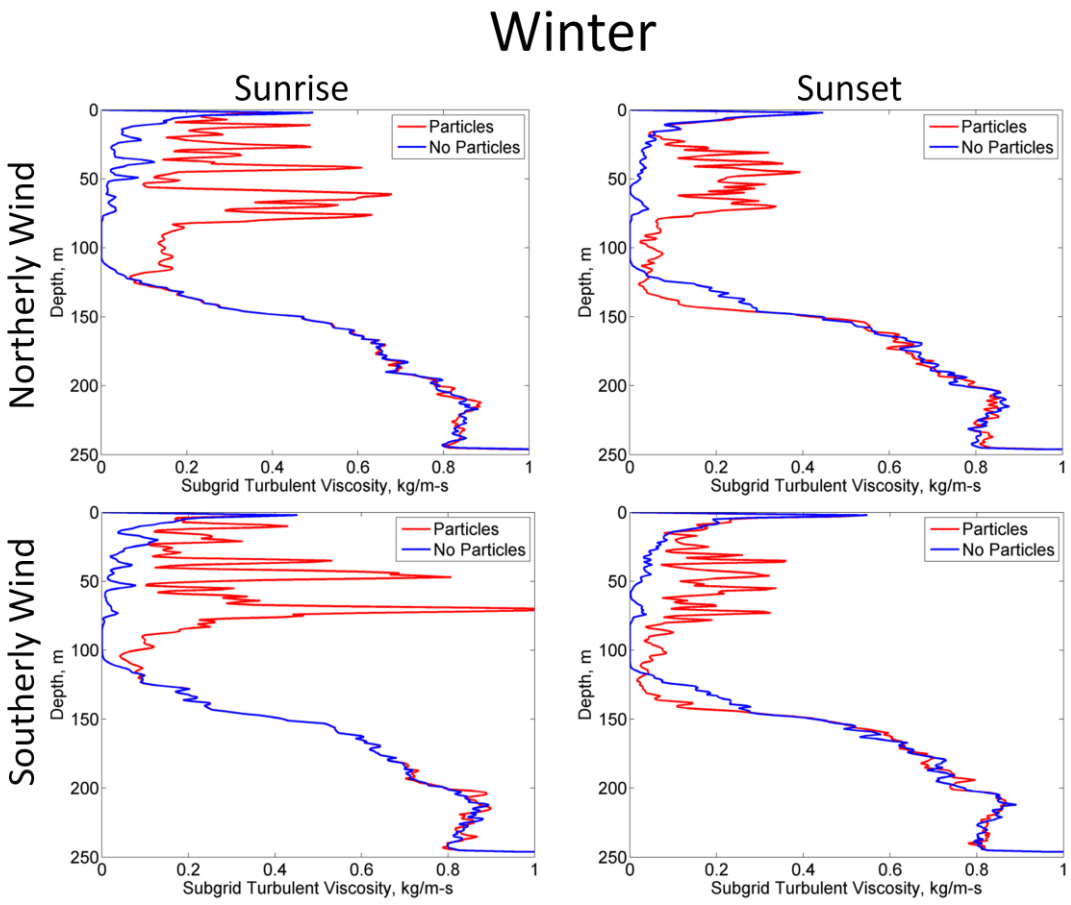

Figure 4-35. Winter average profiles of subgrid turbulent viscosity from CFD model.

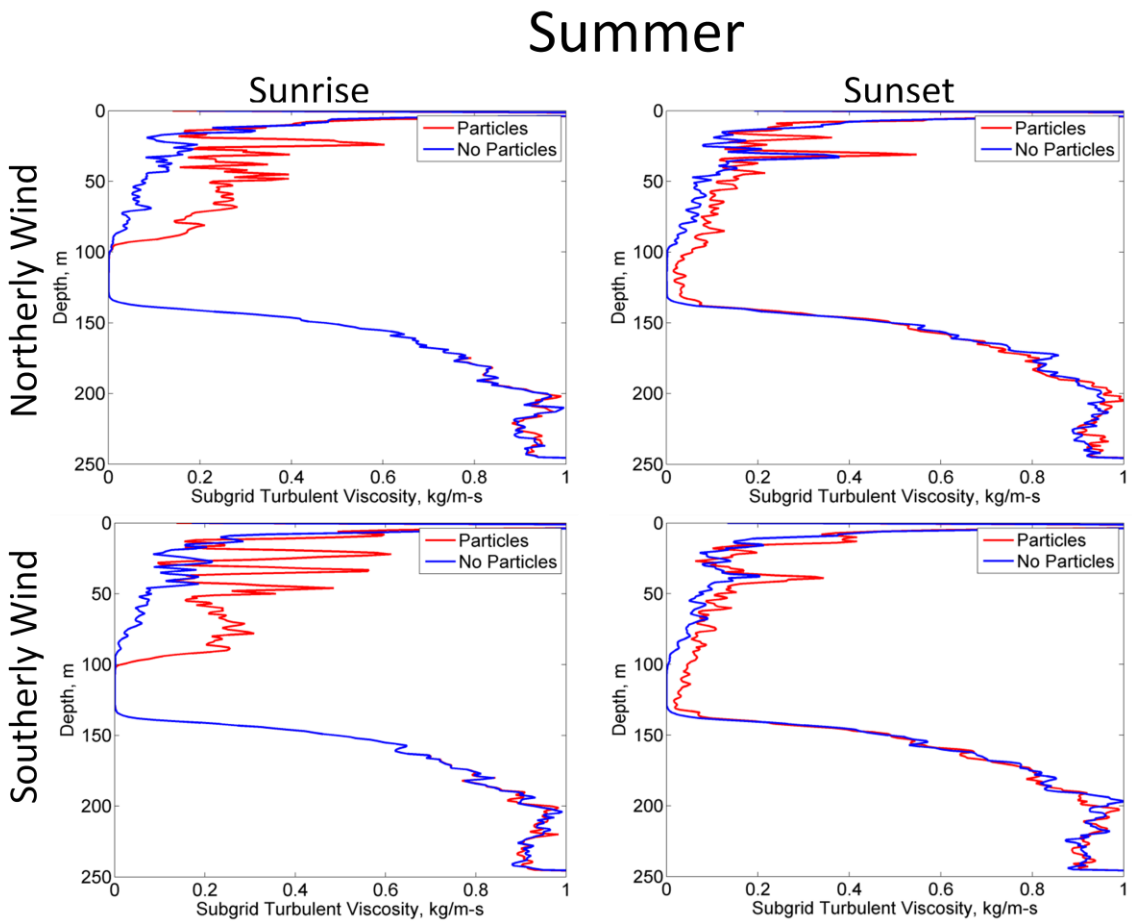

Figure 4-36. Summer average profiles of subgrid turbulent viscosity from model runs.

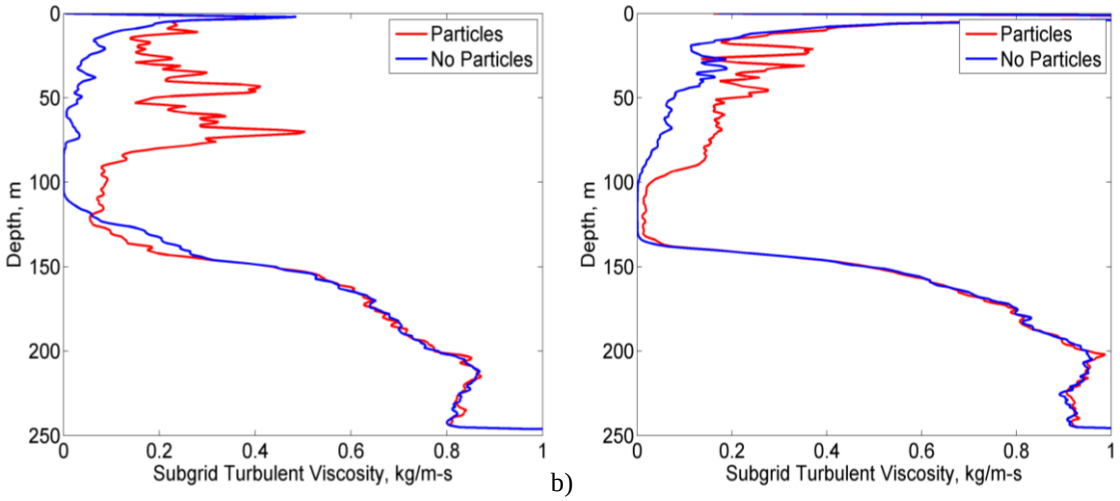

a) b)

Figure 4-37. Season averaged northward velocity profiles from the CFD model. a) Winter cases. b) Summer cases.

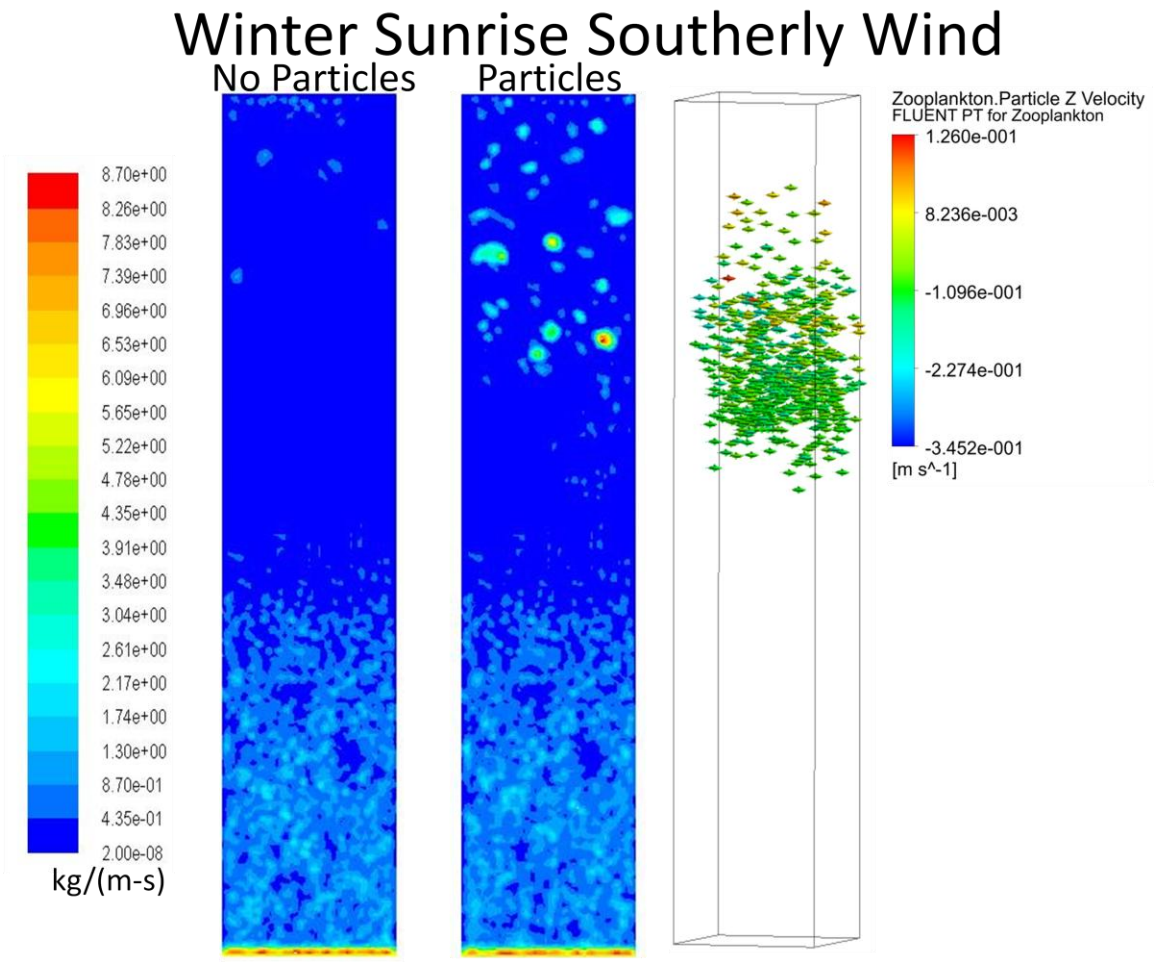

Figure 4-38. Contour of subgrid turbulent viscosity on the center plane in winter sunrise southerly wind condition comparing particles to no particles case. This was 15 minutes after particle injection while they were still in the mixed layer. Image on right shows the location of the particles within the domain.

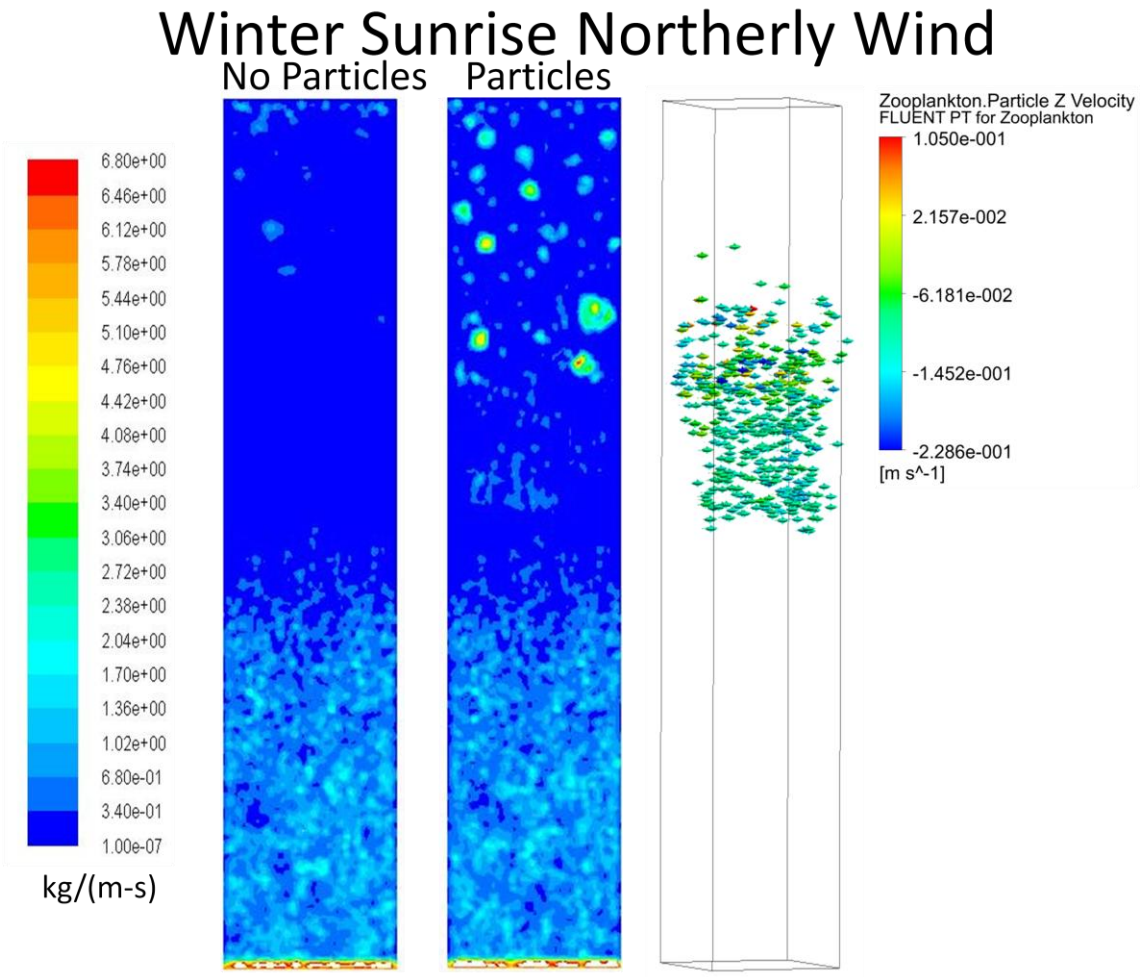

Figure 4-39. Subgrid turbulent viscosity in winter sunrise northerly wind condition comparing particles to no particles case. This was 15 minutes after particle injection while they were still in the mixed layer. Image on right shows the location of the particles within the domain.

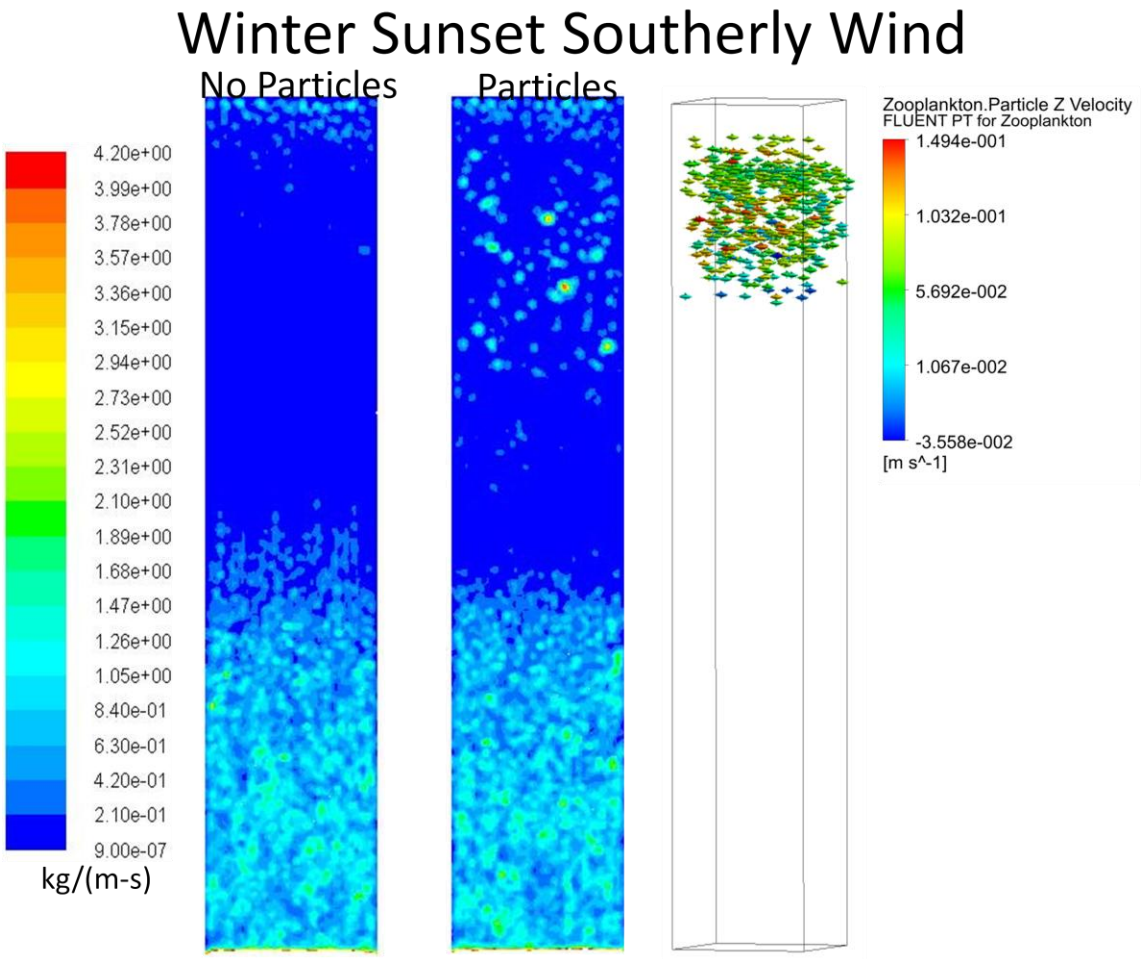

Figure 4-40. Subgrid turbulent viscosity in winter sunset southerly wind condition comparing particles to no particles case. This was 26 minutes and 40 seconds after particle injection while they were still in the mixed layer. Image on right shows the location of the particles within the domain.

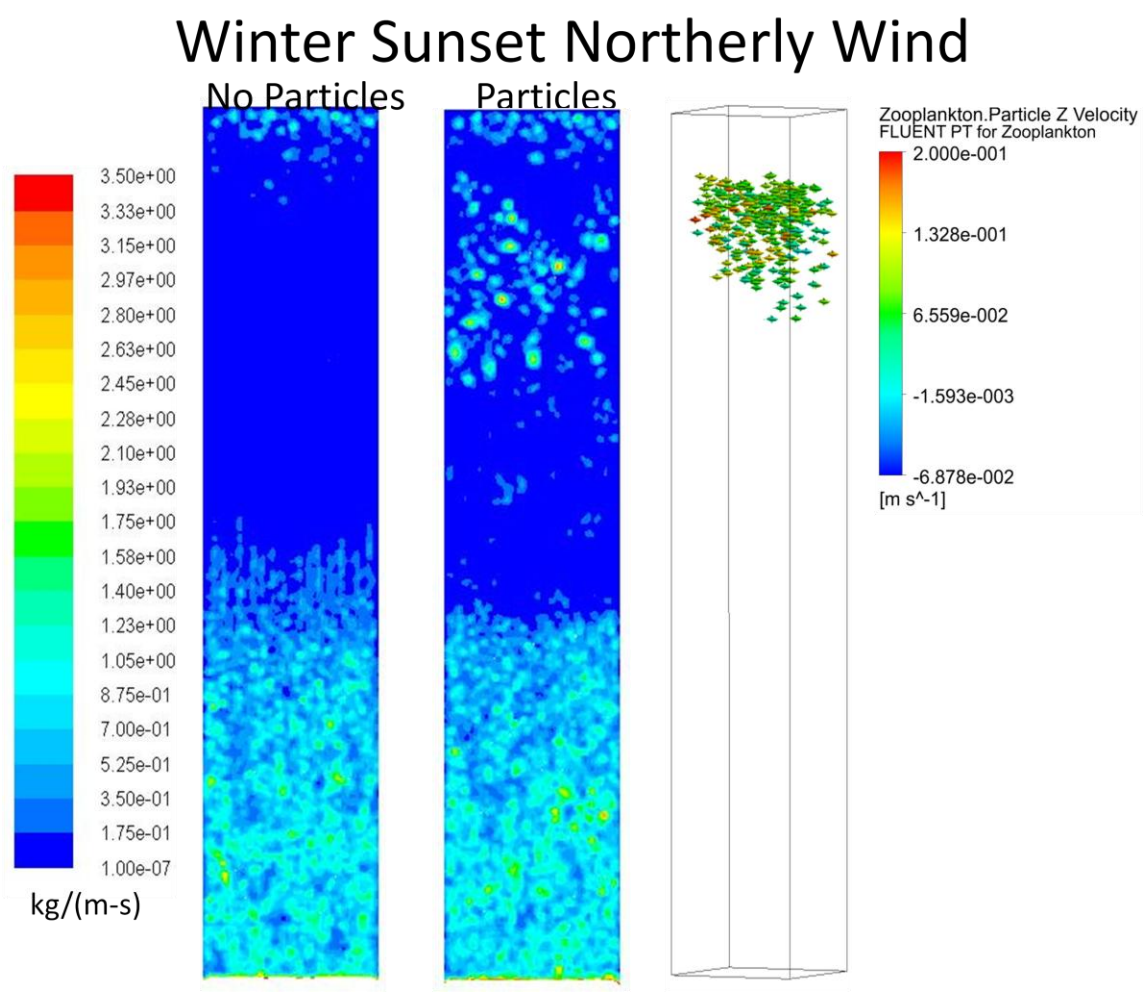

Figure 4-41. Subgrid turbulent viscosity in winter sunset northerly wind condition comparing particles to no particles case. This was 26 minutes and 40 seconds after particle injection while they were still in the mixed layer. Image on right shows the location of the particles within the domain.

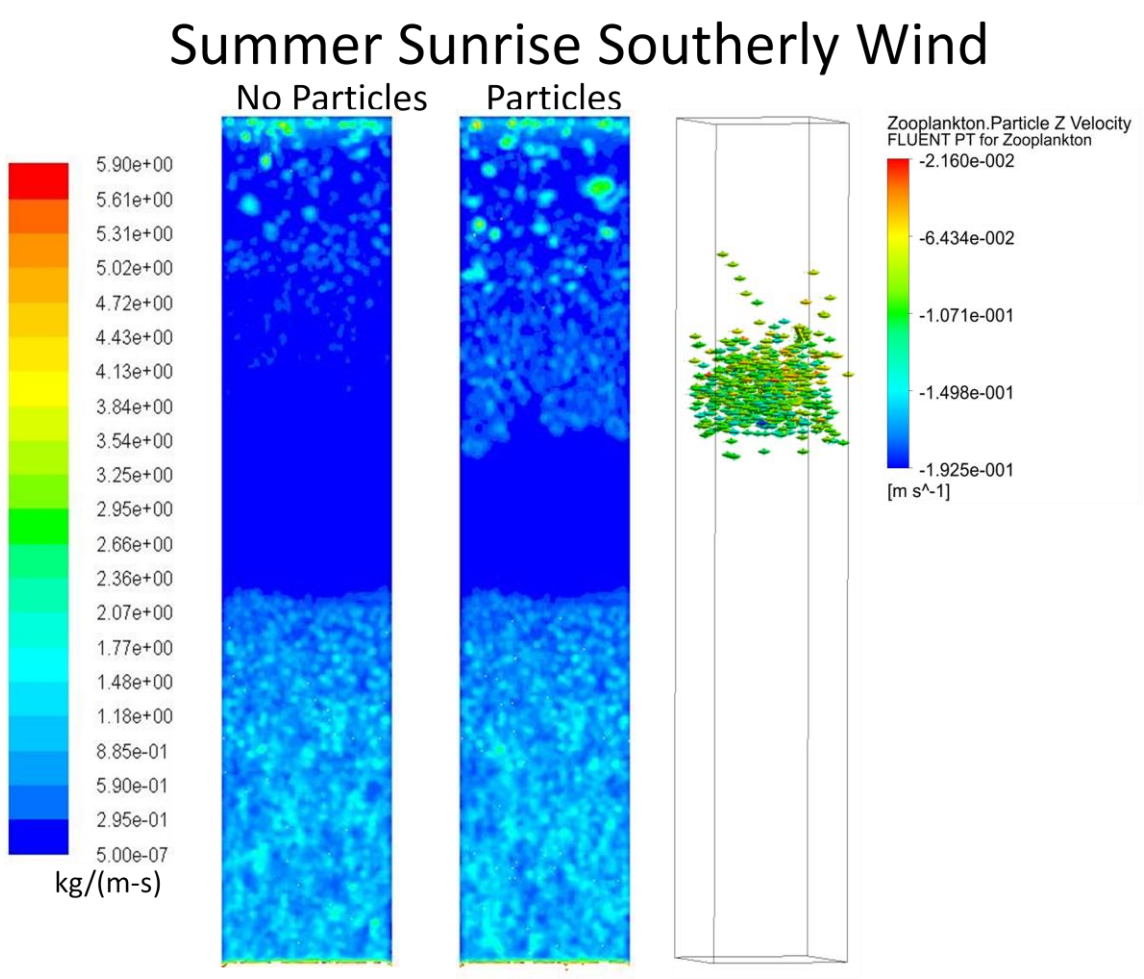

Figure 4-42. Subgrid turbulent viscosity in summer sunrise southerly wind condition comparing particles to no particles case. This was 11 minutes and 40 seconds after particle injection while they were still in the mixed layer. Image on right shows the location of the particles within the domain.

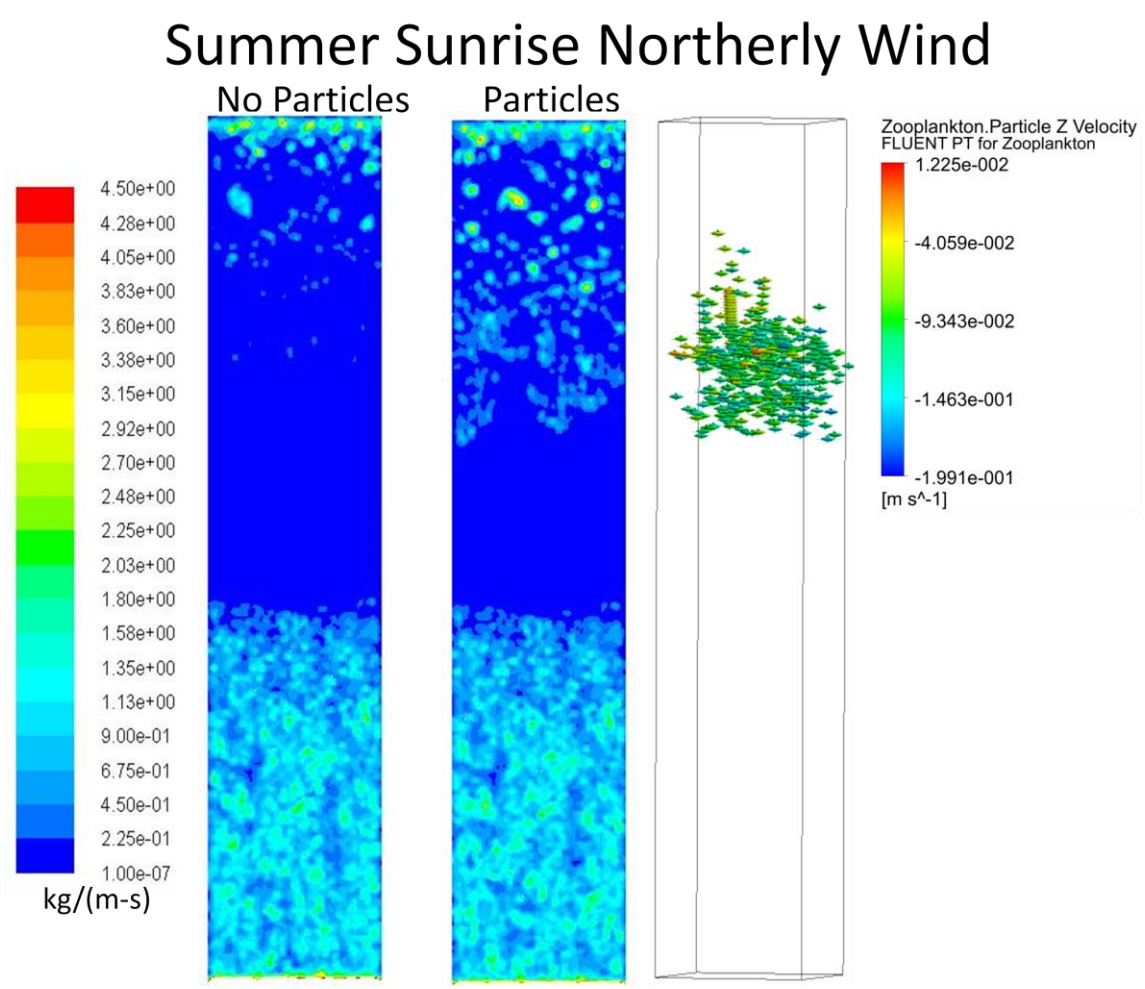

Figure 4-43. Subgrid turbulent viscosity in summer sunrise northerly wind condition comparing particles to no particles case. This was 10 minutes after particle injection while they were still in the mixed layer. Image on right shows the location of the particles within the domain.

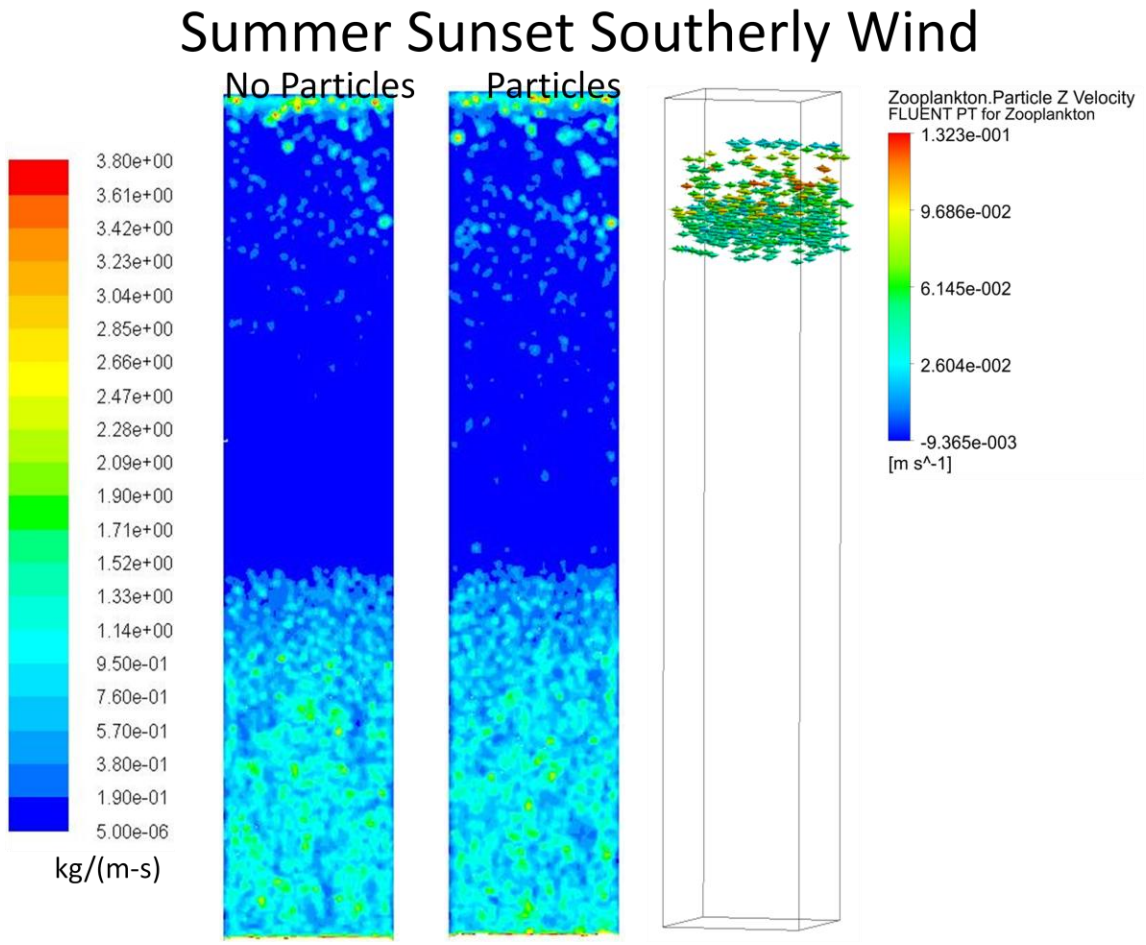

Figure 4-44. Subgrid turbulent viscosity in summer sunset southerly wind condition comparing particles to no particles case. This was 30 minutes after particle injection while they were still in the mixed layer. Image on right shows the location of the particles within the domain.

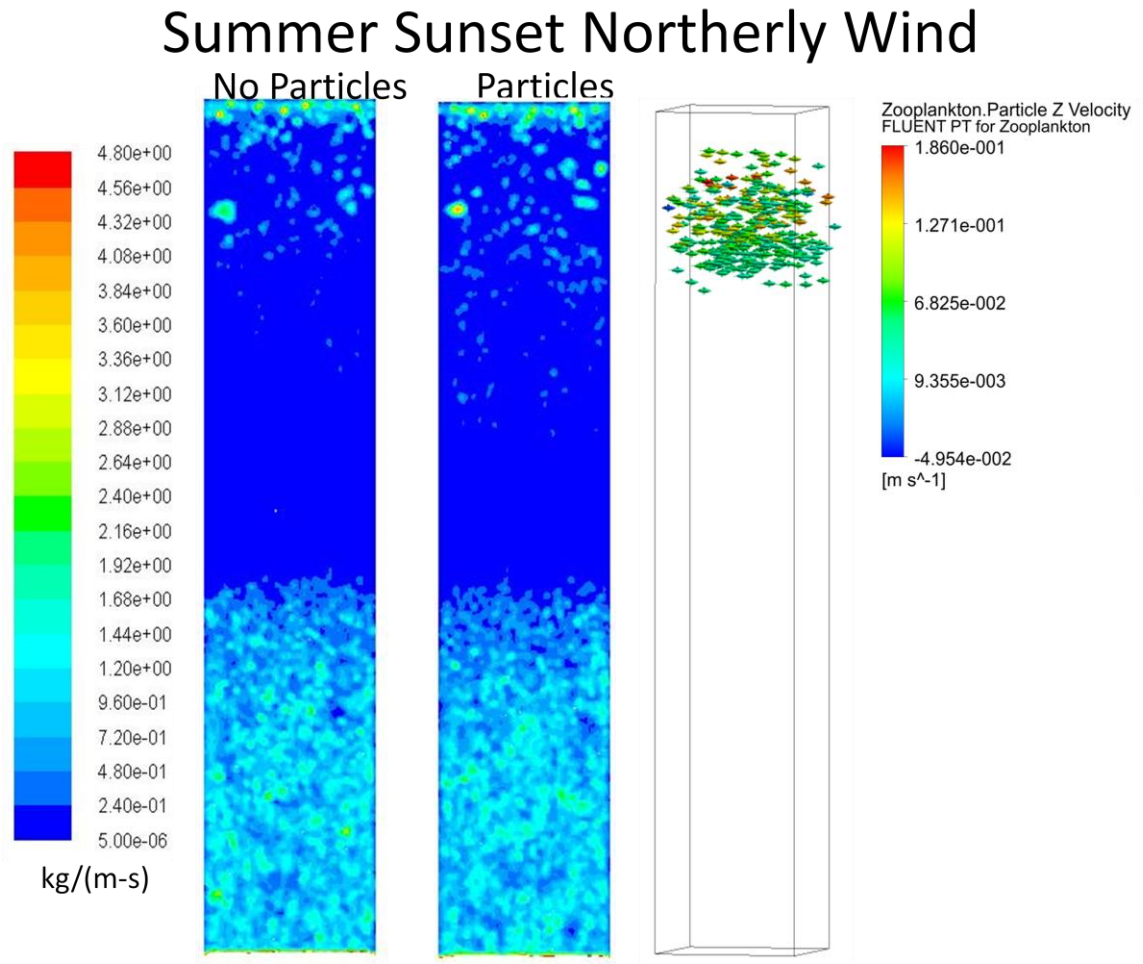

Figure 4-45 Subgrid turbulent viscosity in summer sunset northerly wind condition comparing particles to no particles case. This was 30 minutes after particle injection while they were still in the mixed layer. Image on right shows the location of the particles within the domain.

5 DISCUSSION

5.1 Observational Data

5.1.1 Backscatter

Acoustic data from the ADCP provided an excellent view of some of the major features of the Florida Current. Depth, velocity, tidal oscillations and meandering of the Florida Current were easily observable. These data provided good background information on the physical oceanographic conditions in the study area which helped to create a more accurate model.

From the contour plots of ADCP backscatter (Fig 4-2 to 4-18), there was an obvious periodicity in the strength of the signal. Scattering particles were denser near the surface

layers immediately after sunset. Within an hour of sunset, in almost all cases, the backscatter intensity was much stronger at the surface than before sunrise indicating an upward migration. Within 45 minutes of sunrise, the higher backscatter at the surface had almost disappeared indicating a downward migration. This pattern was consistent with the Nocturnal DVM pattern and appeared in the data from both study sites on most days and when averaged over a season or the full data set.

Zooplankton swimming speeds were calculated for individual cases, as an average over each season, and for the full 11 month data set from Dania Beach (Table 4-1). In many individual cases, such as the one shown in Figure 4-18, there were two different slopes during sunrise and the velocity at sunrise was faster than at sunset. This occurred throughout the Dania Beach data set in all seasons. The two different swim velocities were present but with less frequency during the summer season. There were many spikes in the data during this season due to biofouling of the instrument which could have contributed to this difference.

Seasonal averaged swimming velocities were faster during sunrise than sunset in all cases. Yang (2013) observed the same pattern via acoustic measurements in the Luzon Strait, off the southeast coast of China. Averaged spring sunrise showed two distinct swimming velocities (Fig 4-20). The zooplankton swimming velocity appeared to be faster at the beginning of the downward motion, after which the swimming velocity slowed down. There are two possible hypotheses that may explain this observation. One hypothesis is the zooplankton were, in fact, swimming faster initially to leave the brightly lit surface waters as quickly as possible to avoid detection by visual predators, and then slowed down and sank passively to conserve energy to darker waters at depth. The other hypothesis is that multiple species were migrating down simultaneously. One species was a faster swimmer, which masked the slower speed of other species. Once this faster species migrated back down to depth, it was no longer masking the signal of the other species revealing the slower velocity.

The method used to determine swim velocities from backscatter during migrations averaged the backscatter contours from 60 minutes before and after migrations. These averages did not account for differences in diel vertical migrations due to lunar cycle, cloud cover or other environmental conditions which could alter timing or synchronization of migration. This could have caused blurring of the data masking some features that were present in individual cases. The blurring of the data could account for the lower swimming velocities in seasonal cases as compared to individual cases. This could also be the reason that two swimming velocities were not present in winter or summer during sunrise.

5.1.2 Velocity

Northward current velocity from the ADCP data in Figures 4-23 to 4-31 seemed to show little difference in velocity between sunrise/sunset and three hours prior in most cases. In the Dania Beach data set, however, the northward velocity significantly decreased (95% confidence interval) during a migration time compared to three hours prior in summer and in the averaged complete 11 month data set. The decrease in velocity was likely due to the change of the vertical mixing coefficient produced by additional turbulence from a large mass of zooplankton moving into or out of the area. Increased turbulent friction caused drag, reducing the northward current velocity. Swimming behavior has been known to cause an increase in turbulence on time scales smaller than a few minutes and length scales of a couple of body lengths of the zooplankton (Cheng and Chahine, 2001; Videler et al., 2002; Yen et al., 2003; Catton et al., 2011). An attempt to calculate kinetic energy from the variance of ADCP velocity data was made in order to use it as a proxy for turbulent kinetic energy. These values showed no significant differences because an ADCP is designed to look at velocity data, not turbulence. The bin size was also quite large (4 m), prohibiting the ability to look at small scale processes. All other cases showed no statistically significant change in northward current velocity. This was most likely due to noisy data and other physical factors more powerful than DVM influencing the velocity of the Florida Current, such as wind, tides, and current meandering. Also, the lack of change in the Pompano Beach data set may be due to the long sampling interval of the ADCP. A measurement was only taken once an hour, limiting the number of points available to average.

5.2 Computational Fluid Dynamics Modeling

5.2.1 Velocity

Average x-velocity profiles were analyzed for model runs. These profiles seemed to be consistent with the observational data. A slight difference in x-velocity between particles and no particles model runs was present in both winter sunrise cases and in the summer northerly wind case. No difference was seen in sunset cases or in the summer sunrise southerly wind case. It appeared stratification of the water column was the factor that impacted average velocity profiles the most. When stratification profiles gave a Ri value near critical, changes in average velocity were more likely to occur. Speed of particle motion also appeared to play a role in distortions to the velocity profiles. Particles were set with a larger density difference within water during sunrise cases to mimic the faster swimming velocities found during sunrise times from the ADCP data. A faster motion of the particles might allow for more overturning of the water column, thus a greater change in velocity. A distortion of x-velocity was present in sunrise northerly wind cases for both seasons (Figs. 4-32 and 4-33). This implies that wind direction had a

small effect on changes to velocity profiles as well, but stratification and particle velocity were more important.

When calculating the mass flow rate of particles, the assumption was made that zooplankton were the same density as water. This assumption is not accurate. The density of majority of zooplankton present in the net samples had a significantly lower density than water due to lipid content in the organisms. This assumption was used because the density of particles in the model controls the ascent or descent of diel vertical migrations.

5.2.2 Turbulence

An increase in average subgrid turbulent viscosity was present in all cases when Lagrangian particles were located within the mixed layer of the domain, shown in average profiles (Figs. 4-35 and 4-36) and contour plots (Figs. 4-38 to 4-45). The contour plots revealed higher levels of turbulence in the wake of the moving particles. The increase in turbulence shown in average profiles began deeper in the domain at sunset in both seasons because particles were released from near the bottom of the thermocline in these cases. Both seasons showed a greater increase in turbulence during sunrise which was most likely due to the higher velocity of particles in these cases. Winter cases showed a greater increase in turbulence than summer. This was likely due differences in stratification of the water column between seasons. In winter, the mixed layer was much shallower than in summer and had a sharper temperature gradient. This sharper gradient gave a smaller (near critical) Ri value which allowed for smaller disturbances to cause larger amounts of turbulence. In summer, the mixed layer was deeper than in winter and the temperature gradient was significantly smaller. The smaller gradient gave a Ri value much larger than the critical value near the top of the domain so turnover could not occur as readily. The increase in turbulence began at a deeper depth in the sunset cases because the particles were released near the bottom of the thermocline. The Lagrangian particles in the CFD model simulated zooplankton undergoing DVM; therefore, this result indicates that DVM did cause an increase in turbulence in the upper mixed layer of the ocean.

6 CONCLUSIONS

6.1 Major Findings

In conclusion, this work analyzed the DVM cycle of zooplankton in the Straits of Florida using ADCP data. Average backscatter profiles were used to approximate zooplankton swimming velocities during ascent and descent times. Velocity measurements from the ADCP were analyzed to determine the effect of DVM on northward current velocity profiles. A computational fluid dynamics model was used to simulate the effect of zooplankton DVM in the Florida Current on current velocity and turbulence structure.

An average zooplankton swimming velocity was calculated via average backscatter profiles over each season and over the complete data set for the Dania Beach site. This could not be calculated for the Pompano data set due to the long sampling interval. Swimming velocities during sunrise were faster than sunset in all cases. In many individual cases and in the averaged spring season, two different swimming velocities were observed. It is possible that there are, in fact, two different swimming velocities resulting from an initial quicker swimming rate at sunrise in order to leave the brightly lit surface waters as quickly as possible, followed by a passive sinking phase allowing the organisms to conserve energy once they made it to darker waters at depth. It is also possible that there were organisms swimming at different rates and the faster species masked the signal of the slower swimming species. Once these faster organisms have moved back to depth, the swimming velocities of the slower organisms are observable.

A small, but measurable statistically significant decrease of the northward current velocity of the Florida Current had been linked to the presence of zooplankton undergoing a DVM cycle, but only in a few cases. This decrease in velocity is likely due to an increase in turbulent friction causing drag, thereby, slowing the current velocity slightly. Comparison of the model and average ADCP velocity profiles was complicated by their substantial dependence on the environmental conditions not directly related to DVM including wind, Florida Current meandering, and tides.

An attempt was made to calculate kinetic energy from ADCP variance of velocity fluctuations, used as a proxy for turbulence; however, the differences were not statistically significant. This was likely due to the occurrence of other physical processes stronger than DVM. ADCPs are designed to measure current velocities and not turbulence. The bin size of this instrument is too large to observe small scale processes such as turbulence. To directly measure turbulence, in situ turbulence measurements need to be taken. The effect of DVM on the upper ocean turbulence, as determined from the CFD model, was more visible because the LES subgrid turbulence model is parameterized and physical effects of small scale processes, smaller than the mesh size, are observable. The subgrid turbulent viscosity increases in the wake of particles injected into the model in all cases, indicating that turbulence is increased by DVM on certain time and length scales.

6.2 Limitations

Acoustic measurements and zooplankton net sampling of DVM are limited in the scope of what they can collect. In this case, only organisms or groups of organisms larger than 8 mm could be detected with the 75 kHz ADCP used in this study. There are many migrating zooplankton that are smaller than the detectable size making a true estimation of the number of zooplankton difficult. It is also not possible to determine what species

were present or their swimming behaviors based on acoustics. With net sampling, it was only possible to tell what taxa and densities were present. Also, larger zooplankton can possibly avoid nets like the ones used to contribute to this study. Larger nets with larger mesh size could preclude the collection of smaller organisms.

The acoustic data collected for this project had two components, one with a short sampling interval of five minutes and 11 month duration and the other with a long sampling interval of one hour and 4 year duration. It would be helpful to have a longer data set with a short sampling interval. Direct, in situ turbulence measurements of velocities in the microscale range would also be incredibly helpful to determine instantaneous turbulence structure. Stratification information should have been taken at the sampling site in order to make a realistic initial stratification profile for the model.

As with all models, it is necessary to validate the results with real world conditions. In situ velocity profiles and turbulence structure were not present making it difficult to validate the model. The results of the model can be compared to acoustic data taken from the field, but as mentioned above, there are some limitations to what an ADCP can collect. No one method is able to analyze the effect of DVM on the physical environment so a mixture of methods should be used to acquire a more holistic picture. The optimal experimental design would include acoustic measurements, zooplankton net samples, turbulence profiling with a specialized instrument, particle image velocimetry laboratory experiments and computation fluid dynamics modeling.

REFERENCES

Andersen, V., and P. Nival (1991). "A model of the diel vertical migration of zooplankton based on euphausiids." Journal of Marine Research **49**(1): 153-175.

Anderson, D. L. T. and R. A. Corry (1985). "Seasonal transport variations in the Florida Straits: a model study." Journal of Physical Oceanography **15**(6): 773-786.

Bainbridge, R. (1961). Migrations. "The physiology of Crustacea", *2*, 431-463.

Beer, J. R. (1976) "Determination of zooplankton biomass." In H. F. Steedman (ed) Zooplankton Fixation and Preservation. UNESCO Press. Paris. 35-84.

Blackburn, M. (1981). "Low latitude gyral regions." In: Longhurst AR (ed) Analysis of Marine Ecosystems. Academic Press. London. 3-29.

Bollens, S. M. and B. W. Frost (1989). "Predator-induced diet vertical migration in a planktonic copepod." Journal of Plankton Research **11**(5): 1047-1065.

Brodeur, R. D. and W. C. Rugen (1994). "Diel vertical distribution of ichthyoplankton in the Northern Gulf of Alaska." Fishery Bulletin **92**(2): 223-235.

Catton, K. B., D. R. Webster, S. Kawaguchi, and J. Yen (2011). "The hydrodynamic disturbances of two species of krill: implications for aggregation structure." The Journal of Experimental Biology **214**(11): 1845-1856.

Cheng, J.-Y. and G. L. Chahine (2001). "Computational hydrodynamics of animal swimming: boundary element method and three-dimensional vortex wake structure." Comparative Biochemistry and Physiology Part A: Molecular and Integrative Physiology **131**(1): 51-60.

Cohen, J. H. and R. B. Forward (2002) "Spectral sensitivity of vertically migrating marine copepods." The Biological Bulletin **203**: 307-314.

Cohen, J. H. and R. B. Forward Jr. (2005) "Photobehavior as an inducible defense in the marine copepod *Calanopia americana*." Limnology and Oceanography **50**: 1269-1277.

Cohen, J. H. and R. B. Forward Jr. (2009). "Zooplankton diel vertical migration- a review of proximate control." Oceanography and Marine Biology: An Annual Review **47**: 77-110.

Criales, M. M., C. B. Paris, C. Yeung, D. L. Jones, W. J. Richards, and T. N. Lee. (2004) Horizontal and seasonal distribution of zooplankton biomass and fluorescence from MOCNESS plankton tows in the Florida Straits and the Dry Tortugas. NOAA Tech. Mem. NMFS-SEFSC-525: 24 p.

Dabiri, J. O. (2010). "Role of vertical migration in biogenic ocean mixing." Geophysical Research Letters **37**(L11602): 1-4.

De Robertis, A. and J. Jaffe (2000). "Size-dependent visual predation risk and the timing of vertical migration in zooplankton." Limnology and Oceanography **45**(8):1838-1844.

De Robertis, A. (2002). "Size-dependent visual predation risk and the timing of vertical migration: an optimization model." Limnology and Oceanography **47**(4): 925-933.

De Robertis, A., C. Schell, and J. Jaffe (2003). "Acoustic observations of the swimming behavior of the euphausiid *Euphausia pacifica* Hansen." ICES Journal of Marine Science: Journal du Conseil **60**(4): 885-898.

Dewar, W. K., R. J. Bingham, R. L. Iverson, D. P. Nowacek, L. C. St. Laurent, and P. H. Wiebe (2006). "Does the marine biosphere mix the ocean?" Journal of Marine Research **64**(4): 541-561.

Dickson, R. R. (1972). "On the relationship between ocean transparency and the depth of sonic scattering layers in the North Atlantic." ICES Journal of Marine Science: Journal du Conseil **34**(3): 416-422.

Düing, W. and D. Johnson (1971). "Southward flow under the Florida Current." Science **173**: 428-430.

Enright, J. T. (1977). "Diurnal vertical migration: adaptive significance and timing. part1. Selective advantage: a metabolic model." Limnology and Oceanography **22**(5): 856-872.

Frank, T. M. and E. A. Widder (1996). "UV light in the deep-sea: *in situ* measurements of downwelling irradiance in relation to the visual threshold sensitivity of UV-sensitive crustaceans. Marine Freshwater Behavioral Physiology **27**: 189-197.

Frank, T. M. and E. A. Widder (1997). "The correlation of downwelling irradiance and staggered vertical migration patterns of zooplankton in Wilkinson Basin, Gulf of Maine." Journal of Plankton Research **19**(12):1975-1991.

Frank, T. M. and E. A. Widder. (2002) "Effects of a decrease in downwelling irradiance on the daytime vertical distribution patterns of zooplankton and micronekton." Marine Biology **140**: 1181-1193

Forward, R. B. Jr. (1985). "Behavioral responses of larvae of the crab *Rhithropanopeus harrissii* (Brachyura: Xanthidae) during diel vertical migrations." Marine Biology **90**: 9-18

Forward, R. B. Jr. (1988). "Diel vertical migration: zooplankton photobiology and behaviour." Oceanography and Marine Biology: An Annual Review **26:** 361-393.

Gibson, W. E. (2014)."Cuba presses ahead on offshore oil drilling" *Sun Sentinel*, January 21.

Gliwicz, M. Z. (1986). "Predation and the evolution of vertical migration in zooplankton." Nature **320**(6064): 746-748.

Gordon, R. L. (1996). "Acoustic Doppler current profiler: Principles of operation, a practical primer, second edition for broadband ADCPs." RDI Instruments.

Gray, C. A. (1998). "Diet changes in vertical distributions of larval fishes in unstratified coastal waters off southeastern Australia." Journal of Plankton Research **20**(8): 1539-1552.

Gregg, M. C. and J. K. Horne (2009). "Turbulence, acoustic backscatter, and pelagic nekton in Monterey Bay." Journal of Physical Oceanography **39**(5): 1097-1114.

Haney, J. F. (1988). "Diel patterns of zooplankton behavior." Bulletin of Marine Science **43**(3): 583-603.

Haney, J. F., A. Craggy, K. Kimball, and F. Weeks (1990). "Light control of evening vertical migrations by *Chaoborus punctipennis* larvae." Limnology and Oceanography **35**: 1068-1078.

Huebert, K. B., S. Sponaugle, and R. K. Cowen (2010). "Predicting the vertical distributions of reef fish larvae in the Straits of Florida from environmental factors." Canadian Journal of Fisheries and Aquatic Sciences **67**(11): 1755-1767.

Huebert, K. B., R. K. Cowen and S. Sponaugle (2011). "Vertical migrations of reef fish larvae in the Straits of Florida and effects on larval transport." Limnology and Oceanography **56**(5): 1653-1666.

Huntley, M. E. and M. Zhou (2004). "Influence of animals on turbulence in the sea." Marine Ecology Progress Series **273**: 65-79.

Hutchinson, G. E. (1967). A treatise on limnology. Vol. II: Introduction to lake biology and the limnoplankton.

Ianson, D., G. A. Jackson, M. V. Angel, R. S. Lampitt, and A. B. Burd (2004). "Effect of net avoidance on estimates of diel vertical migration." Limnology and Oceanography **49**(6): 2297-2303.

Irisson, J. O., C. B. Paris, C. Guigand, and S. Planes (2010). "Vertical distribution and ontogenetic 'migration' in coral reef fish larvae." Limnology and Oceanography **55**(2): 909-919.

Iwasa, Y. (1982). "Vertical migration of zooplankton: a game between predator and prey." The American Naturalist **120**(2): 171-180.

Jenkins, W. J. and S. C. Doney (2003). "The subtropical nutrient spiral." Global Biogeochemical Cycles **17**(4): 1110.

Katija, K. (2012). "Biogenic inputs to ocean mixing." The Journal of Experimental Biology **215**(6): 1040-1049.

Klevjer, T. A. and S. Kaartvedt (2011). "Krill (*Meganyctiphanes norvegica*) swim faster at night." Limnology and Oceanography **56**(3): 765-774.

Kunze, E., J. F. Dower, I. Beveridge, R. Dewey, and K. P. Bartlett (2006). "Observations of biologically generated turbulence in a coastal inlet." Science **313**(5794): 1768-1770.

Kunze, E., J. F. Dower, R. Dewey, and E. A. D'Asaro (2007). "Mixing it up with krill." Science (New York, N.Y.) **318**(5854): 1239; author reply 1239.

Kunze, E., J. F. Dower, and R. Dewey (2009). "The role of biologically-generated turbulence in the upper ocean." Victoria, School of Earth and Ocean Sciences, University of Victoria**:** 5.

Lampert, W. (1989). "The adaptive significance of diel vertical migration of zooplankton." Functional Ecology **3**(1): 21-27.

Leaman, K. D., R. L. Molinari, and P. S. Vertes (1987). "Structure and variability of the Florida Current at 27°N: April 1982–July 1984." Journal of Physical Oceanography **17**(5): 565-583.

Lee, T. N. and E. Williams (1999). "Mean distribution and seasonal variability of coastal currents and temperature in the Florida Keys with implications for larval recruitment." Bulletin of Marine Science **64**(1): 35-56.

Loeb, J. (1893). "On the influence of light on the periodical depth-migrations of pelagic animals." Bulletin of the U.S. Fish Commission **13**: 406-411.

Loose, C. J. and P. Dawidowicz (1994). "Trade-offs in diel vertical migration by zooplankton: the costs of predator avoidance." Ecology **75**(8): 2255-2263.

MacKenzie, B. R. and W. C. Leggett (1993). "Wind-based models for estimating the dissipation rates of turbulent energy in aquatic environments: empirical comparisons." Marine Ecology Progress Series **94**: 207-216.

McManus, M. and B. Woodson (2012) "Plankton distribution and ocean dispersal." The Journal of Experimental Biology **215**: 1008-1016.

Morsi, S. A., and A. J. Alexander (1972). "An investigation of particle trajectories in two-phase flow systems." Journal of Fluid Mechanics, **55**(2), 193-208.

Munk, W. H. (1966). "Abyssal recipes." Deep Sea Research and Oceanographic Abstracts **13**(4): 707-730.

Munk, W. and C. Wunsch (1998). "Abyssal recipes II: energetics of tidal and wind mixing." Deep Sea Research Part I: Oceanographic Research Papers **45**(12): 1977-2010.

Niiler, P. P. (1968). "On the internal tidal motion in the Florida Straits." Deep Sea Research and Oceanic Abstracts, **15**(1): 113-123.

Pillsbury, J. E. (1891). The Gulf Stream, methods of the investigation and results of the research, U.S. Coast and Geodetic Survey. 461-620.

Richards, S. A., H. P. Possingham, and J. Noye (1996). "Diel vertical migration: modelling light-mediated mechanisms." Journal of Plankton Research **18**(12): 2199-2222.

Rudjakov, J. A. (1970). "The possible causes of diel vertical migrations of planktonic animals." Marine Biology **6**(2): 98-105.

Schmitz, W. J. and W. S. Richardson (1968). "On the transport of the Florida Current." Deep Sea Research and Oceanographic Abstracts **15**(6): 679-693.

Schott, F., T. N. Lee, and R. Zanotpp (1988). "Variability of structure and transport of the Florida Current in the period range of days to seasonal." Journal of Physical Oceanography **18**(9): 1209-1230.

Smyth, C., A. E. Hay, P. S. Hill, and D. Schillinger (2006). "Acoustic observations of vertical and horizontal swimming velocities of a diel migrator." Journal of Marine Research **64**: 723-743.

Soloviev, A. V., A. Hirons, C. Maingot, R. E. Dodge, A. E. Yankovsky, J. Wood, R. H. Weisberg, M. E. Luther and J. P. McCreary (In Review). "Southward Flow on the Coastal Flank of the Florida Current." Journal of Geophysical Research

Soloviev, A. V., M. E. Luther, and R. H. Weisberg (2003), "Energetic baroclinic super-tidal oscillations on the southeast Florida shelf." Geophysical Research Letters, **30**(9): 1463.

St. Laurent, L. and C. Garrett (2002). "The role of internal tides in mixing the deep ocean." Journal of Physical Oceanography **32**(10): 2882-2899.

St. Laurent, L. and H. Simmons (2006). "Estimates of power consumed by mixing in the ocean interior." Journal of Climate. **19**(19): 4877-4890.

Stich, H.-B. and W. Lampert (1981). "Predator evasion as an explanation of diurnal vertical migration by zooplankton." Nature **293**(5831): 396-398.

Swift, M. C., and R. B. Forward Jr. (1988) "Relative light intensity vs. rate of change: the role of light in the vertical migration of *Chaoborus punctipennis* larvae." Bulletin of Marine Science **43**: 604-619.

United States Coast Guard (USCG) (2008) Environmental impact statement for the Calypso LNG Deepwater Port license application. Volumes 1 and 2. 1657.

Videler, J. J., E. J. Stamhuis, U. K. Muller, and L. A. Van Duren (2002). "The scaling and structure of aquatic animal wakes." Integrative and Comparative Biology **42**(5): 988-996.

Visser, A. W. (2007). "Biomixing of the oceans?" Science **316**(5826): 838-839.

Williams, A. J., (2010). "Historical developments of current, wave, and turbulence measurements including those by MAVS." Proceeding of the IEEE/OES/CWTM Tenth Working Conference on Current Measurement Technology.

Wunsch, C. (2000). "Oceanography: moon, tides and climate." Nature **405**(6788): 743-744.

Wunsch, C. and R. Ferrari (2004). "Vertical mixing, energy, and the general circulation of the oceans." Annual Review of Fluid Mechanics **36**(1): 281-314.

Yamamura, O., T. Inada, and K. Shimazaki (1998). "Predation on *Euphausia pacifica* by demersal fishes: predation impact and influence of physical variability." Marine Biology **132**(2): 195-208.

Yang, C., G Liao, Y. Yuan, H. Chen, X. Zhu (2013). "The diel vertical migration of sound scatterers observed by an acoustic Doppler current profiler in the Luzon Strait from July 2009 to April 2011." Acta Oceanologica Sinica **32**(11): 1-9.

Yen, J., J. Brown, D. R. Webster (2003). "Analysis of the flow field of the krill, *Euphausia pacifica*." Marine and Freshwater Behaviour and Physiology **36**(4): 307-319.